

**SYNTHESIS OF HYBRID NANOSTRUCTURES FOR
LIGHT-INDUCED WATER SPLITTING FOR
HYDROGEN PRODUCTION**

A Thesis

Submitted in partial fulfilment of the requirements for the
award of the degree of

DOCTOR OF PHILOSOPHY

in

(Chemistry)

By

Ruby Gill

(41700240)

Supervised By

Dr Pushendra Kumar



L OVELY
P ROFESSIONAL
U NIVERSITY

Transforming Education Transforming India

LOVELY PROFESSIONAL UNIVERSITY

PUNJAB

2022

DECLARATION

I hereby declare that the thesis entitled “**Synthesis of Hybrid Nanostructures for Light-Induced Water Splitting for Hydrogen Production**” has been prepared and submitted by me under the guidance of **Dr Pushpendra Kumar**, Assistant Professor, Central Instrumentation Facility, Lovely Professional University, Phagwara, Punjab as per the requirement for the award of the degree of Doctor of Philosophy (PhD) in Chemistry is entirely my original work and ideas and references are duly acknowledged. It does not contain any work that has been submitted for the award of any other degree or diploma of any university.



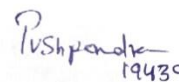
Ruby Gill

Reg.No- 41700240

Department of Chemistry,
Lovely Professional University,
Phagwara, Punjab, India.

CERTIFICATE

This is to certify that **Ms Ruby Gill** has completed her Doctor of Philosophy (PhD) in Chemistry thesis entitled "**Synthesis of Hybrid Nanostructures for Light-Induced Water Splitting for Hydrogen Production**" is a bonafide work carried out by her under my supervision and guidance. To the best of my knowledge, the present work is the result of her original investigation and study. No part of the thesis has ever been submitted to any other University or Institute for the award of any degree or diploma.



Dr Pushendra Kumar

Assistant Professor
Central Instrumentation Facility,
Lovely Professional University,
Phagwara, Punjab, India

Abstract

Exhaustive utilization of conventional fuels and regular increase in energy required per capita is leading to depletion of energy reserves very soon. Therefore, another energy framework is needed to substitute the current energy framework for legitimate human progress of energy for example energy ought to be accessible to each and everybody at a sensible rate. Nature has various rich energy sources but their harvesting is a major concern. Many renewable energy sources are available but either due to low efficiency or high cost, could not be implemented at the grass-root level. To overcome this problem, the research has been turned up towards harvesting renewable energy sources in any direct or indirect mode. Solar energy is a vast energy source and can solve the problem if can be harvested properly with good efficiency.

The hydrogen energy framework has the potential over traditional energy frameworks because of its important properties like high calorific worth and energy content. The end product of hydrogen is water so it is also safe for the environment. There are various methods to produce hydrogen-like steam methane reforming but again it is produced by conventional fuels only so could not solve the purpose. We need a method by which Hydrogen can be produced by utilizing sustainable power sources like sun-oriented energy.

In this thesis, we have reported light-assisted Photoelectrochemical (PEC) Splitting of Water to produce Hydrogen. In short, PEC splitting of water is a process in which a three-electrode cell is constructed by using a working semiconductor electrode, Counter electrode and Reference electrode. Under illumination, the working electrode, and the photocurrent is generated which causes photolysis of water and hydrogen is generated. So the core of the PEC cell is a functioning semiconductor terminal. However, for efficient AEC splitting of water, semiconductors must have certain favourable properties like band edge alignment, high electron mobility, effective charge separation and mobility etc. But to date, no ideal semiconductor has been found which can fulfil all the conditions simultaneously.

In the present report, to find out suitable semiconductor system, various modification tools have been adopted for the formation of nanoarchitecture, nanocomposites, nano-

heterostructures, and dye sensitization. In this study, ZnO Spheres, 1D ZnO Nanorods, SnO₂, TiO₂, TiO₂-MoS₂ based nanocomposites, ZnO based Nanoheterostructures, Dye-sensitized ZnO and mixed oxides were synthesized. The pre-arranged materials were exposed to X-Ray diffraction (XRD) analysis for Phase and crystalline size assurance. All the samples were in the nano range. A single peak in the XRD pattern of ZnO nanorods confirmed the unidirectional growth of ZnO nanorods. The XRD pattern of ZnO powder confirmed the hexagonal wurtzite phase of ZnO. The XRD pattern of TiO₂ showed that strengthening temperature markedly affects the crystallinity of the example and can cause stage change. It was also observed that new peaks evolved depending on the concentration of secondary phases or dopants. Different microcrystalline parameters were evaluated by using XRD data. For optical characterization, UV-Visible spectra of the prepared materials were recorded. The absorption edge of all the samples was found in the expected region. The morphological investigation was done by using FE-SEM equipped with EDS. Different morphologies were observed depending on the method of preparation, annealing temperature and concentration of dopants. The compositional analysis was done by Energy-dispersive X-ray spectroscopy (EDS). The peaks in EDS confirm the presence of respective atoms present in the semiconductor material including nanoheterostructures/ mixed oxides/ doped materials.

To study the photoelectrochemical behaviour, materials were converted into electrodes with the help of copper wire and silver paste. The three electrodes cell was constructed in which semiconductor material was used as a working electrode and NaOH was taken as electrolyte. The electrodes were illuminated by light and photocurrent was recorded with the help of Linear Sweep Voltammetry. By the current-voltage curves, Short circuit current and open circuit potential were assessed. During the photocurrent measurement, small bubbles of hydrogen gas at the Platinum electrode were seen. The amount of hydrogen generated depends on the amount of photocurrent. Therefore, the magnitude of photocurrent can be directly correlated with the amount of hydrogen production.

It was observed that morphology, crystal quality and composition of semiconducting material have a marked effect on photocurrent and short circuit current. The magnitude

of photocurrent and short circuit current does not depend only upon the generation of electron-hole pairs but also depend on their separation and mobility. The low recombination rate of charge carriers and high electron mobility can yield better photocurrent. Electrons in semiconductor material move with the hopping mechanism and may recombine at grain boundaries. Therefore, 1D nanostructures may be a better option as they give an immediate pathway to the electrons. Defects or any other imperfection can lead to electron losses or charge carrier recombinations. To achieve better photocurrent, the crystal quality and band edge alignment are very crucial.

In this study, attempts were made to increase the optical absorption, reduce the charge recombinations and increase electron mobility. The results are encouraging.

Acknowledgement

In the beginning, I would to express my deepest gratitude to the **Almighty God** for his consistent blessings and grace. His guidance allowed me to accomplish this academic venture. Most importantly and firstly, I want to owe a debt of gratitude to my thesis supervisor **Dr Pushendra Kumar**. He has been an excellent advisor to me throughout my journey as a research scholar. He showed big trust in me and my ideas which was the constant source of encouragement for me since the beginning of my Ph. D work.

Additionally, I would like to express gratitude to **Dr Ajit Kumar, Associate Professor, Division of Research and Development** for his treasured support which was influential in shaping my thesis and critiquing my results. He also demonstrated what a brilliant and hard-working scientist can accomplish. I am most grateful to him for lending me his expertise and intuition to my scientific and technical problems.

There are no proper words to convey my deep gratitude and respect for our Head of School, **Dr Kailash Juglan. Professor & Deputy Dean, School of Chemical Engineering and Physical Sciences**. My success in my PhD can never be achieved without his support and motivation.

I have to tender my humble thanks to the technical and supporting staff of **Mr Manoj, Ms Amarjeet Kaur, Mr Nitin, Mr Varun, Mr Sandeep, Mr Amrinder, Mr Manish, Ms Renki and Mr Baljeet** of the Department of Chemistry and Central Instrumentation Facility (CIF) for their help in my research work.

I thank with love **Ms Harpreet Kaur** as she has been a great companion, loved, supported, encouraged, entertained, and helped me get through this agonizing period in the most positive way. My special acknowledge to my friends **Mr. Ashok Singh, Ms Isha Dalal and Ms Shagun Sharma** for encouraging me throughout my PhD. I am also thankful to **Dr Megha Khatri** who supported me whenever I needed her.

I would like to put my deepest sense of regard to my parents for their moral support, selfless love, patience, true blessings and sacrifices they made for my career. It was their love that raised me again when I got weary. I cannot fully express my full depth of appreciation to my brother, **Adv. Karanvir Singh Gill** played a major role in completing my thesis work. He inspired me to pursue research in this area. He always provided me strength during my hard times. Thanks for having faith in me that allows me to keep going.

-Ruby Gill

TABLE OF CONTENTS

Chapter	Title	Page no.
Chapter-1	Introduction	13-37
1.1	Depleting fossil fuels : An emerging threat	13-14
1.2	Sun: A safe and inexhaustible energy reservoir	14-16
1.3	Hydrogen: A feasible energy Carrier	16-18
1.4	Basic Hydrogen facts	18-19
1.4.1	Merits as energy carrier	19-20
1.5	Outline of solar-hydrogen generation	21-23
1.6	Solar water Splitting	23-28
1.7	Photo-electrochemical splitting of water	29-35
1.7.1	Hypothesis of PEC	35-36
1.8	Working of electrolyte	37-38
Chapter-2	Literature review	38-77
2.1	A prospectus of extant findings in the sphere of present work	38-76
2.2	Origin of Problem	76-77
Chapter -3	Methodologies for sample preparation and characterization	78-91
3.1	Outline of Experimental work	78-79
3.2	Materials required	79-79
3.3	Sample synthesis of various materials	80-83
3.3.1	ZnO nanorods	80-80
3.3.2	ZnO nanoparticles at different pH	80-80
3.3.3	SnO ₂ nanoparticles	80-80
3.3.4	ZnO/SnO ₂ Nanoparticles	81-81
3.3.5	TiO ₂ nanoparticles	81-81
3.3.6	MoS ₂ nanoparticles	81-81
3.3.7	TiO ₂ / MoS ₂ nanoparticles	81-81
3.3.8	ZnO/rGO nanocomposites	81-82
3.3.9	Cu doped Fe ₂ O ₃ nanoparticles	82-82
3.3.10	Dye Sensitization by Rose Bengal dye and Erythrosin B	83-83
3.4	Sample Characterization	83-93
3.4.1	XRD study	83-86
3.4.2	Energy Dispersive X-Ray Spectroscopy	86-87

3.4.3	Surface Morphology	87-89
3.4.4	Surface Topography	89-90
3.5	Optical characterization	90-91
3.6	Photoelectrochemical Studies	91-93
3.6.1	Preparation of working electrode	91-92
3.6.2	Current Potential Characteristics	92-92
3.6.3	Mott-Schottky Analysis	92-93
Chapter- 4	Results and Discussion	94-130
4.1	Characterization	94-94
4.2	ZnO nanorods	94-105
4.2.1	XRD analysis	97-97
4.2.2	UV Analysis	97-98
4.2.3	AFM Analysis	99-100
4.2.4	SEM images	102-102
4.2.4.1	Side view	103-103
4.2.5	EDS	104-104
4.2.6	Dye Sensitization & IV studies	104-105
4.3	ZnO nanoparticles at different pH	105-108
4.3.1	XRD	105-105
4.3.2	UV analysis	106-106
4.3.3	SEM images	107-107
4.3.4	EDS	107-107
4.3.5	I-V studies	107-108
4.4	SnO ₂ nanoparticles	108-108
4.4.1	XRD	108-108
4.5	ZnO-SnO ₂ nanoparticles	109-109
4.5.1	XRD	109-109
4.5.2	UV analysis	110-110
4.5.3	SEM images	111-111
4.5.4	EDS	111-111
4.5.5	I-V studies	111-112
4.6	TiO ₂ nanoparticles	112-112
4.6.1	XRD	112-115
4.6.2	UV analysis	115-116
4.6.3	SEM images	117-117
4.6.4	EDS	118-118
4.6.5	I-V studies	118-119
4.7	TiO ₂ /MoS ₂ nanoparticles	119-119
4.7.1	XRD	119-120
4.7.2	UV analysis	120-121
4.7.3	SEM images	121-121
4.7.4	EDS	121-122
4.7.5	I-V studies	122-123
4.8	ZnO/rGO nanocomposites	123-123
4.8.1	XRD	123-124
4.8.2	UV analysis	124-125

4.8.3	SEM images	125-125
4.8.4	EDS	126-126
4.9	Cu doped Fe ₂ O ₃ nanoparticles	127-127
4.9.1	XRD	127-128
4.9.2	UV analysis	128-129
4.9.3	SEM images	130-130
4.9.4	EDS	130-130
4.10	Dye Sensitization By Rose Bengal Dye & Erythrosin B and I-V Studies	131-134
4.10.1	UV-Analysis	131-131
4.10.2	I-V studies	131-132
4.10.3	Open circuit potential and short circuit current	132-134
Chapter-5	Conclusions	134-148
	References	149-191

LIST OF NOTATIONS/ABBREVIATIONS USED

a.u.	arbitrary unit
AFM	atomic force microscopy
BTU	British thermal units
C	capacitance
CB	conduction band
CE	counter electrode
CV	cyclic voltammetry
DW	distilled/deionized water
E	energy
e ⁻	electron
ϵ_s	dielectric constant of the semiconductor
E _c	conduction band edge
ED	electrodeposited thin films
E _F	Fermi level energy
E _g	band gap energy
E _v	valence band edge
F	faraday's constant
Fcc	face centered cubic
f(E)	Fermi-Dirac energy distribution function
FWHM	Full width at half maximum
ΔG	Gibbs free energy change
h ⁺	holes present in semiconductor
hcp	hexagonal close packed
HOMO	highest occupied molecular orbital
h ν	photon energy
I _{ph}	photocurrent density
I-V	current – potential
J _{sc}	short circuit current
K	Boltzmann's constant

L	current under illumination
LCAO	linear combination of atomic orbitals
L_D	Debye length
LUMO's	lowest unoccupied molecular orbital
MS	Mott-Schottky
N_d	charge carrier density
nm	nanometer
NHE	normal hydrogen electrode
PEC	photoelectrochemical
PC	photocatalytic
PDI	Poly Dispersive Index
CE	Platinum counter electrode
q	elementary charge
R	resistance
ϵ	microstrain
SCE	saturated calomel reference electrode
SD	standard deviation
SEM	scanning electron microscopy
SG	sol-gel
SHI	swift heavy ions
t	thickness of the sample
T	temperature
U	potential
V_{fb}	flat-band potential
V	Externally applied potential (measured against SCE)
VB	valence band
V_{oc}	open circuit potential
WE	working electrode
XRD	X-ray diffraction
ZnO	Zinc Oxide

Chapter -1

Introduction

1.1: Depleting Fossil fuels: An Emerging Threat

Energy incorporates the centre of contemporary human progress. It is crucial to the financial progression of any country. With the growing human population and rising reliance on an automated systems, the depletion chart of energy by humans has climbed some folds over the past few decades [Bartlett, A. A. 1986]. The period of fossil fuel emerged not more than two fifty years ago with a further prop on wood and coal-rich energy derivatives and not over a century back the society adapted petroleum age. The thorough take-up of traditional fuels and their troubling rates are creating an imbalance of effective progress for advancing nations like India. There exists a mathematically direct relationship between energy utilization and financial development for quite a while. In India, there is a big discrepancy between the pace of utilization and reserves of fossil fuels and we need to be dependent on Gulf nations to fulfil our energy demand. We are dependent on other countries for about 71% of crude oil and 29% of natural gas [Wang, Y. F. E al. 2014]. Reliance on energy demand in other nations and expensive prices is disturbing for sustainable industrial and social development. Most of the energy need is satisfied by fossil fuels only which will be drained in not so distant future. Moreover, the combustion of fossil fuels gives rise to hazardous gases harming the climate and is also accountable for global warming [Nowotny, J. et al.2014]. Thus, the time has come when we should consider other substitutes of energy sources that can satisfy worldwide energy demand for quite a long period with no irreversible harm to the climate. To settle this global challenge, we need to search for another alternative energy system by which appropriate advancements in energy can be made. In other words, energy should be accessible to every consumer at an economical rate for a long period.

Different substitutes for energy sources are obtainable however, gathering them is still a difficult task because of less proficiency, high expense and restricted accessibility. Geothermal energy, Tidal energy, Wind energy and bio-fuels are the only energy

resources at hand [Wang, J. et al. 2018]. But all of them are bound to a few limits which make them wasteful for the necessary worldwide energy demand.

1.2: Sun: A safe and inexhaustible energy reservoir.

Other than the few potentials and inexhaustible derivatives of energy, solar energy is most favourable. The reserve of energy from the Sun to the Earth is huge: 3×10^{24} joules per year, or around multiple times more than the worldwide population consumes at present [Kreith, F., & West, R. 2004]. While solar energy is the most profuse and clean fuel source accessible at present, the immediate utilization of solar energy is restricted and just 0.04 % of all energy is created by photovoltaics [Feng, X. et al. 2008]. The well-known approaches to limitless solar energy are (I) photovoltaic (PV) cells, (ii) photoelectrochemical (PEC) cells and (iii) concentrated solar thermal systems [Gür, T. M., Bent et al. 2014]. Until now, most of the efforts done for the use of solar energy spin around solar-electricity generation by photovoltaic systems. Such frameworks are already being used in numerous spots. Nonetheless, despite huge mechanical upgrades and cutting in costs in recent years, photovoltaic boards are still extravagant and can't be an answer for the diverse assorted energy needs of the population. The multipurpose, large-scale and effective utilization of solar energy is still fundamentally linked to its conversion to synthetic energy [Walter, M. G. et al. 2010].

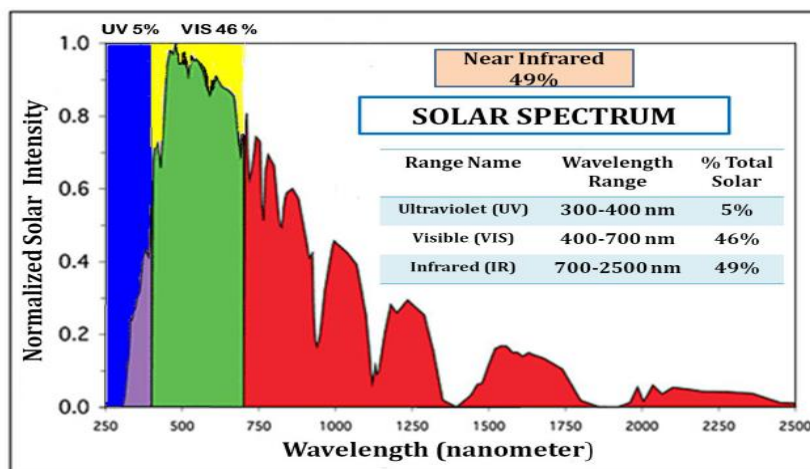


Fig. 1.1:

Graphical distribution of Solar Energy Spectrum

[http://solarcellcentral.com/solar_page.html]

Further, solar-powered energy transition on earth is diffused and relies on schedule, season, climate and district. Consequently, its stockpiling is even more essential and can be accomplished more appropriately by its conversion to a chemical substance. Scientists are focusing on various choices in this specific situation. Some of these are being referred here. The photobiological process, also called man-made photosynthesis, provides some high-energy chemicals, namely carbohydrates, later which can be utilized as an alternative fuel. Fuel creation employing man-made photosynthesis requires: (I) a radio wire/response focus to gather daylight and create electrochemical potential, (ii) impetus for oxidation of water or other electron sources and (iii) impetus for a decrease of carbon-bearing forerunner compounds. Endeavours towards the improvement of the above essential components have brought about just restricted achievement as yet [Gust D et al. 2009]. Photo reforming of biofuels, for example, glucose, ethanol or methanol to create H₂ gas has additionally gotten the consideration of numerous scientists [Peng Q et al. 2009; Lin Y C et al. 2007]. Also, photochemical transformations, including the isomerisation of the natural substance to energy-rich unreliable isomers have been propounded by certain specialists [Lee J H et al. 2010]. But, in the photochemical transformation, the undesired and energy-devouring back electron moves transfers, just as side electron transfers, are significant hindrances [Amouyal E 1995]. It is practically difficult to forestall these undesired electron transfers, especially when the responses are done in a homogeneous arrangement where all the segments encounter one another freely. To combat this issue, the usage of heterogeneous transformation systems, for example, molecular gatherings or polymers has been proposed by a couple of specialists [Connolly, J. (Ed.). 2012]. The single-step thermal splitting of water, known as water thermolysis, has been proposed as a technique for solar energy conversion and capacity. In this strategy, a high-heat source, at or over 2500 K, is required, and it is a major restriction. Furthermore, a powerful method for isolating H₂ and O₂ is required. The extremely high temperature required for the cycle presents serious material issues and can prompt huge radiation loss from the reactor [Steinfeld A 2005]. Water parting thermochemical cycles enjoy an upper hand over thermolysis concerning the present circumstance a H₂/O₂ separation issue is evaded and the cycle occurs at commonly moderate temperatures (\approx 1200 K) [Steinfeld A 2005]. Two cycles that hold an uncommon assurance that needs outstanding

notification concerning the momentum hypothesis are a difference in sun-based controlled energy to Hydrogen, which is seen as a significant compound fuel, by photocatalytic (PC) just as photoelectrochemical (PEC) splitting of water. The basic steps associated with both the cycles are the absorption of photons on some semiconductor photocatalyst/photoelectrode, detachment of charge transporters, surface reactions and transport of reaction species. Photoelectrochemical (PEC) water splitting was shown path back in 1972 by Honda and Fujishima [Fujishima A and Honda K 1972]. A customary PC cell is set up with a semiconductor photoanode and a platinum (Pt) cathode in the electrolyte arrangement. Under illumination ($h\nu \geq$ Energy band gap of semiconductor) at the photoanode, the electrons are empowered and progress from the valence band (VB) to the vacant conduction band (CB). The created layer, created at the semiconductor–electrolyte interface, prompts energy band contorting which energizes the isolation of photogenerated electrons and openings. The electrons moved to the cathode to reduce water to produce hydrogen,

$(2\text{H}_2\text{O} + 2\text{e}^- \rightarrow 2\text{OH}^- + \text{H}_2)$, while the openings (h^+) collect the outside of the photoanode and respond with hydroxyl radicals to form oxygen,

$(2\text{OH}^- + 2\text{h}^+ \rightarrow 2\text{H}_2\text{O} + \frac{1}{2} \text{O}_2)$. A significant yet unsolved task lies in recognizing an appropriate semiconductor system that fulfils all the fundamental standards and in creating/advancing strategies for its large-scale fusion.

1.3: Hydrogen: A feasible Energy Carrier.

Hydrogen, created through the splitting of water is an energy-rich substance that on ignition (for example on oxidation) restores water. Therefore, its formation and utilization form a nearby circle for material flow and it is being viewed as the best energy bearer for the future. With zero outflows of contaminating gases on consumption, hydrogen is superior to all the traditionally utilized fossil fuels. Thus, it anticipates that hydrogen will be a significant part of the spotless energy transporter in future. 'Hydrogen Economy' alludes to a future energy situation where energy would be put away as hydrogen for transportation and electrical grid load balancing. The

hydrogen economy is supposed to take care of the issues of energy supply and combat the evil impacts of utilizing fossil fuels [Veziroglu T Nand Sahin S 2008].

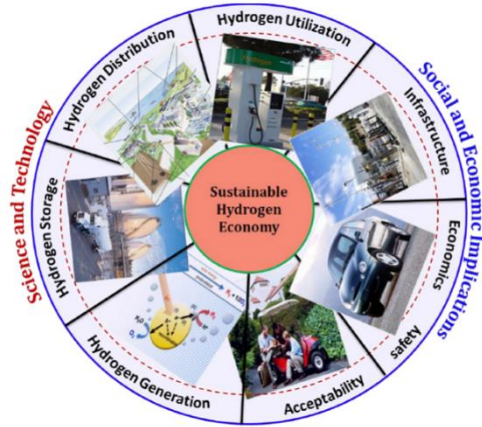


Fig. 1.2: Graphical representation of sustainable hydrogen economy

The effective creation of solar energy-driven inexhaustible hydrogen holds the possibility to supply to the world carbon-free fuel and have a tremendous effect on the feasibility of hydrogen as an energy bearer. Also, it will be a fundamental step while on the way to completely fuel cell technology. It is crucial to refer that the utilization of hydrogen as an energy bearer is eco-friendly (Fig 1.3), as ignition results in the water.

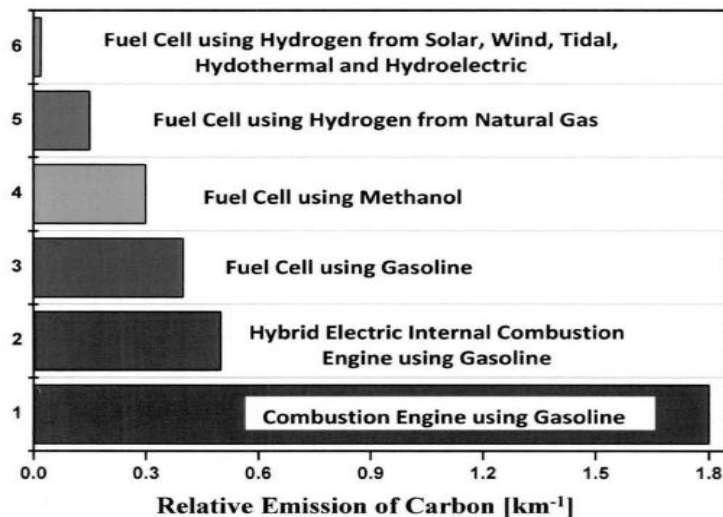


Fig.1.3: Relative discharge of ozone harming substances (communicated in carbon units per km) for vehicles fueled by the present inward ignition motor utilizing gas contrasted with vehicles controlled by energy units [BakaT et al. 2002]

Subsequently, it neither contributes to air contamination nor prompts the outflow of greenhouse gases [Gomez M et al. 1999; Zhao G et al. 1999; Kozuka H et al. 2000; Chandra S 1985]. As raw material for hydrogen creation will be water; it gives off an impression of being realistic since more than 72% of the globe is covered with water. It means, the hydrogen economy starts and finishes with water. It can stay away from every unsafe gas, corrosive downpours, ozone-depleting chemicals and oil spillages because of conventional fuels. In an offer to keep the environment clean and cut off reliance on imported oil for the transport sector, the Government of India is intending to go in for hydrogen gas-based automobiles. Amazingly with the large-scale showing of such vehicles scheduled for the 11th arrangement and commercialization in the coming five-year plan. A national hydrogen energy guide has been drawn and innovation missions recognized. The Government has set up a public hydrogen energy board under the supervision of Mr Ratan Tata having industrialists and researchers as active members. A demonstration Project for setting up hydrogen Dispensing Station at a petroleum station in New Delhi has been authorized as a joint venture of the ministry of New and Renewable Energy and Indian Oil Corporation Limited. Also Maruti's comments in support of hydrogen also come weeks after Mukesh Ambani, chairman of refiner Reliance Industries, said it would invest \$10 billion in clean energy, including setting up a Giga factory to produce fuel cells and green hydrogen. To reduce fuel consumption and emissions, Maruti is pushing sales of cars that operate on compressed natural gas (CNG), and is also investing in hybrid technology, he said, adding that "the use of hydrogen is also an interesting alternative". Suzuki Motor Corp, which controls Maruti, is also prioritising the development of clean technologies suitable for the Indian market, Bhargava said, adding that Suzuki's alliance with Toyota Motor Corp in Japan would prove valuable for this effort [The Economic Times 2021].

1.4: Basic Hydrogen facts [fchea.org]

Hydrogen is the first element of the periodic table, comprising one proton and one electron making it the lightest and least among all the elements. It was discovered in 1766 by the English scientist and physicist H. Cavendish. Hydrogen reacts with various materials and is perhaps the most abundant element known to us, 90% of the

atoms in the known universe are hydrogen. It is a drab, scentless, nontoxic gas, which is lighter than air and can be produced from different sources. The main source is "water-splitting" [Fujishima, A., & Honda, K. 1972; Bolton, J. R. 1996; Khan, S. U., & Akikusa, J. 1999; Khan, S. U., Akikusa, J. 1998; Khaselev, O., & Turner, J. A. 1998; Licht, S. et al. 2000; Heidt, L. J. 1951; Khan, S. U., & Akikusa, J. 1999; Licht, S., & Peramunage, D. 1990; Bard, A. J., & Fox, M. A. 1995; Maeda, K. et al. 2006], what isolates water into hydrogen and oxygen by electrolysis/photolysis. These can be joined again in a fuel cell, making power and heat with water as the sole discharge.

1.4.1: Merits as energy carrier [energy.gov 2021; fuelcell.pdf 2004]

Hydrogen can be appropriately named a future fuel as it scores over traditional fuel in every aspect whether be its non-dangerous results or its energy carrying effectiveness or security regarding its use.

- (1) Hydrogen can create power without discharging any poisons; their sole bi-products are water and heat. It creates no ozone-depleting gases and can be produced with clean, inexhaustible sources of power to completely affect public security, the environment, and general public health.
- (2) It can both convey and store energy and can be used in a wide assortment of uses, including compact contraptions that burn through batteries, vehicles, and different fixed force sources. The lion's share of hydrogen is presently produced by handling fossil fuels (which emits toxins through the underlying cycle), however, it can likewise be made from sustainable energy sources and feedstocks through the electrolysis of water.

Hydrogen is much safer [Hydrogen fuel cell safety report 2021] as being the lightest component in the universe and significantly more secure than gas or some other hydrocarbon fuel in the event of a break or disaster including a vehicle's fuel stockpiling and movement framework. Spilling hydrogen rapidly disperses up and moves well hidden from its source. Whenever touched off, hydrogen consumes rapidly with a non-glowing fire that can't quickly sear a person a good ways off. It transmits only one-tenth of the brilliant warmth of a hydrocarbon fire and devours a 7% cooler than gas. By and large, casualties don't burst into flames by hydrogen except in case they are not actually in the fire, nor are they gagged by the smoke. The primary advantage of utilizing

Hydrogen as the vehicular fuel is that it contains no Carbon atoms, and in this way combusting it as a fuel brings about no Carbon discharges. The essential emanation of hydrogen combustion is water vapour. During burning, oxides of Nitrogen can be framed from the Nitrogen in the environment, yet the Hydrogen Car Company (HCC) [h2caro.com] has limited the formation of Nitrous Oxide (NOX) by bringing down the temperature of ignition. HCC's vehicles use oil as a lubricant, just a single quart for every 30,000 miles. HCC's vehicles are the sole pick-ups and sports utility vehicles that meet ultra low-emissions vehicle (ULEV) discharges guidelines. a BMW is persuaded that hydrogen can make a significant commitment to supportable versatility close by BEVs later on – given the essential hydrogen framework is set up and offers a decent cost for hydrogen, and the cost of the vehicles falls. In those conditions, hydrogen power device vehicles can be the zero-discharge innovation that permits clients to keep up with the adaptable driving propensities they are acclimated with. The Hydrogen Council, a worldwide drive of driving energy, transport and industry organizations, is likewise persuaded of this. The chamber sees hydrogen not just as a practical future method for the impetus for power device vehicles yet in addition as a perfect energy hotspot for warming, power and industry [bmw.com].

While taking off fuel costs, the Union Transport Minister Nitin Gadkari on Wednesday crashed into Parliament in a first-of-its-sort green hydrogen-powered vehicle, the Toyota Mirai. Mirai is one of only a handful of exceptional Fuel Cell Electric Vehicles (FCEVs) on the planet and just sudden spikes in demand for hydrogen-produced power. On March 16, Gadkari sent off this green hydrogen-based progressed FCEV in the first venture in quite a while means to bring hydrogen-powered vehicles to the country. The vehicle was sent off as a component of the Toyota Kirloskar Motor (TKM) pilot project with the International Center for Automotive Technology (ICAT). The minister headed out from his home to the Parliament in the FCEV and underscored the need to change to renewables and environmentally friendly power energy. Toyota Kirloskar Motor (TKM), alongside the International Center for Automotive Technology (ICAT), is directing a pilot task to study and assess Toyota Mirai on Indian streets and climatic circumstances. The organization guaranteed that Toyota Mirai is controlled by a hydrogen power module battery pack and fit for giving a reach up to 650 km in a solitary

charge, with a refuelling time of five minutes. This could cut down the expense of travel to simply Rs 2 for every km. In Japanese, the word 'Mirai' signifies 'future'. Gadkari's office tweeted that India would before long turn into green hydrogen exporting country, adding that the government would focus on "green and clean energy" under the National Hydrogen Mission. Gadkari told columnists outside Parliament that "Gas and petroleum costs are taking off on the planet market. This has caused a ton of misery among individuals. Be that as it may, Narendra Modi's fantasy is an Aatmanirbhar Bharat. We import Rs 8 lakh crore worth of petroleum, and unrefined, diesel. Consequently, we should create ethanol, methanol, bio diesel, bio CNG, bio LNG, power, and green hydrogen."The minister said the authorities were hoping to clean up grimy water and reuse natural waste to deliver efficient power energy.



Fig. 1.4: Union Transport Minister Nitin Gadkari on 16th March 2022 crashed into Parliament in a first-of-its-sort green hydrogen-powered vehicle, the Toyota Mirai. [<https://www.businesstoday.in/auto/story/nitin-gadkari-drives-indias-first-hydrogen-powered-car-to-parliament-327937-2022-03-30>]

- (3) It can displace oil and other fossil fuels on a global basis for all time, and its utilization can increase national security by finishing dependence on imported oil. In energy terms, 1 kilogram of hydrogen is equivalent to around 1 gallon of gas in energy value (Table 1).

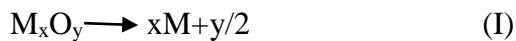
	Hydrogen	Gasoline	Diesel	Natural gas	Methanol
Density (kg/L)	0,0000898	0,702	0,855	0,00071	0.799
Density (kg/m³)	0,0898	702	855	0,71	799
Energy density (MJ/kg)	120	42,7	41,9	50,4	19,9
Energy density (MJ/L)	0,01006	31,2	36,5	00,0361	15,9
Energy density (MJ/m³)	10,783	31200	36500	36,1	18000
Energy density (kWh/kg)	33,3	11,86	11,64	14	5,53
Energy density (kWh/m³)	2,79	8666,67	10138,88	10,02	4420

Table 1: Hydrogen density compared to other fuels [minihydrogen.com]

1.5: Outline of solar-hydrogen generation: In-hand technologies

Strategies/innovations for hydrogen formation utilizing solar energy can be classified comprehensively into four classes, viz., photovoltaic, solar thermal energy, photoelectrolysis, and bio photolysis. Since the start of the 1970s, the photo-voltaic panels are being used to generate electricity, which is then used to produce hydrogen by electrolysis of water [Yilanci A, Dincer I and Qzturk H K 2008; Bilgen E 2001]. This strategy for sustainable hydrogen generation requires a higher and broad examination as the hydrogen formed by this technology is over the top expensive, mainly because of the extravagant cost of photovoltaic panels. Another disadvantage of this technique is that solar energy is changed over to hydrogen in two stages, consequently diminishing the proficiency of energy conversion. For example, if the proficiency of photovoltaic converters and electrolyzers is 20% and 80%, respectively, the general productivity of solar radiant energy changed over to hydrogen energy would not be over 16% [Yilanci A, Dincer I and Qzturk H K 2008]. Solar photo-biological hydrogen production utilizes a cycle similar to plant and algal photosynthesis. The biological hydrogen creation may happen through two cycles. The principal cycle, which is light-reliant, incorporates direct or indirect biophotolysis and photo-fermentation; while the other cycle, which is light-free, incorporates dark fermentation [Kotay S M and Das D 2008]. plant and algal photosynthesis bring the parting of water into oxygen and a decreasing specialist. The reducing agent at that point lessens CO₂ to carbohydrates or protons to hydrogen. The benefit of natural cycles is that these happen in a watery environment at surrounding temperature and pressure. Nonetheless, most natural techniques for hydrogen generation

need supportability and have been shown only in a research facility or limited scope outside the demonstration system. Such frameworks have not yet been formed for business use and the innovation is as yet under the formative stage [Benemann J R 1997]. The single-step thermal splitting of water is known as water thermolysis. The response requires a high-temperature heat source at or more than 2500 K and this is a significant limitation of the method. Additionally, the need of a proficient strategy for isolating H₂ and O₂ would also be required. The high temperature needed for the cycle shows extreme material issues and can prompt critical radiation loss from the reactor [Steinfeld A 2005]. Water splitting thermochemical cycle has an upper edge on thermolysis as in this cycle H₂/O₂ division issue is maintained at a strategic distance and the cycle happens at generally moderate temperatures (~ 1200 K) [Steinfeld A 2005]. An effective two-venture thermochemical cycle utilizing metal oxide can be addressed as [Steinfeld A et al. 1998],



M means a metal and M_xO_y the comparing metal oxide. The principle, of endothermic advance, is the sunlight-based warm parting of the metal oxide to the metal or the lower valence metal oxide. The second, non-sun controlled, exothermic advance is the hydrolysis of the metal to shape H₂ and relating metal-oxide. Since H₂ and O₂ are created in various advances; the prerequisite for high-temperature gas division is cleared out [Steinfeld A 2005]. One more technique to convert sunlight into hydrogen is by utilizing a photoelectrochemical (PEC) cell to power the electrolysis of water [Fujishima A and Honda K 1972]. when presented to daylight, a semiconductor photoelectrode (anode or cathode) lowered in a watery electrolyte, creates a satisfactory voltage to isolate water atoms. The other terminal utilized in such a framework is the metal cathode [Nowotny J et al. 2005]. Photons with energies more than the semiconductor bandgap can be devoured by the semiconductor, making electron-opening sets what partition in the space charge district created between the semiconductor and electrolyte. The electric field in the space charge district displayed in the band bending of the conduction and valence band edges is important to supply free charge transporters to drive the water-parting response. Photoelectrolysis in a PEC cells integrate solar energy absorption and water electrolysis into a single system. The

device does not require a separate power generator and an electrolyser. The maximum theoretical efficiency for PEC splitting of water using solar energy has been estimated to be about 35% [Dincer I 2002]. However, the maximum efficiency demonstrated experimentally to date has not gone beyond 18%. One of the drawbacks of PEC cells is that even though the fact that they are simple and do not require complex manufacturing steps, yet, they demand high land space and semiconductor necessities. Moreover, most semiconductor photoelectrodes suffer corrosion in contact with electrolyte solution and have low life. Also, some operational/technical details of PEC cell functions are yet unknown. Therefore, broad research is expected to saddle the full potential of PEC cells for solar-light driven photo-splitting of water to produce hydrogen.

1.6: Solar-water splitting: Role of nanomaterials

To meet future necessities for inexpensive, eco-friendly and inexhaustible hydrogen, better approaches to its production are needed. An answer, that holds high potential, is isolating hydrogen by the direct parting of water with the assistance of sun-powered energy. The shot at the photoelectrochemical (PEC) parting of water was first shown in 1972 by Fujishima and Honda. They prevailed with regards to parting water by the brilliance of titanium dioxide semiconductor cathode. However, titanium dioxide frameworks yield low efficiencies in changing sunlight-based energy over to hydrogen, as TiO_2 retains just in the UV district. Upheld by the underlying report by Honda and Fujishima, in the previous 3 - forty years that followed, a monstrous number of semiconductor materials were investigated by various specialists for the creation of hydrogen by parting water in PEC cells. Water parting is a wide term used to allude to any substance interaction wherein water is changed over into oxygen and hydrogen. Photoelectrochemical parting of water is an interaction where sun-based energy is utilized to isolate water into oxygen and hydrogen, a significant fuel. Now and again, this cycle is additionally called counterfeit photosynthesis. Sunlight-based water parting is perhaps the most reassuring approach to recognising hydrogen economy for the accompanying three reasons: (I) this advancement depends on photon (or sun-oriented) energy, which is a perfect, tenacious wellspring of energy, and basic water,

which is an economical asset; (ii) it is an environmentally protected innovation without unwanted side-effects and poisons; and (iii) the photochemical change of sun-powered energy into a storable type of energy, for example, hydrogen, permits one to deal with the sporadic person and occasional variety of the sun-powered inundation. The development of sun-oriented hydrogen creation innovation, in light of photoelectrochemical gadgets, needs new photosensitive semiconductor materials filling in as photograph cathodes. Photograph anodes are probably going to be made of reasonable polycrystalline single or composite materials rather than expensive single precious stones. Comprehend that the photosensitivity of polycrystalline material is firmly affected, still up in the air, by the advancement in the science and designing of material -interfaces. Additionally, there is a need to expand the comprehension of the neighbourhood properties of interfaces, for example, deformity issues, electronic construction, and related semiconducting properties, on the effect of interfaces on photoelectrochemical properties. In the continuous journey for a proficient PEC cell for sun-powered hydrogen age, the plan of photoelectrode with fitting qualities has been central, and in this specific situation, a few new measurements have been remembered for past years. A huge piece of the past work relied upon planar metal oxide semiconductor films, where the usefulness of PEC gadgets has been confined by a couple of key components, for example, the restricted light maintenance proficiency in the ideal apparent locale and recombination of photoexcited electrons and openings. During the earlier decade, nanomaterials have arisen as better than ever light energy gatherers. Joined with this, their extraordinary semiconductor properties have opened up new freedoms for their application in the PEC parting of water. Nanomaterials have pulled in enormous thought recently [Li Y and Zhang J Z 2010].

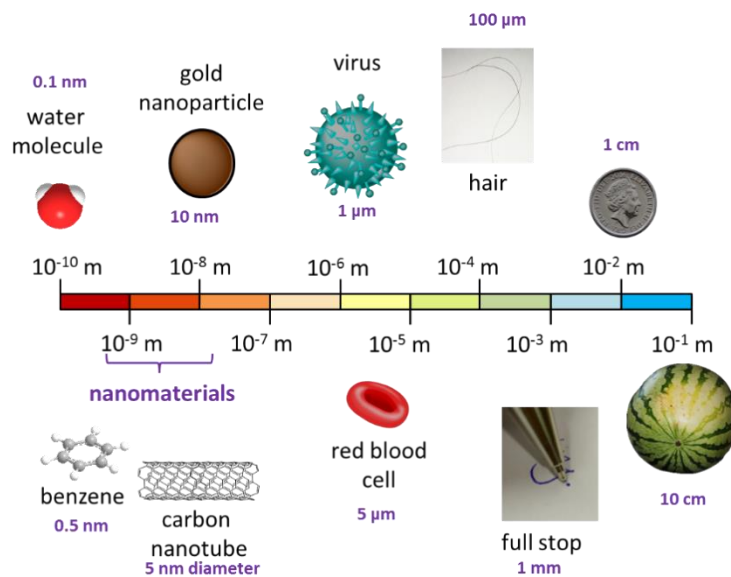


Fig. 1.5: Nano-scale materials

[<https://chembam.com/definitions/nanotechnology/>]

The essential explanation is their one-of-a-kind physical and synthetic properties contrasted with mass materials just as their likely applications in various innovations including energy change. Photoelectrodes dependent on nanostructured semiconductor materials have been investigated for PEC parting of water and the results are very amazing. Size quantization impacts in semiconductor nanoparticles and quantized charging impacts in metal nanoparticles give the premise to growing new and fruitful systems. The essential explanation is their exceptional physical and synthetic properties contrasted with mass materials just as their expected applications in various advances including energy transformation. Photoelectrodes dependent on nanostructured semiconductor materials have been investigated for PEC parting of water and the results are very great. Size quantization impacts in semiconductor nanoparticles and quantized charging impacts in metal nanoparticles give the premise to growing new and fruitful frameworks. The structures provide innovative methodologies for designing next-generation energy-conversion devices [KroIRR V D, Liang Y and schoolman J 2008]. Nanotechnology is earth-shattering development for sharing and reproducing nature at the sub-atomic and nuclear levels. It is being seen as the premise of the following mechanical upheaval and will help in changing and developing a wide scope of new materials, gadgets, innovative frameworks and surprisingly living life forms.

Nanomaterials, portrayed by something like one measurement in the nanometer range, can be considered to involve a scaffold between single particles and boundless mass frameworks. Nanostructured materials, as opposed to their mass partners, show colossal adjustment in their properties viz. bandgap, porosity and surface region, which are significant for PEC applications. Utilizing nanomaterials to accomplish effective PEC parting of water had been created a couple of years back [Chaudhary Y S et al. 2004]. Nanotechnology opens a huge possibility to tailor-make materials having remarkable properties. Future PEC innovations dependent on nanotechnology are relied upon to play an important role in the field of energy and harnessing alternative sources like solar energy. The materials might be customized by band edge designing to make new plans of semiconductor mixture blends like couple cells, triple crossing points, p-n mixes and forte plans. Among different central necessities for a proficient photoanode to accomplish better photograph transformation viability, both high surface zone and unrivalled charge transport abilities are incredibly critical. As of late exploration has been gone to complex nanostructures which offer a high surface area, unrivalled electrical conductivity and splendid mechanical strength and are made by a gathering of anisotropic nanostructures, for example, nanorods or nanowires or nanotubes associated through single-translucent intersections [Qifeng Z et al. 2009]. Such new materials offer the accompanying advantages: (i) the single-glasslike nature of every constituent shaft and the convergences convey the whole construction to perform superiorly in gathering and moving charges; (ii) the perplexing thought of the design offers surface regions like that found in structures shaped by nanoparticles; (iii) the mechanical strength presented by the translucent intersections helps in isolating the singular light emissions complex design, keeping the construction from falling that will prompt surface region decrease. Regardless, it is perceptible that paying little heed to the above benefits, the plan rule of complex nanostructures stays an overwhelming test when sunlight-based energy transformation is pointed. hetero nanostructures containing more than one part might hold to answer this test because each part may be improved freely to accomplish wanted generally properties in a deliberate way [Li Y and Zhang J Z 2010]. The blend of nanostructured materials keeps on being an exceptionally powerful exploration field in modem times. The ability to manufacture and measure nanostructured materials lies at the centre of nanotechnology, clearing a path for

understanding novel properties and understanding their possible applications. As of not long ago, different advances have been investigated to incorporate nanostructured materials [Schmidt-Mende L and MacManus-Driscoll J L 2007]. These specific methodologies can be collected in two forms: 'hierarchical and 'base up. In particular, a more flexible 'base up' technique dependent on science has pulled in noteworthy thought on account of its generally minimal expense and high throughput. 'Granular perspectives' allude to the advancement of material from the base; iota - by - particle, atom - by - particle, or group - by - bunch. Development species, like particles, particles, and atoms, after impinging on the development surface, collect into gem structures at the same time. Recently, different methods, including coprecipitation, sol-gel measure, microemulsion, freeze-drying, aqueous cycle, laser pyrolysis, shower pyrolysis, ultrasound, microwave illumination and substance fume affidavit have arisen in this particular part. In every engineered strategy, size impacts set up a charming piece of nanomaterials. The effects affected by size identify with the advancement of exceptional underlying, thermodynamic, electronic, spectroscopic, electromagnetic and compound provisions. Size impacts can be grouped into two sorts, one managing explicit incidental effects and the other including size scaling appropriately to commonly greater nanostructures. The previous remembers the presence of new provisions for the electronic construction. Layered heterostructures have likewise been manoeuvred into the thought of scientists utilizing nanomaterials. [Liu D. and Kamat P V 1993; Hotchandani Sand Kamat P V 1992; Innocenti M et al. 2004]. A blend of little and huge bandgap material saved one over the other may acclimatize the full sun-based range all the more adequately and, if energy band edges co-ordinate at the intersection, proficient partition of electron-opening is conceivable. Additionally, they offer widely high photocatalytic action by photogenerated electrons and openings which can expeditiously move toward the interlayer spaces of the response locales. Besides, multi-material cross-breed nanomaterials, which comprise a mix of two distinct material sorts, can prompt novel functionalities that are autonomous of the singular parts and might be customized to fit unequivocal application necessities [Sharma P et al. 2010]. The mix of chemically dynamic metals with nanostructured semiconductors might show an assurance as great materials for sustainable power transformation, unequivocally photograph electrochemical water parting. The possibilities that are accessible as such

now include: (I) recognizing and planning new semiconductor materials with noteworthy transformation effectiveness and solidness; (ii) setting up multi-facet frameworks or utilizing sharpening colours to solid ingestion of sun-powered radiation; (iii) figuring multi-intersection frameworks or coupled frameworks to streamline and use the potential areas of sun oriented radiation, and creating synergist frameworks which can proficiently separate water. Here is a rundown of the essential benefits of nanostructured materials concerning their utilization in PEC parting of water might be referred to as:(i) Nanostructured photoelectrodes including zero-dimensional nanocrystals and one-dimensional nanorods and nanotubes offer a possible benefit over their mass accomplices as they give a very huge surface region for the redox responses to happen, which would altogether be able to extend the capability [Hagfeldt A and Gratzel M 1995]; (ii) Quantumsizeconfinement in nanomaterials brings about increased band gap energy just as increased absorption coefficient [Khan SUM and Bockris J 1984]; (iii) The little sizes of nanomaterials diminish the distance for photogenerated openings to diffuse to the photoanode/electrolyte interface for the oxidation of water [aHagfeldt Aaand GratzelaM 1995], as such, the deficiency of transporters by means of electron-opening recombination might get diminished; (iv) The essential optical and electronic properties can be tailor altered through a controlled assortment of nanomaterial structure. For the model, the bandgap of semiconductor nanocrystals can be tuned by changing their size to assemble the light maintenance in the sunlight-based range [Oriol-Instruments 1999; Wenham S R et al. 1994]. In addition, the partition of electrons and openings would be essentially upgraded in nanorods if their distances are similar to the width of the consumption layer; (v) When utilized, the 'base up' manufactured technique permits the improvement of single-precious stone nanomaterials on different substrates without the courses of action of detachments because of the cross-section jumble between development substrate and semiconductor. These astounding nanostructured photoelectrodes with a low thickness of deformities decrease the catching or recombination of electrons and openings [Nowotny J 1994]; also, (vi) conversely, with the traditional planar PEC anode, the covering of nanomaterials on leading substrates normally frames an antireflection layer, thus, lessening the energy misfortune because of light reflection. With all the above potential benefits, nanostructured semiconductor photoelectrodes could generally

change the plan of PEC cells and work on the sunlight based on hydrogen transformation effectiveness. All things considered, the current research in nanotechnology faces numerous difficulties to the extent of the application in PEC splitting of water. These difficulties include the integration of nanostructures and nanomaterials into or with a macroscopic system that can yield high proficiency. The most critical undertaking to be taken in the field of PEC cells is to develop highly efficient, consumption safe and corrosion-resistant photoelectrode material.

1.7: Photo-electrochemical splitting of water

1.7.1: Hypothesis

The indispensable components of a PEC cell are the semiconductor terminal and the electrolyte (Fig 1.6).

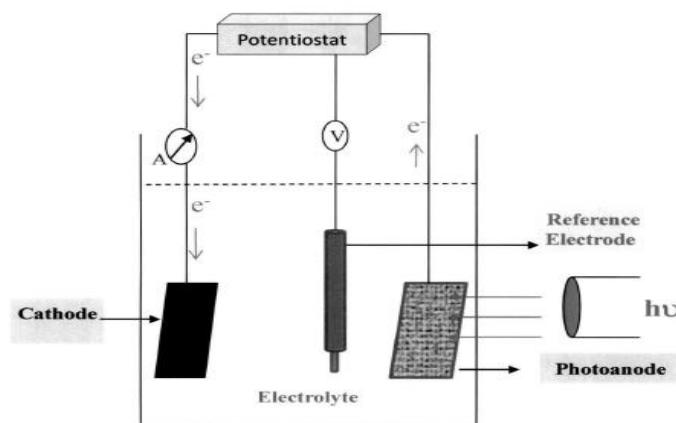


Fig. 1.6: Schematic view of a typical photoelectrochemical cell

The semiconductor-electrolyte intersection is the essential useful unit and to fathom the system of the cycles going on in a PEC cell, an unmistakable thought of the Chemistry and Physics of semiconductors in touch with the electrolyte arrangement and the idea of redox measures happening in that, particularly under enlightenment, is normal. Under this section, an endeavour has been made to exhibit this viewpoint.

Electron dissemination and holding in a strong material are communicated discretely. Holding in metals is generally seen as an unbendable network of metal cations in a pool of free electrons. In any case, this model is crude and has confined materialness. The sub-atomic orbital hypothesis gives a superior perception of the marvel that drives electrons to tie cores together to shape particles. The hypothesis expects that electrons have wave properties and are addressed by wave capacities, which have come about because of their connection with cores in the particles. Indeed, even by utilizing the Schrodinger condition, it is very hard to track down a precise answer for the wave capacities. Subsequently, a guess of sub-atomic orbitals is created by the straight mix of nuclear orbitals (LCAO). While framing a strong material, nuclear orbitals join to create a comparable number of atomic orbitals, with energy dividing between the diverse energy levels. The energy dispersing decreases with an expanding number of consolidating molecules for example expansion in the number of atomic orbitals. At the point when the amount of orbitals is sufficiently adequate, the ensuing atomic orbitals are so mutually dispersed that a continuum is shaped with uncountable little spacings between the discrete energy levels. Happening as a continuum, this blend of energy levels is known as an energy band. At low temperatures, following Pauli's avoidance rule, electrons will get comfortable in all open states in a gem up to a specific energy level. The most involved band at zero degrees Kelvin is known as the valence band (VB) and the neighbouring band with more energy, is known as the conduction band (CB). The contrast between the most elevated energy in the filled valence band and the least energy in the empty conduction band is known as the bandgap energy (E_g). It demonstrates a scope of energies where no orbital exists for electrons.

A huge view in the clarification of semiconductors is that of the Fermi level, (E_F) which is portrayed as the energy level where the assumptions for the level being involved by an electron are 0.5 (i.e., where almost certainly, the level is either involved or empty) [Bardakci J and Faulkner L Ra2001]. In a metal, the conduction band is vivaciously either contiguous or covering the valence band. Subsequently, electrons can be handily empowered from the valence band into the conduction band by warm excitations. Attributable to the smallest energy distinction between the valence and conduction groups, conduction happens successfully in a metal. On account of semiconductors, in

the ground express, all electrons are in the valence band and there are no electrons in the conduction band, so the odds of discovering an electron quickly change from 100% at the highest point of the valence band to 0% at the lower part of the conduction band.

At higher temperatures, hardly any electrons secure energy over the Ferrier level and arrive at the conduction band. The likelihood of control of an allowed energy state, proportionate to energy E, can be numerically determined from the Fermi-Dirac dispersion work $f(E)$, communicated as condition (1.1),

$$f(E)=1/[1+\exp((E-E_F)/kT)], \quad (1.1)$$

In this equation, k is Boltzmann's constant and T is the temperature. The expected variation of function $f(E)$ with E, as per equations (1.1), is shown in Fig. 1.6. In semiconductors covers the most noteworthy involved energy level of the valence band and the least empty energy level of the conduction band are known as the valence band edge (E_v) and the conduction band edge (E_c), individually (Fig.a1.7). Additionally, electrons in the valence band can't convey current. In any case, at temperatures over zero Kelvin, electrons can be invigorated by the warm movement of the iotas, achieving a few electrons populating orbital in the conduction band. The electrons in the conduction band are versatile and convey current. In light of the excitation of electrons, there will be unfilled spaces in the valence band (named as an opening), which moreover add to the progression of current.

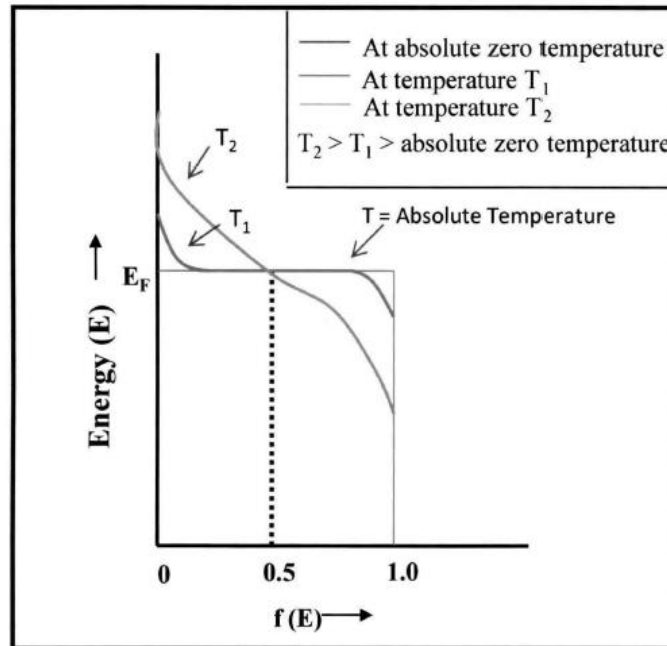


Fig.1.7:The variation of Fermi-Dirac distribution function, $f(E)$, with energy (E)

From now on, the current stream in a semiconductor is a result of the measure of the movement of electrons in the conduction band and openings in the valence band. Electronic conductivity in the semiconductors anticipates that electrons should be eager to the conduction band. This may be refined thermally (as depicted above) or ideally. On the off chance that the energy hole among conduction and valence band edges (for example E_g) is huge, at the same time, not many electrons will be advanced thermally at standard temperatures and the conductivity will remain nearby zero, giving a separator. Henceforth, Solid-state materials would now be able to be ordered as, directors, semiconductors and encasings dependent on their band structure (Fig. 1.7). Directors have an electronic construction with the objective that E_F exists in a permitted band. This is either a direct result of inadequate electrons being accessible to fill an open band or the presence of covering groups. Encasings have one band involved by electrons and there exists a tremendous hole between this band and the higher band where the E_F is arranged. Encasings have bandgap energy of 4 eV or more. At low temperatures, the semiconductor doesn't lead, however at higher temperatures, the Fermi-Dirac dispersion allows a couple of levels in the valence band to be empty and some in the conduction band to be involved. Consequently, a semiconductor where the

transporter focus and the electrical conductivity are provoked by the temperature is called an inherent semiconductor [Tien, H. T., & Chen, J. W. 1992].

All genuine precious stone cross-sections go astray from ideal nuclear designs and have imperfections that influence different actual properties of the material, including the electrical conductivity. The idea of a natural semiconductor is hard to control because a slight temperature variety can change the entire conductivity. Natural semiconductors (like exceptionally high-immaculateness Si) have some negligible pollutants, while extraneous semiconductors have debasements that give electrons to the conduction band or acknowledge electrons from the valence band. For the most part, inherent semiconductors are sedated with new pollutions to create an outward semiconductor. Giver or acceptor energy levels are contrived just underneath the conduction band edge or simply over the valence band edge, individually. Benefactor debasements achieve n-type conductivity, where conduction is constrained by electrons, the negative charge transporters. The conductivity of the extraneous semiconductor depends essentially on the quantity of debasement or dopant iotas and may even be autonomous of the temperature inside a particular temperature range. Then again, acceptor contaminations bring about p-type conductivity, where conduction is constrained by sure charge transporters (for example openings). When there is an n-type semiconductor, the prevailing charge transporters (electrons) are known as larger part transporters and the openings as minority transporters. Furthermore, on account of an inherent semiconductor, warm excitation of electrons from the valence band (VB) to the conduction band (CB) happens, forsaking an equivalent number of openings as electrons, $n = p = n_i$ (characteristic transporter thickness). The mass activity law is shown in Eq. 1.2 communicates that the consequence of the electron focus (n) and the opening fixation (p) is identical to the characteristic transporter focus (n_i) squared, where N_c and N_v are the number of charge transporters in the conduction band and valence band, separately.

$$n.p = N_c N_v \cdot \exp(-E_g/kT) = n_i^2 \quad (1.2)$$

Metal-oxide semiconductors are of much lower immaculateness than traditional semiconductors, like Si and Ge, and regularly have ionic deformities (like opening and

interstitials) that go about as contributors or acceptors. These Ionic imperfections like opening and interstitials are called point defects. Electronic imperfections, for example, additional electrons from dopants and polarons (electron and neighbourhood grid bending made by the charge transporter) are electrically unique and can bring charge transporters into mid-bandgap energy levels. Metal-oxide semiconductors can't be viewed as inherent semiconductors. Even though the inborn transporter thickness to a great extent relies upon temperature, there exists a high-temperature range where the amassing of inherent charge transporters outperforms that of the extraneous transporters, so the electrical properties of the semiconductor are free of the debasements inside the material and the semiconductor shows characteristic conduct. At lower temperatures, the conductivity is impacted by pollution conduction systems coming about because of the generally temperature-autonomous extraneous imperfections. For, example, as shown in Fig. 1.8, four of the electrons participate in the covalent holding measure, while the extra electron enters an energy level in a benefactor state under the conduction band. Since the extra electron isn't firmly bound to the molecules, simply a little extension in energy is required for the electron to enter the conduction band. This sort of doping is called n-type doping. Likewise, when contamination having lesser valence is added there will not be adequate electrons to finish the covalent holding measure. An electron (opening) is, subsequently, made in the valence band that can be loaded up with electrons from various areas in the band (Fig. 1.9). The opening goes about as acceptors of electrons. These opening destinations have a fairly more significant level than typical energy and make an acceptor level of conceivable electron energies over the valence band. An electron ought to secure energy to make an opening in the valence band. The opening then, at that point moves and conveys the charge. This is known as a p-type semiconductor [Askland D R 1996].

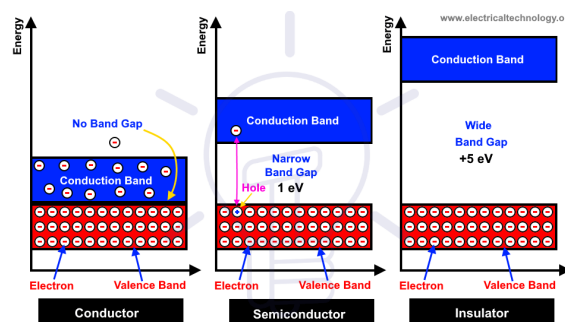


Fig. 1.8: Schematic presentation of bandgap (E_g) and band edges (E_c and E_v)
[\[https://www.kngac.ac.in/elearning-portal/ec/admin/contents/2_18K4CSAP3\]](https://www.kngac.ac.in/elearning-portal/ec/admin/contents/2_18K4CSAP3)

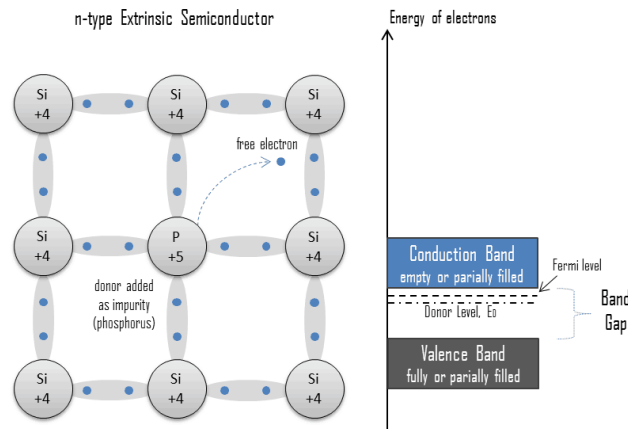


Fig. 1.9: Creation of donor energy state in an n-type doped semiconductor
[\[https://www.radiation-dosimetry.org/what-is-electron-donor-and-electron-acceptor-definition/\]](https://www.radiation-dosimetry.org/what-is-electron-donor-and-electron-acceptor-definition/)

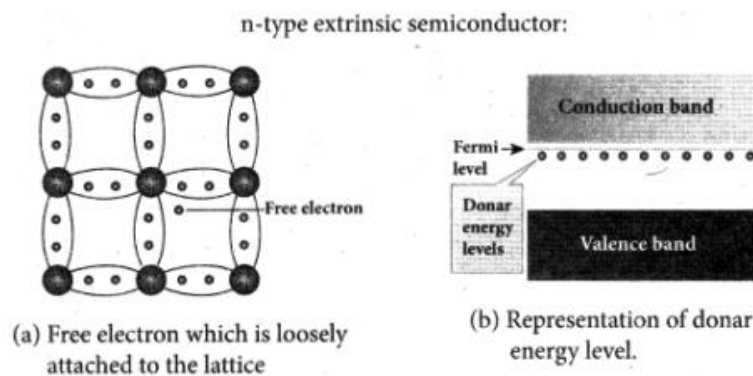
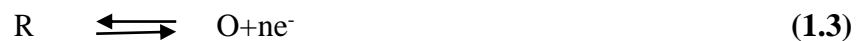


Fig. 1.10: Creation of acceptor energy state in a p-type doped semiconductor
[\[https://www.sarthaks.com/883212/elucidate-the-formation-of-a-n-type-and-p-type-semiconductors\]](https://www.sarthaks.com/883212/elucidate-the-formation-of-a-n-type-and-p-type-semiconductors)

1.8: Working of electrolyte

An electrochemical cell typically involves two terminals in contact with an ionic conductor or electrolyte (which might be an answer, a fluid or a strong). Unendingly all electrochemical cell cycles may be seen as a bunch of redox responses. A redox

response is a response wherein there is an exchange of electrons starting with one animal categories then onto the next. The oxidizing specialist is the electron acceptor and the diminishing specialist is the electron giver. Each redox response might be communicated as two half-responses, which express the misfortune and gain of electrons. The decreased and oxidized substances in a half-response structure of a redox couple indicated O/R, with the comparing oxidation half-response as:



In electrochemical cells, half-responses of oxidation and decrease happen at various terminals and these are called anode and cathode, separately. A cell wherein the general cell response isn't at synthetic harmony can do electrical work as the response drives electrons through an external circuit. The work that a given exchange of electrons can achieve depends upon the expected qualification between the two terminals. This potential qualification is known as the cell potential. The capability of more than one cathode has no precise worth and must be assessed concerning the other anode. The reference terminal picked is fundamentally the typical hydrogen anode (NHE) and its latent capacity, by definition, is set to zero under the conditions composed underneath for the relating half cell,



wherein, all species are at a standard state. The possibilities of all redox couples can be mathematically communicated, concerning this terminal. The potential with regards to the NHE is known as the standard cathode likely U^0 . The cathode potential for a half-cell response that isn't in the standard state can be estimated with the accompanying Nernst condition [Bard A J and Faulkner L R 2001].

$$U = U^0 - (RT/nF) \ln(a_R/a_O) \quad (1.5)$$

Here at and up are the actions of R and O, respectively and are stated as $a_R = \gamma_R [R]$ and $a_O = \gamma_O [O]$, where $a[O]$ and $[R]$ are the molar concentrations and γ_O and γ_R are the activity coefficients of O and R, respectively. The standard electrode potential is an element of the standard Gibbs free energy ΔG° , and the relationship is explained by equation (1.6),

$$\Delta G^0 = -nFU^0, \quad (1.6)$$

n is the number of electrons moved in the overall cell reaction and is Faraday's constant. If the components in the system are not in the standard states, at that point, the above relation can be explained as an equation (1.7).

$$\Delta G = -nFU \quad (1.7)$$

Exactly when a semiconductor terminal is in touch with an electrolyte, two particular logical regions are joined together; strong state physical science and electrochemistry. The strong state of physical science and the semiconductor speculations were fundamentally concentrated by physicists and they framed an energy scale dependent on the nuclear and sub-atomic orbital hypothesis utilizing the energy of the electron in a vacuum as a source of perspective level. Then again, electrochemistry and electrolyte hypotheses are a result of scientists opposing the physicists, they utilized the standard decrease possible scale to clarify the redox framework. On this scale, the typical hydrogen anode (NHE) is by definition set to nothing. Appropriately, an assessment between cell possibilities identified with the redox couple in the electrolyte, and the energies of the groups in the semiconductor is needed. This differentiation is conceivable because the Fermi level in the semiconductor and the redox capability of the electrolyte are similar species as the electrochemical capability of the electron. The potential terms can be changed over to comparing energy terms by increasing with the rudimentary charge (q). The absolute worth of E_F depends upon the choice made for the reference state. Oftentimes this is considered as zero for a free electron in a vacuum, for example for an electron that is very still at an endless separation from the strong. The Fermi levels in metals and semiconductors can be chosen by ascertaining work capacities or electron congruity. Since the electron is in a condition of lower energy in practically all materials that stood out from its energy in a vacuum, E esteems are generally negative[Bard A J and Faulkner L R 2001]. The Fermi level in the arrangement stage is determined by estimating U qualities against NHE. The association between the energy (communicated in electron-volt, and the potential (U) of any redox couple can be communicated by condition (1.8).

$$a-E = 4.7+aqU \quad (1.8)$$

In this way, the energy scale and the potential scale are oppositely coordinated. When the potential of electron increases, its energy decreases for an n-type semiconductor.

Chapter-2

Literature review

Contemporaneous state of erudition in the research

2.1: A prospectus of extant findings in the sphere of present work

This part takes a view of literature representing nearly all substantial and currently penned published on the preparation, characterization and application of semiconductor photoelectrodes for splitting of water using photoelectrochemical cells. In this introduction, a few potential semiconductors and systems/perspectives, received by various labourers, have been explained, so far allowing unique accentuation on the utilization of ZnO as photoanode and the part of electrolyte all the while. Aside from basic doping and the changes in representative composing circumstances, few novel methodologies have likewise been endeavoured lately by certain specialists, to adjust the properties of semiconductors for PEC parting of water. The literature review introduced features such as outlines also.

Jakani et al (1985) considered the properties of ZnO photoanodes doped with transition elements (Cr, Mn, Fe, Co, Ni) have been examined for photodecomposition of aqueous arrangements. A huge expansion of the photoresponse happens in the apparent locale, especially with Co^+ and Mn^+ doped samples. The doped particle harmonization, the energy criteria, and the tool of the conduct transfer are examined.

Bahadur and Rao (1992) contemplated the photoelectrochemical properties of polycrystalline ZnO thin film electrodes doped with cobalt with specific accentuation on the expansion of the photoresponse to the obvious area. The film arrangement is constructed to vary from the arrangement of the spray solution. Films with conductivity as peak 34 S cm^{-1} were gotten. The photocurrent potential curves, absorption and action spectra of Co-doped ZnO electrodes demonstrated the critical expansion to the obvious locale of its spectral reaction, affirming subsequently the presence of Co^{2+} in tetrahedral sites of the ZnO

lattice.

Yoshida et al (1999) declared that dye-adjusted semiconductor photoelectrodes assumed a conclusive part in dye-sensitized solar cells. They arranged dye-adjusted ZnO thin films by electrodeposition. Crystallographic, morphological and spectroscopic investigation of the product uncovered that arranged patterns were created both for ZnO and dye molecules in the placed films. They additionally talked about materials characterization, growth mechanism and photoelectrochemical resources of these exceptional matters.

Bozleea and Exarhos (2000) reported gold and ruthenium colloids brought into meagre movies of ZnO by turn covering metal particle doped courses of action of zinc acetylacetonate onto quartz or Pt substrates, followed by warming to 400°C. The two sorts of film uncover a blue colour because of M, for example, light reconciliation by metal nanoparticles. Examination of the recognizable mix spectra suggested particle radii of the solicitation of 2 nm. Regardless, electron micrographs revealed some greater atoms and particles sums as well. While the Au colloid coordination band was developed to a greatest at about 575 nm, Raman excitation diagrams of the colloidal movies exhibited red-moved most elevated almost 700 nm. They credited the striking Raman power improvement at an innervations frequency of 700 nm to Surface-upgraded Raman (SER), scattering of the El technique for ZnO. Ru colloids likewise persuaded SER to scatter from an excess RuO₂ covering that covered the Ru metal particle. In the present circumstance, the SER scattering was articulated when the laser innervations were changed into the most elevated of the Ru colloid joining band, assumed with the alleged electromagnetic hypothesis of SER coordination. While not the whole of the Ru in Ru-doped movies was gathered in the zero oxidation region, XPS assessments uncovered that the entirety of the gold in the gold-doped movies was in the zero oxidation places.

Ohta (2000) tracked down that simultaneous H₂ and O₂ progress can be accomplished simply by interesting the powder of a p-type semiconductor like Cu₂O, NiO, Co₃O₄, or

Fe_3O_4 in refined water at room degrees. The grinding back rubs of the exciting bar onto the foundation of the glass holder was the principal state. They analyzed that the back rub between the exciting bar and the glass region directed sufficient electrostatic circle to make a circle spread of the productive well from the semiconductor powder which was connected at the little hole spaces on the vessel region. The spread positive ghetto responded with water atoms to foster O_2 and protons which move to the vessel region and along with the electrons emanate H_2 . In this paper the energy changed over the system, the formation of back rub power, the results of water, the haulier exhume spread assumption; the bound conduction in semiconductor and the results of liquid elements were expressed.

Singh et al (2001) organized the astoundingly conductive and straightforward aluminium-doped zinc oxide slender movies by eliminating the errand controlling 2wt% Al_2O_3 with Ar Fexcimer laser ($\lambda=193$ nm). The movies were joined at a rehashed pace of 10 Hz, energy thickness of 2-3 J/cm^2 and shaft season of 10-60 min (6000-36000 laser shots). The noticeable and electrical things of the movies were uncovered to be the turn on the substrate temperature and oxygen pressure all through film release. They analyzed the sharpened decrease in conveyance and sharp ascent in reflectance intently the plasma line in the nearly infrared range because of pollution reconciliation which was created by aluminium doping.

Lee et al (2001) investigated Cu-doped ZnO (denoted by ZnO: Cu) films made barf magnetron co-sputtering of a ZnO target with few towards Cu chips. X-Ray deflection (XRD) spectra of settled ZnO: Cu films were noted and character coefficient (TC) numbers for (002)-induction were calculated. Optimal areas of RF powers and substrate degrees for making increase TC numbers were calculated. Results of Cu-doping assumptions on TC numbers, electrical resistances, and relative Cu- configuration of settled films were consistently examined. X-ray photoelectron spectroscopy (XPS) results observed that the similar substances of metallic copper (Cu) atoms and CuO (Cu^{+2})-cycles within settled films may part a crucial character in directing their electrical resistances. Extremely resistive ZnO films with maximum TC numbers (80%) were targeted by Cu-doping. Surface acoustic wave (SAW) patterns with

ZnO: Cu (or ZnO) inter electronic transducer (IDT) SiO₂ Si up-gradation was also forged to calculate the productive electro-mechanical dualing cooperative and introducing damage.

Mathew et al (2002), arranged CdTe by near dispersed transformation on stretchable metallic substrates. The p-CdTe has remained in solutions with a pH following 7 to 10. Undergoing one sun illumination the hydrogen progress possible of the p-CdTe /electrolyte structure moved remarkably. The hydrogen progress possible of a p-CdTe /electrolyte pattern (pH=4.04) moves by about 220 mV when revealed to sun illumination. The V_{fb} stated a linear dependence on the pH of the result. The hydrogen progress onset prospective was minimum in results having less pH. It was found that the unlocked circuit possibilities under dark and light have dissimilar dependence on the pH of the results. The changing of the p-CdTe region with Ru improved both the hydrogen progress productive and the balancing of the photocathode.

Noack and Eychmuller (2002) inspected the move arising during the strengthening of the release of ZnO slim movies and powders by estimations realities strategies (TEM and powder X-beam wonder) and by warm assessment. They saw that water and carbon dioxide vanished from the surface at the level of around 100 °C. At higher degrees (somewhere in the range of 300°C and 500°C), two stages were discovered: an alteration in the synthetic arrangement of the stage by the warm insult of adsorbed atoms and a limit of the mathematical particle measurement. An example forms for nanometer-sized. ZnO nanocrystals were started as expressed by to which the focal point of the particles involved generally of unadulterated ZnO covered by a concentrate limiting Li⁺ and ZnO. Acetic acid derivation particles are adsorbed on this contrived definitive sheet. To proclamation for the least energy move in the assimilation scope of the greater particles, a trade of the adsorbed acetic acid derivation particles with the electrons internal to the ZnO was suggested which partook in the saw size-quantization of the little semiconductors.

Samarasekara et al (2002) propagated the narrow films of ZnO on conductive glass substrates by DC sputtering. The sputtering framework was changed to get ZnO

films with the highest open-circuit photovoltage sustained in the electrolyte KI/I₂. They found that a photovoltage as maximum as 40.66 V/m² could be got for the film synthesized at the constraint of 6 mbar for the time of 23.75 hours and ZnO thin films could be utilized to soak the short wavelengths in the ultraviolet (UV) sector of the solar orbit.

Shi et al (2002) examined acrylic corrosive polymer meagre films kept on the surfaces of nanoparticles of ZnO utilizing a plasma polymerization treatment. The normal size of nanoparticles was of the request for 50 nm in sporadic shapes. High-goal transmission electron microscopy (HRTEM) tests showed that an amazingly dainty film of the acrylic corrosive layer (15 nm) was consistently kept on the surfaces of the nanoparticles. The HRTEM results were affirmed by season-of-flight auxiliary particle mass spectroscopy. The impact of plasma power on the polyacrylic dainty film was concentrated by Fourier change infrared examinations. The statement instruments and the impacts of plasma treatment boundaries were suggested.

Zhou et al (2003) announced the doping impacts of Cu on the electrical conductivity of ZnO in the typical parallel framework through air conditioner obstruction spectroscopy. The Cu doping declined the electrical conductivity of ZnO both in the grain and in the grain regions by various significant degrees. Hydrogen was initiated into the Cu-doped ZnO samples by the ion implantation methods. The electrical conductivity of the hydrogen-implanted layer peak by about 9 orders of magnitude at most. The device for such hydrogen consequences was also suggested.

Seelig et al (2003) observed a novel technique for the directed synthesis of mono scattered ZnO colloidal layers. Optical estimations counting consideration style optical microscopy and dissemination and single-domain reflection spectroscopy found that the time arrays disclosed a photonic band slot in the (1 1 1) supervision of the fee lattice and computations were awarded to calculate the productive number of the refractive indices of the colloidal layers. Lastly, photoluminescence (PL)

estimation told that the ZnO lasing thresholds were lesser in time patterns than in random arrangements of the same domain.

Jayatissa (2003) reported the narrow films of Ga-doped ZnO by oxidation of vacuum vaporized ZnS and GaO compositions. The electrical and systematical properties of ZnO films were inquired for several oxidation degrees and GaO matter in vaporized ZnS powder. They revealed that the electrical conductivity of Ga-doped ZnO was peak by one sequence of magnitude compared with undoped films. The carrier potency and absorption were also maximum for Ga-doped ZnO films.

Kresse et al (2003) arranged the thickness-useful computations for the (0001)- Zn surface of wurtzite ZnO. A few adjustment gadgets, for example, metallization of the external coated, adsorption of OH gatherings or O atoms, the rise of Zn circumstances, and tremendous scope of three-sided modification were contemplated. They tracked down that secluded Zn circumstances or O particles were unfriendly adjusted to three-sided reconstruct. In the delinquency of hydrogen, these three-sided attributes stayed under any even-minded degree and power.

Norris et al (2003) reported a ZnO transparent thin-film transistor (TTFT) with a means coated sheet consisting of spin-coating discharge. The TTFT was maximizing clear and revealed n-channel,improvement-mode efforts with channel potency as bigger as $0.20 \text{ cm}^2\text{V}^{-1} \text{ s}^{-1}$ and a sewer current on-to-off ratio of closely 10^7 .

Salem et al (2003) suggested a plain empirical correlation to gauge the peak frequency refractive index (n) for compound semiconductors out of the electro negativities of the atoms of the elements. The aforesaid relation construct on the bond energy slit interrelation was $n = F/(X-D)^{1/4}$, where X was the electronegativity contrast between the constituent atoms of the compound semiconductor and D was a distinctive numerical constant. The parameter F was established on the semiconductor class and its number was set up to be proportional to the ratio of the

valence electron plasmon and the Fermi-energies.

Qiu et al (2004) analyzed Ni-doped ZnO (ZnO: Ni) films made on Si(0 0 1) substrates by reactive electron pillar dissipation at little substrate temperature. The developed movies were then tempered in oxygen encompassing at raised temperatures. X-ray diffraction (XRD) result pointed that 5 at.% Ni-doped examples were still of the single-stage with the ZnO-like wurtzite structure. Photoluminescence (PL) evaluation of Ni-doped examples showed the UV-PL discharge focused at around 384 nm, which was ascribed to the close to band-edge (NBE) outflows of ZnO-like band forms. The UV-PL power turned out to be very much worked alongside the development of strengthening temperatures and arrived at the most prominent extent after annealing at 450°C. In any case, alongside the further broadening of toughening temperatures, UV-PL power blurred again. The UV-PL force of 450°C-strengthened examples was multiple times more grounded than that of doped examples, which might deliver conceivable use in optoelectronic gadgets, for example, UV brilliant gadgets.

Chien et al (2004) expected ferromagnetism in 3d change metal-particle doped ZnO inspected by abdominal muscle electronic example calculations rely on the summed up angle estimation (GGA). They likewise addressed GGA+U calculations to additional reasonable their examination. Mn-doped ZnO had the greatest attractive moment and Sc-doped ZnO was nonmagnetic. Additionally, Mn-Co-or Cu-doped ZnO were ferromagnetic semiconductors. The coming of ferromagnetism in these frameworks suggested the opportunities for the creation of an invisible ferromagnet which might have a big effect on modern applications in magneto-optical gadgets.

Tang et al (2004) found the progress of ZnO by epitaxial methods was crucial for the growth of new optoelectronic tools. In sequence to initiate control over the progress, it was dominant to estimate dopant profiles through the coating to alternative Hall effect facts. In this cover, C-V profiles from metal-organic chemical haze accumulation enlarge ZnO thin films were accorded.

Lee et al (2005) scrutinized the differences in physical attributes of ZnO with doping impurities: K, Cr, and Cu ions. K ions doped in ZnO have diverse stable positions bounded by the doping rate of 2 mol%. For the Cu- or Cr-doped ZnO, the feature $3d$ energy level could be given as carrier trap level because of the deep level in the ZnO and could alter the magnetism *via* a shift of the Fermi level. It was also stated that ferromagnetism depended on the carrier density in Cr-doped ZnO and Cu-doped ZnO.

Liang et al (2005) blended cubic translucent MgZnO on p-type Si (100) by a receptive e-pillar vanishing framework at low temperature. AES profundity profiles for the MgZnO films showed great consistency in Mg, Zn and O segments. MIS capacitors were created and C-V and I-V portrayals were performed to assess the tempering impact on the electrical properties of MgZnO films. High temperature strengthening up to 900 °C under 0.2 Torr surrounding essentially improved C-V and I-V characteristics. The interface got charges lessened from $5.30 \times 10^{12} \text{ cm}^{-2}$ to $2.48 \times 10^{11} \text{ cm}^{-2}$ as the hardening temperature extended from 550 °C to 900 °C, showing the quality improvement of the interfacial layer. Meanwhile the thickness of flexible charges extended from $1.93 \times 10^{10} \text{ cm}^{-2}$ to $1.72 \times 10^{11} \text{ cm}^{-2}$ as the reinforcing temperature extended from 550 °C to 900 °C, which was attributed to the dispersal of O near the surface and movement of Zn^{2+} towards the surface from MgZnO compound film under such high temperatures.

Maeda et al (2005) contemplated the hydrogen gas development from water prompted with γ -beam light of silica gels and metal oxides scattered in water by inspecting the hydrogen gas advancement. Hydrogen gas was identified by gas chromatography after ^{60}Co γ -beam light of the example arrangement in a shut vial at room temperature. They saw that water adsorbed on the outside of metal oxides showed more advancement of hydrogen gas than unadulterated water. Hydrogen gas development was amplified in the silica gels when the size of a silica gel pit was around 2 nm, being on the request for spike size. The most dynamic surface toward the deterioration of water upon γ -beam illumination was that of SiO_2 dried

at 100 °C after the example arrangement.

Gao and Nagai (2006) detailed the reproducible low-temperature arrangement-based interaction for the readiness of ZnO movies of nanorod clusters and their application to colour-sharpened sun-powered cells (DSSCs). A two-venture approach was utilized for the epitaxial development of ZnO. They began with the planning of a (002)- situated ZnO seed layer by the electrochemical affidavit strategy. After the treatment, the substrate was absorbed in a watery arrangement containing ZnCh and complex specialists. A large- scale creation of ZnO nanorod clusters on straightforward conductive oxides was accomplished after dousing at 95 °C for 1-48 h. The as-kept ZnO film had a huge surface zone, accordingly allowing a lot of colour stacking. The independently isolated nanorod framed a direct nanorod which showed more viable electron transportation than that in the movie got from ZnO powders. The DSSCs utilizing these ZnO films as photoelectrodes showed transformation productivity of about 0.6% at AM 1.5. h.

Moreno et al (2006) considered the thin films of ZnO and Co grown on ShN_4 buffered (100) Si substrates at 673 K by using the supporting electron microscopy approach which gave local details regarding structural, electronic and magnetic attributes. No proof of secondary stages at interfaces resulted. For this growth temperature, Co was incorporated into the ZnO lattice by replacing Zn, and its oxidation state was 2+. Off-axis electron holography disclosed no quantifiable magnetic signal, either at domains or at interfaces, in assent with macroscopic calculations that specified a non-ferromagnetic behaviour.

Roeb et al (2006) examined a promising technique for the change and capacity of sun-based energy into hydrogen created by the separation of water into oxygen and hydrogen, completed through a two-venture measure utilizing metal oxide redox frameworks like blended iron oxides, covered upon multi-diverted honeycomb earthenware upholds equipped for retaining sun oriented light, in an arrangement like that experienced in car fumes exhaust systems. They depicted that with this setup, the entire interaction could be done in a

solitary sun-based energy converter, the cycle temperature could be altogether brought contrasted down with other thermo-synthetic cycles and the recombination of oxygen and hydrogen was forestalled by fixing the oxygen in the metal oxide.

Sharma et al (2007) considered the mass examples of Mn-doped ZnO combined with the ostensible structures $Zn_{1-x}Mn_xO$ ($x= 0.02, 0.05, 0.10, 0.15$) by the strong state response and sol-gel strategies. In both the strategies the examples were at last sintered at $\sim 700^\circ\text{C}$ in air. The X-beam diffraction (XRD) investigations of the examples integrated by the strong state response technique showed the presence of wurtzite (hexagonal) precious stone construction like the parent compound (ZnO) in every one of the examples proposing that doped Mn particles sit at the ordinary Zn locales. In any case, the same examinations over the examples with Mn content 5% and blended by the sol-gel technique uncovered the presence of some optional stage notwithstanding the greater part wurtzite stage. The attractive estimations by vibrating test magnetometer (VSM) demonstrated ferromagnetic communication at room temperature in every one of the examples. The Curie temperatures (T_c) and charge fluctuated with the convergence of Mn particles in the examples. Be that as it may, the examples orchestrated by sol-gel strategy were found to have lower T_c esteems and lower polarization when contrasted with the comparing tests blended by strong state response technique. It might be because of the presence of antiferromagnetic islands and more modest crystallite sizes in the examples arranged by the sol-gel technique.

Benouis et al (2007) revealed the correlation of material science properties between undoped ZnO and aluminium AZO and indium IZO doped zinc oxide slender movies. The fundamental, optical and electrical properties were depicted by X-pillar diffraction plans, reflectance and transport spectra and resistivity assessments at room temperature. To be specific the zinc oxide with wurtzite structure was saved by splash pyrolysis on corning glass substance at a specific kept temperature. Photoconductivity was altogether changed by doping.

Jeong et al (2007) researched the Al-doped ZnO (AZO) film kept at room temperature by RF magnetron sputtering with custom-made targets. The reliance of optical and the electrical properties of the sputtered AZO movies on the dopant substance were explored in the targets. The favoured direction of the AZO movies was in the [001] heading. As the proportions of the dopants were changed, the glasslike and the movement changed. The electrical resistivity furthermore changed with changing aluminium doping totals. The AZOamotion pictures were used as anode terminals for normal light-releasing diode (OLED) devices.

Wang et al (2007) explored the p-type doping in ZnO arranged by metal-natural compound fume testimony with dimethylhydrazine (DMH) as the nitrogen dopant source. Results got by x-beam photoelectron spectroscopy showed that DMHy displayed a tight temperature window from 500 to 550 °C for proficient nitrogen consolidation and that nitrogen doping was impacted by development conditions, for example, the N/Ga motion proportion in development. The impact of the N/Ga transition proportion on the conductivity transformation of ZnO was additionally revealed. The extraneous nitrogen acceptor level was determined to be around 160 meV from low-temperature photoluminescence spectra.

Chikoidze et al (2007) orchestrated weakened attractive semiconductor epitaxial slender movies of $Zn_{1-x}Mn_xO$ become on c-sapphire by the MOCVD procedure. Varieties of an and c grid boundaries adhered to Vegard's law and verify the fuse of substitutional Mn^{2+} particles. Transporter focus (n-type) and electron portability were read versus temperature for various centralizations of manganese. Joining of manganese led to the launch of the band hole, seen as a blue move in energy concerning unadulterated.

Hou et al (2007) examined ZnO and MnO powder and slight movies arranged by standard strong state response cycles and radio-recurrence (RF) magnetron sputtering. Attractive estimations showed that the powder was paramagnetic for temperatures above 3K, while the slight movies toughened in vacuum are

ferromagnetic room temperature with a change temperature of around 400 K. The biggest immersed charge (Ms) was discovered to be about 1.05 B/Mn, while the coercive power was discovered to be 100 Oe at room temperature. The altogether different outcomes for the powder and dainty movies demonstrated that development conditions and imperfections assumed a significant part in delivering ferromagnetism.

Zhu et al (2008) concentrated exceptionally Cu doped ZnO nanowires created by fume liquid- strong (VLS) measure. The typical centralization of Cu in the ZnO nanowires was surveyed to be 6 at. %. The ultrafine fused nanowires had widths of just about 80 nm, while their typical length lay in the extent of 40 to 90 μm . Raman spectroscopy showed that the Cu-doped ZnO nanowires had an ordinary wurtzite structure. Significant standard transmission electron microscopy (HRTEM) assessments of individual nanowires showed that the nanowires included a single glasslike structure in which the improvement bearing was orchestrated along with the c turn. Room temperature photoluminescence scope of as-prepared nanowires showed two releases in UV and clear regions that could be ascribed to the near band edge (NBE) change and defects independently, while the scope of the hardened nanowires showed a red move in UV and covering in perceptible gatherings. In addition, the low temperature (10 K) PL range laid out an original winning blue release relating to the unmistakable valence territories of Cu particles in ZnO, which was explained dependent on the Dingle model.

Singh et al (2008) considered undoped and Cr-doped ZnO polycrystalline examples incorporated artificially. Optical estimations affirmed the presence of a Cr in the ZnOagrid. Microstructural investigations of mass examples uncovered an organization of petal-like designs that were discovered to be extraordinary for Cr-doped examples. Essential planning of these examples uncovered uniform circulation of Cr and Zn molecules. Cr doping suppressed the recombination radiation close to 385 nm and expanded the security of ZnO films in an O₂ environment.

Ilican et al (2008) put away the zinc oxide (ZnO) and indium-doped zinc oxide (IZO) slight films onto glass substrates by the shower pyrolysis procedure. The assortments of the essential, electrical and optical properties with the indium combination were inspected. The diamond development and course of the ZnO and IZO thin motion pictures were investigated by XRD plans. They found that all of the saved films were polycrystalline. The gram is not set in stone pretty much 31-36 nm. Morphological depiction and syntheses of the films were performed by SEM and EDX assessments, separately. The optical absorbance through the films was assessed spectrophotometrically in the recurrence range of 200-900 nm. The optical band opening and optical limits were furthermore settled. The electrical resistivity was gotten by the Vander Pauw strategy in dull and under UV light.

Shamla et al (2008) studied tin oxide slender movies by a novel strategy called changed SILAR. The preparative boundaries were enhanced to acquire great quality dainty movies. As-stored films were strengthened in O₂ environments for 1 h at 500 °C. The tempered movies were lighted utilizing Au⁸⁺ particles with an energy of 100 MeV at various fluences of 1×10^{11} , 1×10^{12} , 5×10^{12} and 1×10^{13} particles cm⁻² utilizing a couple of pellets on a gas pedal. The illumination prompted changes in tin oxide flimsy movies which were examined utilizing XRD, AFM, optical band hole, photoluminescence and I-V estimations. XRD considers showed arrangement of tin oxide with tetragonal construction. AFM uncovered uniform testimony of the material with expansion in grain size after illumination. The diminishing in-band gap from 3.51 eV to 2.82 eV was seen with expansion influence. A lessening in PL force and an extra pinnacle were seen after light. I-V estimations showed a diminishing in obstruction with expansion influence.

Wang et al (2008) exhibited the 1.6 GHz surface acoustic wave (SAW) age utilizing interdigital transducers designed by e-shaft lithography on a slender ZnO piezoelectric film saved on an InP substrate. The profoundly arranged, thick, and fine- grain ZnO film with high resistivity was kept by radio recurrence magnetron faltering and was portrayed by an X-beam diffraction, filtering electron microscopy, nuclear power

microscopy, and a four-point test station. The acoustic frequency of the 1.6 GHz SAW produced by energizing the interdigital transducer on ZnO/InP with a microwave signal was 1.6 μm . They showed that this SAW channel gadget could be solidly incorporated with optoelectronic gadgets, opening new freedoms to utilize SAWs for applications, for example, gigahertz-recurrence channels on optoelectronic gadgets and novel broadly tunable quantum course lasers.

Xu et al (2008) combined oneself collected roselike ZnO nanostructures through the warm vanishing of zinc powders without synergist help at the moderately low temperature of 550 °C. The roselike structures are comprised of an enormous number of ZnO nanorods consistently orchestrated into hexagonal multi-facets. The unconstrained nanoindentation impacts under mathematical requirements could be utilized to clarify the structures. The cathodoluminescence spectra showed a wide obvious emanation band identified with Zn buries trials and oxygen opportunities. Field outflow estimations exhibited that the roselike ZnO nanostructures have great electron emanation qualities with a tum-on field of 4.3V/ μm . rs.

Asenjo et al (2008) studied slender film sun-based cells dependent on CuInS₂/ZnS/ZnO arranged with ZnS cradle film of various thicknesses. ZnS films were developed by substance shower testimony (CBD) from acidic arrangements of ZnSO₄ and thioacetamide (TA). The difference in the development rate with time was concentrated by methods for the quartz precious stone microscope. Movies with various thicknesses showed variable physical, synthetic and morphological properties. The construction is concentrated with X-beam diffraction, showing diverse crystallinity with statement time. The retention coefficient likewise relied upon the CBD testimony time and showed ingestion edges somewhere in the range of 2.70 and 3.65 eV. The compositional examination did with XPS (surface) and EDAX (mass). Mass compositional movies were exceptionally stoichiometric with Zn/S proportions near the unit. Fundamental outcomes with CuInS₂-based sunlight-based cells showed efficiencies around 5%, lower than generally found with standard CdS cradle films (near 9%).

Liu et al (2008) uncovered porous ZnO feeble films organized on glass substrates through sol- gel procedure using polyethene glycol (PEG) as normal configuration, zinc acidic corrosive determination as a trailblazer, ethanol as dissolvable and diethanolamine as chelating subject matter expert. A model concerning the pore improvement suggested that a PEG taking zinc oligomers kept away from the ethanol dissolvable which achieved the stage segment of this system. The investigation results showed that the thickness of the film got by six dive covering is around 220 nm. The valuable stone development of the ZnO films was hexagonal wurtzite by X-pillar diffraction plan examination. In addition, the transport range gave a high movement of 80% in the conspicuous region.

Guillen et al (2008) reported the photovoltaic properties of nanostructured ZnO terminals masterminded from monetarily available ZnO nanoparticles and honed with xanthene colours. They used a Eosin Y, a Eosin B and Mercurochrome and stood out from their performance from that of the more ordinary N719 tone. They saw that these shadings capably honed business ZnO nanopowder and yielded efficiencies that were especially significant concerning those given by N719. Neighbourhood photocurrent and transport assessments as a component of the recurrence avowed the extraordinary execution of the xanthene colours in the digestion maxima. They moreover organized polymer-fixed cells and assessed the short-out current of the contraptions under constant illumination at 200 mW/cm² contrasting with twofold the standard sun-fueled light power. The normal tones showed wonderful strength properties under these conditions. The blend of a versatile metal oxide, for instance, ZnO and prudent normal tones should be considered a promising choice in the field of shading-honed sun-based cells.

Zaidi et al (2008) examined the impacts of N doping on zinc oxide (ZnO) slim movies arranged by metal natural fume stage epitaxy (MOVPE) utilizing diethylzinc (DEZn) and 0.2 antecedents and NH₃ as the doping source. N-doped ZnO slim movies were saved on c-plane sapphire substrates with NH₃ stream rates from 0.2% to 4% during development. Profoundly resistive ZnO slender movies

with p-type transporter groupings of $4.24 \times 10^{14} \text{ cm}^{-3}$ and portability of $16.55 \text{ cm}^2/\text{Vs}$ were gotten. Resistivity for the as-developed movies was of the request for $2.3 \times 10^6 \text{ cm}$. The PL consequences of the N-doped ZnO showed concealment of the band-edge radiance and two expansive pinnacles focused at 480 and 600 nm inferable from profound N acceptor radiance were seen. Quick warm strengthening at $800 \text{ }^\circ\text{C}$ in N_2 surrounding turned all the N-doped ZnO films, independent of doping focus, to exceptionally conductive n-type with transporter fixation was of the request for $5.92 \times 10^{18} \text{ cm}^{-3}$, the versatility of $34.91 \text{ cm}^2/\text{Vs}$ and resistivity of 0.09 n cm .

Su et al (2009) examined the electronic design of Be and Mg co-doped wurtzite ZnO frameworks utilizing the primary standards approach dependent on the thickness utilitarian hypothesis. In contrasted and Be-doped ZnO frameworks, Be and Mg co-doped frameworks were more steady. It was shown that for certain doping fixation a sun-powered visually impaired district bandgap can be accomplished.

Schneider et al (2009) concentrated top-notch Cr-doped ZnO nanoparticles arranged from the gas stage and examined their primary, optical and attractive properties. The lengthy x-beam assimilation fine design and the x-beam ingestion close to edge construction of the particles confirmed that after nanoparticle readiness Cr was fused as Cr^{3+} at least somewhat on destinations with a 4-overlay oxygen design, in all likelihood on a Zn site, into the wurtzite cross-section. Despite the way that Cr is referred to go about as an effective non-radiative misfortune community for close to band hole emission (NBE), a pronounced NBE was acquired up to room temperature in any event, for an ostensible Cr centralization of 10 at.%. Strengthening at $1000 \text{ }^\circ\text{C}$ brought about a critical improvement of the photoluminescence productivity and a decreased PL linewidth down to 2.9 meV at low temperatures while the underlying and attractive information demonstrated the arrangement of ZnCr_2O_4 clusters.

Holladay et al (2009) discussed that as of now, hydrogen was basically used in the compound business, yet soon it would transform into an enormous fuel. There were

various cycles for hydrogen creation. In this paper, they reviewed the progressions related to hydrogen creation from both fossil and unlimited biomass resources including improvement (steam, midway oxidation, auto warm, plasma, and watery stage) and pyrolysis. In addition, electrolysis and various systems for delivering hydrogen from water, hydrogen amassing related philosophies, and hydrogen cleaning strategies like desulfurization and water - gas-move were discussed.

Huang et al (2010) uncovered twofold recurrence emissive ZnO tetrapods by Er⁺³ particles, both with and without a germanium (Ge) sensitizer layer, introduced onto the outside of ZnO tetrapod structures. Such developments, depicted by electron microscopy and X-ray diffraction, are found to communicate at both the UV/perceptible and close infrared because of the presence of ZnO/Er⁺³. The presence of picked maintenance features in the recognizable glow spectra proposed the energy move from ZnO to Er⁺³ particles in the doped materials. The introduction of Ge onto the tetrapod surface redesigned the force of Er⁺³ photoluminescence basically with a corresponding blue move of 11 nm in the transmission maxima.

Zhang et al (2010) revealed the amalgamation of ZnO nanocrystallite totals within the sight of lithium particles and movies comprising these totals for colour-sharpened sun-oriented cell applications. A most extreme in general transformation effectiveness of 6.1% was accomplished with these movies. This worth was a lot higher than the 4.0% got for the movies that contained ZnO totals orchestrated without lithium particles. The lithium particles were found to impact the development and gathering of ZnO nanocrystallites, leading to an increment in the nanocrystallite's size and a polydisperse circulation in the size of the totals. The expansion in the nanocrystallite size was because of a lithium-actuated expansion in the diffusivity of interstitial zinc molecules, which led to an improvement in crystallinity. This, in turn, gave an oxygen-enhanced ZnO surface which acted to stifle the disintegration of zinc molecules at the ZnO surface on account of an acidic colour. Accordingly, the development of a Zn²⁺/colour complex was stayed away from. This teamed up with an expansion in the pores size of the totals considering

the increment in the nanocrystallite size, permitting colour particles to go through an exhaustive invasion into the photoelectrode film to be more adsorbed. The polydisperse size conveyance of the totals was accepted to support light dispersing so the voyaging distance of light inside the photoelectrode film could be altogether broadened. Both the further developed colour adsorption and the upgraded light dispersing served to expand the light-gathering proficiency of the photoelectrode and, consequently, advanced the general change effectiveness of sun-powered cells.

Valentin (2010) announced the electronic design of GaN: ZnO strong arrangements as a promising framework for photocatalytic or photoelectrochemical water parting under noticeable light illumination. Nonetheless, the beginning of their movement at a longer frequency regarding the parent materials (GaN and ZnO) engrossing in the UV spectrum is still a matter of discussion. Past hypothetical investigations depended on standard GGA or GGA + U computations which generally thought little of the band hole upsides of the two semiconductors and are in this manner not the most appropriate techniques for the necessary examination. They did a crossover thickness practical investigation (B3LYP) which gave a more exact portrayal of the electronic construction of the parent semiconductors and was accordingly more dependable for the assessment of the blended GaN: ZnO framework. For little convergences of ZnO in GaN, neighbourhood inhomogeneity of Zn or O focus should be summoned to notice a redshift of the ingestion edge. For bigger focuses, some irregular composite dispersions, enthalpically more costly yet entropically more good, were found to introduce decreased band hole esteems due to a positive shift of the N 2p states from the GaN part interfacing the ZnO sections as a result of the ghastly connection with the Zn 3dstates.

Richter et al (2010) concentrated by utilization of surface-upgraded Raman spectroscopy, noticed the level of charge-move for Ag/PATP/ZnO sandwich compounds as a component of both ZnO nanoparticle size and as an element of the excitation frequency. They showed that there were a few probably charge-move resonances. The clearest was the reverberation at a molecule breadth of 27.7 nm for

all frequencies. In a hypothetical report, it was recommended that when there was an electron acceptor on the nanoparticle surface it might shape a complex with the semiconductor exciton and that this was probably the source of the size-subordinate reverberation. At the littlest size (18.2 nm) concentrated here, there was an expansion in the level of charge-move (comparative with adjoining sizes), showing the chance of another, lower-lying charge-move state, which likewise could be brought about by the acceptor-exciton complex. The other reverberation recommended by our information was higher excitation energy for all molecule sizes. It very well may be seen that the level of charge-move raised as the excitation frequency was abbreviated, showing an extra charge-move reverberation in the bright.

He et al (2010) itemized a direct and green technique to decorate the ZnO nanorod group, considering electrophoresis testimony in the Au colloidal game plan masterminded by laser expulsion in water and coming about additional laser enlightenment. The outside of nanorods was homogeneously upgraded with Au nanoparticles. The Au nanoparticles have incredible interfacial affiliation and strong confining with ZnO nanorods. The adornment morphology was viably obliged by the size of Au colloids. Further examinations revealed that sensible electrophoretic potential, little Au colloid's size, and enough between nanorods isolating were pressing to the improvement of a homogeneous and strong surface beautification. Such Au nanoparticle-advanced ZnO nanorod group was functionalized and shown brilliant surface-further developed Raman scattering execution and showed the shot at molecule level ID. This examination allowed one more opportunity to the controllable surface difference in I D semiconductor nanostructures and broadens the perception of the genuine arrangement of electrophoretic declaration.

Inamdar et al (2010) manufactured nanocrystalline zinc oxide flimsy movies by utilizing twofold heartbeat potentiostatic electrodeposition in oxygen immersed zinc acetic acid derivation shower onto FTO-covered directing glass substrates. The zinc oxide development system was concentrated by utilizing straight scope

voltammetry (LSV) and electrochemical quartz microbalance (EQCM) in the presence of oxygen. The impact of heartbeat boundaries like nucleation beat potential (E_1) and development beat potential (E_2) of a potentiostat twofold heartbeat on the size dissemination of zinc oxide slight movies were examined. The primary, morphological and optical properties of zinc oxide nanocrystalline slim movies were examined. The outcomes uncovered how to tailor nanoparticles concerning the size, monodispersity and thickness of the store. Zinc oxide nanoparticles were orchestrated by upgrading beat boundaries of the twofold heartbeat strategy in an oxygen-immersed zinc acetic acid derivation shower. The quantum size impact on optical band hole energies was additionally read for the ZnO nanocrystalline dainty movies.

Flickyngerova et al (2010) examined the impacts of photograph helped electrodeless and particle RF-falter carving on the underlying and optical properties of falteredzZnO: Al slim movies were researched. The photograph helped electrodeless carving was fitting for getting "smooth" surfaces and particle RF-falter scratching by high force has essentially altered the surface unpleasantness with an increment of the light diffuse conveyance.

Garcia-Belmonte (2010) mulled over the assortment in the open-circuit voltage of bulk- heterojunction regular sun fueled cells with temperature and light power was researched reliant upon the dynamic congruity among photogeneration and recombination rates, by choosing the Fermi level dislodging with temperature and inhabitation of the thickness of-states. A negative temperature coefficient of solicitation $dV_0/dT = -1 \text{ mK}^{-1}$ was gotten at temperatures higher than a fundamental worth T_c , which hailed the change between high-to low-inhabitation conditions.

Monda et al (2010) revealed their investigations on cross-breed photoelectrochemical cells made of thionine and zinc oxide nanoparticles. Nanostructured zinc oxide was integrated into the laboratorily by time and savvy technique. The photoelectrochemical cell yielded a voltage of high size (401.5 mV)

and effectiveness (1.21%) contrasted with other traditional photoelectrochemical cells. The morphology of the nanostructured zinc oxide was distinguished by X-beam diffraction and electron microscopy examines. Unearthly examinations showed adsorption of the colour particles on zinc oxide nanoparticles, the justification for proficient assimilation of the episode photons. During photoexcitation, the thionine atoms and the zinc oxide nanoparticles went about as giver acceptor groups which created photovoltage.

Chang et al (2010) detailed the finished ZnO side of the equator cluster films which comprised of development prevented ZnO nanorods of various lengths were created on ITO glass substrates and utilized for sun-oriented cell applications. The manufacturing interaction included an arrangement of ZnO seed, self-amassed polymeric empty particles as nanosphere veil, development of ZnO nanorods, and evacuation of nanosphere cover. Fixing the nanosphere cover on the substrate and controlling the size of the interstices between nearby circles were vital to the manufacture of ZnO nanorods at specific destinations. The surface unpleasantness, including the size and state of the side of the equator pore, can be tuned by changing the ZnO pole development time and the nanosphere size.

Solanki et al (2011) investigated the effect of 120 MeV Ag particle illumination on photoelectrochemical properties of SrTiO₃ dainty movies kept on Indium doped Tin Oxide (ITO) covered glass by sol-gel turn covering techniques. Irradiation of SrTiO₃ narrow films were analyzed to be useful in refining its photoelectrochemical properties. A detectable decrease in the middle grain measurement from 36 to 26 nm, consumption in-band uncovered from 3.55 to 3.43eV and sharply in cruelty following illumination was uncovered which set up in increase photoelectrochemical quest for SrTiO₃ slender movies. Slender movies illuminated at fluence 3×10^{-12} particles cm², when used in PEC cell showed improved photocurrent of 0.16 mA cm⁻² at zero inclination conditions, which was multiple times greatest than that of the uni transmitted preliminaries.

Ko et al (2011) explored the specific improvement of "nanoforest" made out of high

thickness, since a long time ago extended "treelike" multi-age progressive ZnO nanowire photoanodes. The PEC assessments were performed using electrolyte arrangement (0.1 M LiI, 0.5 M 1,2-dimethyl-3-propylimidazolium iodide, 0.03 M h, and 0.5 M tertbutylpyridine in acetonitrile) under AM 1.5G 100 m W/cm² illumination from a sun based test framework. For the most part, the light-change capability of the drawn-out ZnO nanowire DSSCs was right multiple times greater than the viability of DSSCs worked by upstanding ZnO nanowires. The extended adequacy was a result of inconceivably working on the surface zone for higher shading stacking and light procuring, and because of declined charge recombination by giving direct conduction pathways join with the translucent ZnO "nano trees" multi-age areas.

Wong et al (2012) showed the impact of ZnO nanoparticle qualities on the dye-sensitized sun-based cell execution. There was a compound connection between local shortcomings, colour adsorption, charge transport and sunlight-based cell execution. The presence of a high grouping of nonradiative harms was initiated to be hindering photovoltaic demonstration, though, for radiative obligation, preliminaries showing orange-red deformity discharge displayed better execution contrasted with tests with green defect emanation (when the preliminaries had similar discharge powers).

Kumar Daand Khare N. (2016) researched nanotechnology raises a ton of opportunities for fitting materials that have assorted properties as per their size, shape, as well as gathering. Future nanotechnology-based advancements are anticipated to assume a huge part in energy and the double-dealing of elective energy sources like sun-oriented energy. Band edge designing can be utilized to alter materials to make new semiconductor mixture mixes such as pair cells, triple intersections, p-n mixes, and claim-to-fame designs. In expansion, multi-material cross-breed nanomaterials, which join two distinct material sorts, can bring about clever capacities that are autonomous of the singular parts and can be custom-made to meet explicit application prerequisites.

X. Xu et al (2016), Graphene-based half and half materials have been utilized with extraordinary achievement in sensors, sun-based cells, and photocatalysis. Progress metals (e.g., Cu, Co) and their oxides have additionally provoked mainstream

researchers' curiosity because of their assorted applications in gadgets, attractive capacity, photocatalytic water parting, and sun-oriented energy change to electricity. In these composites, graphene and dynamic parts coincide in fluctuated types of microstructures, for example, sandwich-like, secured, wrapped, embodied, layered, and blending modes to frame 3-D, 2-D, or 1-D macroscopic architectures and these composites are typically alluded to as graphene-based materials (GBMs). Currently, GBMs with tailorable nanostructures proposed invigorating freedoms to deal with the challenges and inquiries set off by the developing worldwide energy requests.

Li Chao et al (2018) graphene, a planar monolayer of sp^2 -fortified carbon particles firmly stuffed into a two-dimensional (2D) honeycomb cross-section comprising carbon-carbon bonds, has gotten a great deal of consideration given its astounding properties like high surface region ($2630\text{m}^2\text{g}^{-1}$), incredible warm conductivity ($5000\text{Wm}^{-1}\text{K}^{-1}$), high charge transporter portability ($250.000\text{cm}^2/\text{Vs}$), and compound stability. The molecule-thick 2D graphene design might alter its surface properties using substance adjustment, which opens up different opportunities for the improvement of functionalized graphene-based materials.

UzmaJabeen et al (2018) used the co-precipitation approach to synthesise and characterise un-doped and noble metal-doped zinc sulphide quantum dots. A definite examination of the optical underlying, morphological, and photovoltaic properties of zinc sulfide and honourable metal-doped zinc sulfide uncovered that the presence of silver and gold pollutions in the quantum dab grid essentially affected the properties of the un-doped example.

XiaotianGuo et al (2018), nanostructured transition metal oxides with a high theoretical capacity have limitations such as high irreversible capacity loss during initial cycles and large volume expansion during lithiation, which severely limit their uses. Combining transition metal oxides with conductive nanosize metals significantly boosts conductivity and accelerates the electrochemical kinetics of lithium conversion processes, which improves the electrochemical performances of transition metal oxides.

Chao Li et al (2018) studied the 3D N-doped graphene-supported metal oxide that has been synthesized as the sulfur host of Lithium-sulfur batteries. The SEM images and XRD spectra confirmed that nanoparticles with few tens of nanometers distributed on the surface of the graphene sheet.

Wei Hau Low et al (2018) found that the hybridisation of blended progress metal oxides with graphene is a grounded way to deal with upgrading the electrical conductivity and explicit surface space of the nanocomposite through the advancement of a more limited dispersion pathway for the electrolyte ions. Furthermore, these nanoarchitectures' enhancements in coulombic productivity, explicit energy/force, and cycle life were exhibited specifically. The 2D adaptable nature of graphene and graphene congregations with the enormous explicit surface region and high porosity, specifically, guarantees that electrolyte particles are available to the mass cathode, bringing about unrivalled charge stockpiling, rate ability, brilliant cycles life, and momentous energy thickness.

JulienLoste et al (2018) worked on transparent nanocomposites made from polymer matrices loaded with inorganic nanoparticles, demonstrating that a wide range of transparent nanocomposites can be made using a variety of thermoplastic and thermoset transparent matrices. The use of rare-earth for semi-conductors has followed the evolution of the particles incorporated in nanocomposite clays used to increase the mechanical properties of the polymers.

Sunil P. Lonkar et al (2018) conveyed that ZnO-graphene and nanocomposites have potential uses in sensors, photocatalysis, solar cells, and energy storage. Graphene-ZnOnanocomposites are currently made using multistep solution-based processes, which have low productivity and produce a lot of liquid waste.

D.Kishore Kumar et al (2018) graphene quantum spots (GQDs) created from graphene spaces have been broadly inspected to investigate their photoluminescence properties, which can be tuned by size. GQDs are biocompatible, low cytotoxic, exceptionally brilliant, and scatter well in both polar and non-polar solvents, making them ideal for use in bioimaging, light-discharging, and photovoltaic frameworks.

BeataBajorowicz et al (2019) reasoned that the photocatalytic action of QD-sharpened semiconductor composites is influenced by the accompanying:

(I) The band hole design of the semiconductors (e.g., the qualities and the general places of the valence and conduction band edges);

(ii) morphology (size and shape),

(iii) arrangement,

(iv) surface ligands,

(v) gem design and crystallite size

(vi) surface properties (e.g., opportunities, BET surface region) and

(vii) the sort and weight proportion of semiconductors used to frame QDs and the grid

Wang et al (2019) presumed that the porous MoS₂/CdSe/TiO₂ ternary photocatalysts were effectively prepared by a basic methodology. The SEM and TEM results show that MoS₂/CdSe/TiO₂ ternary composites have a permeable construction, which can supply more mass charge transport pathways. The optical estimation demonstrates that such ternary composites display a more extensive scope of visible light retention than binary composites of MoS₂/TiO₂, CdSe/TiO₂, and unadulterated TiO₂. In particular, the PEC estimation results show that such ternary photocatalysts display a higher photocurrent execution than a double composite and pure TiO₂, which can be credited to areas of strength for the impact of the MoS₂ sheets, CdSe nanoparticles, and TiO₂ porous designs. These unrivalled outcomes demonstrate that porous MoS₂/CdSe/TiO₂ photocatalyst is a promising decision for PEC water splitting.

Wang Z et al (2019) planned a SnO₂ NSs/TiO₂/CdS QDs have visitor-type photoanode and are manufactured for sunlight-based water parting application through a blend of aqueous strategy, ALD procedure, and typical SILAR technique. The thickness of the as-developed SnO₂ NSs can be tuned by how many synthetic compounds are utilized in the antecedent answer for the aqueous response. To lessen the charge recombination rate between CdS guest and SnO₂ host, a thin TiO₂ interlayer has been presented for the band arrangement of the host-visitor photoanode. The streamlined SnO₂ NSs/TiO₂/CdS QDs visitor have photoanode shows better PEC execution contrasted with SnO₂ NSs/CdS QDs and SnO₂ NSs/TiO₂ reference photoanodes. This improved PEC execution is credited to the high apparent light ingestion of the CdS visitor, huge explicit surface region and powerful light-catching impact from the SnO₂ NSs have as well as the great band arrangement from the ALD TiO₂ interlayer. Because of the great

porosity and straightforwardness of the as-created SnO₂ NSs cluster, it has extraordinary possible applications in different fields, for example, photoelectrodes for sun-powered hydrogen generation, energy capacity, and smart windows.

Kavan et al (2019) played out a drawn-out autoclave treatment at a low temperature were taken on to develop TiO₂/SnO₂ forerunners arranged by a sol-gel response. The aqueous circumstances seem to advance an improvement in anatase TiO₂, all the more so within the sight of little (5%) Sn sums. Bigger Sn contents (20%), all things being equal, upheld the development of rutile TiO₂ as the fundamental part, albeit no glasslike stages connected with Sn oxides can be valued in diffractograms. The surface confinement of finely scattered SnO₂, with grain sizes beneath the limit of XRPD perceptibility, was rather upheld by XPS judgments. Besides, the outer layer of the composites turns out to be profoundly hydrophilic as evident from both FTIR and XPS determinations. The probability to tune at low temperature the TiO₂ stage arrangement while keeping up with the surface exceptionally hydrophilic is profoundly advantageous in a few utilizations of TiO₂/SnO₂ composites, going from photocatalysis (as here answered) to additional imaginative applications, for example, in biomaterials. In this regard, the utilization of TiO₂/SnO₂ heterojunctions has been as of late proposed in titanium bone inserts in this application, the profoundly hydrophilic surface would advance cell connection and bone mineralization.

Ranjan, R et al (2019) worked to have detailed planning of MoS₂-CdS-rGO photocatalysts by the aqueous procedure. The movement of MoS₂ supposedly enhanced altogether when CdS and rGO were consolidated to MoS₂. Results affirm electronic cooperation at the strong connection points of the three parts. In presence of MoS₂ and rGO, the CdS was generally in the cubic stage. Essentially, notwithstanding the hexagonal stage, a three-sided (metallic) period of MoS₂ was additionally seen at the point of interaction. The morphological examinations uncovered that both rGO and MoS₂ had shaped plate-like designs and these plates were in cosy contact with one another. Discs supposedly form particles that were on the outer layer of rGO and MoS₂ and are furthermore embedded between the layers of MoS₂. The XPS and FTIR investigations have uncovered the development of heterojunction at the strong - strong points of interaction. Since there exist several lingering bunches on the outer layer of rGO, it is reasoned that compound association has occurred between 'S' of CdS/MoS₂ and 'C' of rGO through the p* orbital of C and n orbital of S. Correspondingly Mo being more electronegative than Cd the electronic connection among MoS₂ and CdS has occurred because of close contact between them. These electronic cooperations have brought about the arrangement of heterojunctions. The development of heterojunctions has worked with a charge move at a strong e strong connection point and in this manner a more prominent charge detachment. The impedance spectroscopy results show that

the conductivity of MoS₂eCdSerGO expanded when CdS and rGO were integrated into MoS₂. This is because of (i) the development of the three-sided period of MoS₂ which has a metallic person and (ii) because of the high conductivity of rGO. The M-S examination has shown p-type semiconductivity. It has been likewise uncovered that the expansion of CdS and rGO to MoS₂ has brought about a more prominent level band potential and a high charge transporter thickness. Hence, the more noteworthy charge division and the high electronic conductivity, high-level band potential with high transporter thickness have brought about a better movement than the MoS₂eCdSerGO impetus detailed in the current work.

N.Reddy et al (2019) have effectively combined Cu-doped Fe₂O₃ and honourable metal plasmonic Ag nanostructures utilizing an aqueous and polyol strategy. The combined nanostructures researched with different examination strategies concentrated on the impact of Cu dopant on precious stone design, morphology, optical band hole, and photoelectrochemical water parting movement of Fe₂O₃. XPS examination affirmed the presence of Cu dopant in the Fe₂O₃ have nanostructures. The Nyquist plots uncovered the most minimal opposition for 0.2 mol% Cu doped Fe₂O₃ with plasmonic Ag nanowires, which implied the practicality of interfacial electron-opening exchange in these photoanodes. The superior water parting trial of these hematite nanostructures could be achieved by controlling the Cu dopant sum with and without the metal layer. Further, the PEC examination showed 135 and 28-overlay expansions in the photocurrent thickness for the enhanced 0.2 mol% Cu-doped α -Fe₂O₃ (1.48 mA/cm², with Ag layer) and (0.31 mA/cm², without Ag layer) photoelectrodes, separately, contrasted with the unadulterated α -Fe₂O₃. These outcomes affirmed that the doped photoanodes with respectable metal plasmonic layers can fundamentally work on the photocurrent thickness for water splitting applications.

Guo, J. et al (2020) utilized a one-venture fume warm method to union a mesoporous film dependent on TiO₂-diminished graphene oxide (RGO) crossovers without the necessity for an extra tempering interaction. This straightforward technique for planning TiO₂/graphene crossover mesoporous films with super high photocatalytic action and photovoltaic execution is relied upon to be valuable in functional applications for getting ready another metal oxide/graphene half and halves with super high photocatalytic movement and photovoltaic execution.

P. Sheng et al (2020) implemented a free-standing nanosheet-nanorod ZnO substrate with CdS as a host for indium, copper, manganese, and cerium doping. The dynamic photoelectrochemical catalytic activity of ZnO-CdS-Mn and ZnO-CdS-Ce model photocatalysts is also well demonstrated by measuring the OH content during irradiation. This work is a nice complement to what we're doing. The effects of doping indium, copper, manganese, and cerium ions on photoelectrochemical activity are precisely assessed.

Jiang, H. et al (2020) used PbS quantum dots to decorate ZnO nanorod/ZnFe₂O₄ nanosheet core/shell nanoarray photoanodes and facilitate charge transport and operate as light absorbers. The photoanode made of ZnO/ZnFe₂O₄/PbS has a much higher photocurrent density and outstanding photoelectrochemical stability. This research demonstrates a simple method for designing highly efficient and stable photoelectrodes for photoelectrochemical water splitting.

C.V.Reddy et al (2020) utilized a format-free hydrothermal technique, and effectively blended unadulterated, mono-doped, and co-doped hematite photoanodes. The co-doped (Y, Cu) hematite photoanode showed 36 and 1.8 overlaps more noteworthy photocurrent thickness at 1.23 V versus RHE over immaculate and mono-doped photoanode. Complete primary and PEC investigation uncover that the superior PEC water oxidation movement can be credited to the synergistic impact between two metal dopants. Besides, the dopant could act passivation impact to further develop the photograph invigorated voltage and lesser the beginning potential by lessening the recombination pace of the charge transporters and expanding the surface PEC energy to upgrade the photocurrent by surging the partition of the surface charge and use. The phenomenally improved electrical conductivity (as proven by electrochemical impedance spectroscopy) of the co-doped (Y, Cu) hematite photoanode feature the meaning of co-doping.

Marlinda et al (2020) had done investigations on graphene and have demonstrated the way that GO sheets can show different highlights as 2D delicate matter. Decreased or part of the way diminished GO has been broadly utilized as an electron sink for metal-containing photocatalysts to advance exciton division and later transportation and additionally stockpiling of electrons for H₂ for water decrease because of its high surface region and p-formed basal plane. Moreover, the testimony of metals, for example, Pt, on the outer layer of GO makes a Schottky hindrance, which works on the creation of H₂. The inward electric field in the pen intersection advances exciton partition by constraining GO electron infusion into the n-type partner, and for later water oxidation, GO gets and moves openings. GO can work as a photocatalyst for water deterioration. The primary undertaking of examination of GO-helped photocatalytic water parting with this information is to explore and characterize the interfacial contact and holding among GO and the semiconductors in the composites. This assignment needs elaborate endeavours to recognize tests and hypothetical estimations of electronic construction. The subsequent test is to make a blended strategy that precisely changes the properties of the GO material. GO's properties depend on the size, number of layers, and implanted usefulness of the graphene sheets, and point of fact, these qualities decide the component of charge transport in the composites. The last undertaking, or speculative goal, is to plan a cross-breed structure for in general water parting for the prompt development of H₂ and O₂. To accomplish this objective, it could be important to take advantage of GO further. For instance, compound change

procedures can be additionally used to grow new nanostructured GO composites that productively transport charges inside composites and infuse charges for responses at the water-composite point of interaction. GO's particular attributes offer superb conceivable outcomes to foster high photocatalytic effectiveness in water splitting utilizing solar energy.

Yang, X. et al (2020) effectively manufactured RGO-NS@TiO₂/SnO₂ photoanode by utilizing a fast extinguishing strategy joined with photoreduction treatment. The presentation of the RGO nanoscroll upgrades the optical adsorption property in UV-noticeable light districts and advances the partition of photogenerated charges. The presence of SnO₂ goes about as an electron pool to accumulate the abundance of photoelectrons. The nanoscroll design of the composite likewise adds to the photocathodic security impact on 304SS both under light illumination and in dark.

Mu, J., Teng, et al (2020) have effectively developed 0D/2D SnO₂/SnS₂ novel S-plot heterojunctions by solvothermal strategy and in-situ oxidation procedure by controlling the toughened temperatures in N₂/H₂ air. The SS-400 uncovers the most elevated photocurrent (0.33 mA cm⁻²) at 1.23 V versus RHE under AM 1.5G brightening, which is around 1.9 and 1.2 times that of SS-300 (0.17 mA cm⁻²) and SS-500 (0.27 mA cm⁻²), separately. The SS-400 shows the hydrogen and oxygen advancement of 5.5 and 2.7 μmol cm⁻² h⁻¹, and the relating faradaic productivity is around 89.4% and 87.7%, individually. The principally upgraded justification for SS-400 is that a proper measure of SnO₂ NPs framed on the surfaces and edges of SnS₂ NSs create in-situ S-conspire heterojunctions, which are speeding up the recombination of transporters with frail redox limit and advancing the division of transporters with generally solid redox limit. Interim, the boundary factor, interior electric field, coulomb communication, and applied predisposition variables can likewise advance the recombination of transporters with frail redox limit (electrons of SnO₂ and openings of SnS₂). This work gave an original idea for planning and building the instrument of S-plot heterojunctions for photoelectrochemical water splitting.

Ghosh, D et al (2020) introduced the nanotextured hexagonal microwell of p-GaN [pGaN(Et)] combined through a wet compound carving course as a photocathode (PC) for PEC water parting. The p-GaN(Et) was additionally adjusted by interconnected nanowall organization of two-dimensional (2D) change metal dichalcogenide (MoS₂) [2D-MoS₂/p-GaN(Et)]. The two PCs were portrayed for their morphology, structures, and optical and electronic properties. Generally speaking, PEC execution was approved through photocurrent values followed by how much hydrogen and oxygen advancement. This mix of 2D-MoS₂/p-GaN(Et) outflanked flawless pGaN(Et) by a few significant degrees in generally PEC execution. The phenomenal steadiness under a persistent working condition with 1 sun brightening (100 mW/cm²) gives the genuinely necessary kind of a productive photocathode. The upgraded photocathode

[2D-MoS₂/pGaN(Et)] shows the most elevated applied predisposition photon-to-current transformation proficiency of ~3.18% with a hydrogen development pace of 89.56 $\mu\text{mol/h}$ at -0.3 V versus RHE. This wafer-level savvy combination of 2D-MoS₂/GaN heterostructure-based PCs opens another way for enormous scope solar–fuel conversion.

Ke. J et al (2021) sunlight-based driven photoelectrochemical (PEC) water dividing frameworks are exceptionally encouraging for changing over sun-powered energy into perfect and economical substance energy. An incorporated photoelectrode in such PEC frameworks comprises a light reaper that retains sun-powered energy, an interlayer that transports photogenerated charge transporters, and a co-impetus that triggers redox responses. Accordingly, it is basic to grasp the connections between the natural underlying attributes and elements of photoelectrodes. Here we inspect different 2D layered photoanodes/photocathodes, including graphitic carbon nitrides, change metal dichalcogenides, layered twofold hydroxides, layered bismuth oxyhalide nanosheets, and MXenes, joined with cutting edge nanocarbon (carbon specks, carbon nanotubes, graphene, and graphdiyne) as co-impetuses to gather incorporated photoelectrodes for oxygen development/hydrogen advancement reactions. The key ideas of PEC water parting, just as the physicochemical provisions of photoelectrodes and the synergist responses associated with them, are analyzed. The article presents elaborate ways for collecting 2D photoelectrodes with nano carbons to further develop PEC execution. The mechanics of association between 2D photoelectrodes and nanocarbon co-impetuses are analyzed in better detail. The field's troubles and potential are laid out to direct future examination into further developing PEC water parting transformation proficiency.

Yu Z et al (2021) contemplated that 1D nanostructured photoelectrodes are promising for application as photoelectrochemical (PEC) gadgets for sunlight-based energy change into hydrogen (H₂) due to the optical, primary, and electronic advantages. Titanium dioxide (TiO₂) is the most tried competitor as a photoelectrode because of its great photostability, low creation cost, and eco-invitingness. The impediment to TiO₂'s reasonable application is the inborn wide bandgap (UV-lights reaction), helpless conductivity, and restricted opening dispersion length. Here, a far-reaching audit of the flow research endeavours toward the improvement of 1D TiO₂-based photoelectrodes for heterogeneous PEC water parting is furnished alongside a conversation of nano architectures and energy band designing impacts on interfacial charge move and

partition of 1D TiO₂ composited with various dimensional photoactive materials. Understanding charge move measures at interfaces, just as the connection between photogenerated charge division and photoelectrochemical execution, is a significant focal point of this investigation. This audit is relied upon to give extra understanding into the judicious plan of nano architectures, doping, and heterojunction interfaces for 1D TiO₂-based photoelectrodes to accomplish high proficiency in sun-based energy transformation.

Siavash Moakhar et al (2021) examined that 1D nanostructured photoelectrodes are promising for application as photoelectrochemical (PEC) gadgets for sun-based energy change into hydrogen (H₂) due to the optical, underlying, and electronic advantages. Titanium dioxide (TiO₂) is the most tried applicant as a photoelectrode because of its great photostability, low creation cost, and eco-agreeableness. The impediment to TiO₂'s reasonable application is the innate wide bandgap (UV-lights reaction), helpless conductivity, and restricted opening dispersion length. Here, an exhaustive audit of the momentum research endeavours toward the advancement of 1D TiO₂-based photoelectrodes for heterogeneous PEC water parting is furnished alongside a conversation of nano architectures and energy band designing effects on interfacial charge move and detachment of 1D TiO₂ composited with various dimensional photoactive materials. Understanding charge move measures at interfaces, just as the connection between photogenerated charge partition and photoelectrochemical execution, is a significant focal point of this investigation. This audit is relied upon to give extra knowledge into the objective plan of nanoarchitecture, doping, and heterojunction interfaces for 1D TiO₂-based photoelectrodes to accomplish high proficiency in sunlight-based energy change.

According to Han J et al (2021) hydrogen as an energy source has started broad consideration because of its eco-accommodating, inexhaustible, high energy thickness, and long haul manageability. Hydrogen age utilizing the photoelectrochemical water parting (PEC-WS) framework must be demonstrated to be a practical alternative for tending to future energy and ecological difficulties. Temporary metal oxides (like ZnO, TiO₂, SnO₂, and others) were normally utilized as photoanodes in a standard PEC-WS

framework given their great electron versatility, extraordinary solidness, and OK conduction band area, among a few others. Various improvement and adjustment methodologies for photoanodes dependent on ZnO were thoroughly summed up in this survey, including morphology and design control, crystallization energy regulation, doping designing, another semiconductor coupling, cocatalyst stacking, piezoelectric/ferroelectric/pyroelectric impact coordinating, and metallic nanoparticle consolidation. The potential and viewpoint of ZnO-based photoanodes, just as their advancement strategies, were additionally talked about. This audit likewise gives a bit-by-bit manual for elective metal oxide advancement and adjustment methods.

Kyesmen et al (2021) in their research, studied that nanostructured heterojunction of hematite (α -Fe₂O₃) and permeable copper (II) oxide (CuO) composites addressed as α -Fe₂O₃/CuO was ready and utilized as photoanode for photoelectrochemical (PEC) water parting. X-beam diffraction (XRD) and Raman spectroscopy studies affirmed the high virtue of α -Fe₂O₃/CuO heterostructures created. Upgraded photocurrent thickness of 0.53 mA/cm² at 1.0 V versus reversible hydrogen anode (versus RHE) was accomplished for α -Fe₂O₃/CuO photoanodes, addressing a 19-overlap increment when contrasted with the worth recorded for α -Fe₂O₃. The arrangement of a heterojunction combined with the permeable surface morphology of α -Fe₂O₃/CuO heterostructure worked with charge detachment of photogenerated electron-opening sets, upgrading PEC water parting. The diminished bandgap recorded for α -Fe₂O₃/CuO brought about expanded retention of photons in the noticeable range by the heterostructure, which additionally impacted the improvement of the photocurrent thickness. Also, expansion in control transporter thickness and the decrease of charge move obstruction at the fluid/strong interface accomplished for α -Fe₂O₃/CuO were extra proof related to the improvement in the recorded current thickness. This exploration introduced the arrangement of α -Fe₂O₃/CuO heterojunction structure with the permeable surface as a practical course to accomplishing eminent improvement in the photograph reaction of α -Fe₂O₃ photoanodes for PEC water parting.

Swathi S et al (2021) examined whether photoelectrochemical (PEC) water parting is useful and has drawn interest because of the expanded potential to fabricate hydrogen

and oxygen from water using bountiful sun-powered light to address the energy emergency. In PEC water dividing applications, an assortment of dynamic semiconductor materials is explored. Nevertheless, in past many years, the vast majority of the analysts recommended that titanium oxide (TiO₂) is the best photoanode for this sort of use. Presently, Zinc oxide (ZnO) is viewed as an ideal replacement for TiO₂ because of its equivalent energy band construction and predominant photogenerated electron move rate. In this investigation, uncovered and phosphorus-doped ZnO nanorods were effectively evolved on fluorine-doped tin oxide-covered glass (FTO) substrate by synthetic fume testimony. X-beam diffraction (XRD) design validated hexagonal construction arrangement with solid diffraction pinnacle of (101), which showed that ZnO nanorods were impeccably evolved along with c pivot. The optical and morphological properties were investigated by UV–Vis and filtering electron microscopy pictures. The energy-dispersive X-beam spectra exhibited that doping specialist phosphorous was available in ZnO nanorods. The PEC properties of the created ZnO nanorods were additionally researched and gotten results recommended that a limited quantity of phosphorus-doped ZnO nanorods improves their PEC execution.

Ghosh N.G et al(2021) have detailed the combination of two natural semiconductors which are anthraquinone and Benzonia/selenadiazole-based π -formed D–A1–D–A2 (D-contributor, A-acceptor) type co-polymers. They have coupled these natural semiconductors with the Ti³⁺ self-doped TiO₂ nanorods (Ti³⁺/TiO₂ NRs)—developed on the fluorine-doped tin oxide-covered glass substrate—to get type-II n-n inorganic/natural nano-heterostructures (NHs). Ti³⁺ self-doping successfully creates oxygen opening which, thusly, joins many sub-bandgap states in TiO₂—making them noticeable light active. Under apparent light enlightenment, the NHs cathodes filling in as photograph anodes start water oxidation. The NHs increment noticeable light absorbance, however, they additionally accelerate photogenerated transporter delocalization and transportation because of their great sort II band alignments. The NHs including benzothiadiazole (TP1) have been found to display preferred photoelectrochemical exhibitions over the Ti³⁺/TiO₂ NRs just as the NHs containing benzoselenadiazole (TP2). The soaked photocurrent densities presented by the TP1 and

TP2 NHs anodes at 1 V versus Ag/AgCl are 0.50 mA/cm² and 0.30 mA/cm², separately, connoting practically 466.7% and 233.3% augmentations over the photograph current thickness shown by the Ti³⁺/TiO₂ NRs terminal at 1 V versus Ag/AgCl. All things considered, the TP1 NHs flimsy film has shown the best execution. The photocatalytic effectiveness for both of the NH's meagre movies generously increased within the sight of 1 mM H₂SO₄. This marvel is owing to the photochemical arrangement of H₂O₂ due to the underlying uniqueness of the polymers. Also, trying different things with the electron and opening scroungers concede the photocatalytic responses are for the most part overwhelmed by electron interceded courses for both of the NHs. The photogenerated electrons produce •OH extremists which administer the all-encompassing corruption system.

Zhou N et al (2021) contemplated that the inadequate usage of daylight of ZnO, because of its expansive band hole, brings about low effectiveness for photocatalytic hydrogen creation. To work on the photocatalytic adequacy of ZnO in the apparent light reach, plasmonic honourable metal nanoparticles (NPs) of different structures (circles and bars) were blended in with mesoporous ZnO to shape a centre shell nanostructure. The photoelectrochemical water dividing exercises of the metal@ZnO centre shell nanocomposites (NCs) were explored. The photocurrent reaction of metal@ZnO NCs was found higher than unadulterated ZnO or the combination of metal NPs and ZnO credited to the viable charge move system. It was likewise tracked down that the photocurrent of metal@ZnO NCs was identified with the thickness of ZnO and there was an upgraded shell for every sort of metal centre. Also, the presentation of Ag shell can get a higher photoelectrocatalytic proficiency contrasted with unadulterated Au NPs centre because of lower Schottky obstruction among Ag and ZnO and more extensive annihilation range in the apparent light of Au@Ag nanoparticles.

According to Huang X et al (2021), the confusing interfaces of heterojunctions ordinarily include many deformities, which bring about recombination of delivered electron-opening sets. Homojunction interfaces, then again, are believed to be invaluable for charge transporter partition because of the similar provisions of the different sides of the homojunction. TiO₂ has rutile and anatase two commonplace

photoactive stages in nature. In this work, TiO₂-rutile/anatase (TiO₂-R/A) homojunction photoanode is manufactured by in situ development of anatase TiO₂ on the TiO₂-R surface. By appearing differently in TiO₂-rutile/rutile (TiO₂-R/R) photoanode, TiO₂-R/A showcases higher photocurrent thickness (1.70 mA cm⁻² at 0.6 V versus SCE). A profound understanding of the instrument proposes that TiO₂-R/A homojunction has serious band twisting and improved surface region, which work with the charge partition and transmission. This research gave new bits of knowledge into the plan and creation of semiconductor photoanodes for high-productivity photocatalytic measures.

Sivagurunathan, A. T. et al (2021) expressed PEC is the most encouraging way to deal with making hydrogen in a spotless and manageable way. In any case, immense obstructions should be defeated to upgrade sun-powered water parting proficiency, which is connected to energy misfortune during the significant light-gathering stage because of photogenerated charge transporter recombination and the subsequent corruption of fabricated cathodes. The dependability and charge-move components that influence in general PEC proficiency are represented by interfacial associations between the cathode and the electrolyte. The advancement of nanostructured materials on the nuclear scale, designing of bandgaps, passivation of surfaces, improvement of impetuses, and alteration of the light-reaping properties of a surface have all gotten a great deal of consideration since the coming of cutting-edge designing procedures. Post-surface alteration utilizing nuclear layer affidavit (ALD) has gotten a great deal of consideration since it can work with the advancement of nanostructured materials on the nuclear scale, designing of bandgaps, and passivation of surfaces. The current audit centres around utilizing ALD to work on the underlying and surface properties of planned anodes using different ALD-kept materials, just as investigating their suggestions on PEC proficiency and giving a short outline of PEC basics. Recent ALD projections that have supported the upgrade of PEC gadget activities are likewise referenced. This paper likewise traces the future possibilities and capability of PEC water parting, which has started a great deal of interest in the present academic local area.

2.1 ORIGIN OF PROBLEM:

The reserves of petroleum products that presently power society will miss the mark concerning its interest in not so distant future. Besides their use in continuously increasing quantity has started threatening human health as it is leading to some adverse climatic changes. Elective inexhaustible powers, however at present a long way behind from being cutthroat with non-renewable energy sources in cost and creation limit, are the lone arrangement left. Solar energy holds an edge over other renewable sources of energy on account of its huge potential and widespread availability.

Photoelectrochemical applications of metal oxide semiconductors in the conversion of solar energy to a valuable chemical fuel viz., hydrogen are well documented. However, the efficiency and durability of the PEC system are still a challenge to launch this technique at the commercial level.

The principle accentuation on work in PEC water parting concerns expanding the effectiveness and soundness of the photoactive materials to accomplish the necessary proficiency focus of 10% that will be reasonable for commercialization. Right now stable photoelectrode (PE) materials dependent on metal oxide have rather low proficiency of a few per cent while high effectiveness materials dependent on a multijunction regular semiconductor can accomplish marginally above 10% yet corrupted inside a brief time frame.

In the quest for **appropriate semiconductors**, that have all the required characteristics, intense research is going on around the world. The central theme of all such research is to induce the desired properties in the semiconductor by some suitable material modification techniques, especially during the preparation and processing of such semiconductors.

Chapter-3

Methodologies for sample preparation and characterization

The recent research focuses on the synthesis, characterization and use of nanostructured semiconductor thin films/powders for photoelectrochemical/photocatalytic water splitting. Table 3.1 lists the specifics of the samples which were prepared. The samples were examined for crystal phase, microstructural, and optical characteristics, as well as their potential use in PEC and PC water splitting. An overview of the experimental methods used is shown below.

3.1 Outline of Experimental work

Parameters of the study	Description
Preparation of samples <ul style="list-style-type: none">• Materials of interest	<ul style="list-style-type: none">• ZnO, Cu₂O, Fe₂O₃, TiO₂, rGO, SnO₂, MoS₂• Dyes: Rose Bengal, Erythrosin B
<ul style="list-style-type: none">• The proposed method of preparation	Sol-gel process and/ or Spray pyrolysis and Sputtering
<ul style="list-style-type: none">• Variables	<ul style="list-style-type: none">▪ The relative concentration of metal oxides▪ Sintering temperature

	<ul style="list-style-type: none"> ▪ Dopant concentration ▪ Dye concentration
Characterization	<ul style="list-style-type: none"> ▪ Phase analysis by XRD ▪ Crystalline size and Strain measurements ▪ Surface morphology by SEM ▪ Surface topography by AFM ▪ Bandgap energy by UV-Vis spectrophotometer ▪ Film thickness by surface profilometer ▪ Film density ▪ Film resistivity ▪ Flat band potential and carrier density
PEC measurement variables	<ul style="list-style-type: none"> ▪ Current-Voltage curves under darkness and illumination. ▪ Photovoltage ▪ Photocurrent ▪ Open circuit potential ▪ Short Circuit current ▪ Photocurrent density ▪ Qualitative analysis of evolved gases

3.2: Materials Used

Co-precipitation, sol-gel, and electrodeposition were used to make the samples (powders/thin films). Precursor salts included zinc acetate dihydrate $[\text{Zn}(\text{CH}_3\text{COO})_2 \cdot 2\text{H}_2\text{O}]$, zinc nitrate $[\text{Zn}(\text{NO}_3)_2 \cdot 6\text{H}_2\text{O}]$, tin chloride $[\text{SnCl}_2]$, and iron (III) nitrate nonahydrate $[\text{Fe}(\text{NO}_3)_3 \cdot 9\text{H}_2\text{O}]$. Ammonium hydroxide, natural graphite, Potassium permanganate $[\text{KMnO}_4]$, Copper (II) nitrate trihydrate, rose bengal dye, erythrosin B, sodium hydroxide, hexamethylene-tetramine (HMT), and was all AR grade reagents used in the research. Phosphoric acid, urea, and silver nitrate were used as source compounds in the synthesis of phosphorus, nitrogen, and silver integrated ZnO thin films, respectively. Sigma–Aldrich Corporation in the United States provided the platinum gauze (0.1 mm thick, 99.9%) used in the formulation of the

counter/auxiliary electrode in PEC studies. To make electrical contacts with the sample film/pellets, conductive silver paste (RS Components, Northants, NN17 9 RS, UK) and industrial-grade copper wire (1 mm thick) were used. Only double-distilled water (DDW, basic conductivity $0.8 \times 10^{-6} \text{ ohm}^{-1} \text{ cm}^{-1}$ at 25 °C) was used to make reagent solutions.

3.3: SAMPLE SYNTHESIS OF VARIOUS PARTICLES

3.3.1 ZnO Nanorods:

(i) Seed layer formation: A sufficient amount of zinc Acetate was dissolved in isopropanol and diethanolamine was added as a stabiliser to make a thin film on the ITO substrate as a seed layer. At 30°C, the whole solution was stirred for 4 hours. The prepared sol was kept overnight to ensure that it was stable. A spin-coating system at 2500 rpm was used to coat two layers on an ITO substrate. The excess solvent was evaporated by drying the film on a magnetic stirrer after each coating. The films were then annealed for one hour at 500°C in a muffle furnace.

(ii) In distilled water, an equimolar solution of zinc acetate and hexamethylenetetramine was prepared and stirred for 1 hour. To slow down the rate of precipitation, various quantities of ammonia solution were slowly applied to this solution. This solution, along with ITO glasses with a ZnO seed layer, was autoclaved for 6 hours at 90°C in a Teflon-sealed autoclave. The ITO glasses were then washed in distilled water and annealed for one hour at 500°C.

3.3.2 ZnO Nanoparticles at different pH:

A suitable amount of zinc Acetate Dihydrate was dissolved in water in different beakers and a solution of NaOH was added dropwise to maintain the pH at 8,9,10 and 12. Precipitation occurred when NaOH solution was added. Solutions were stirred continuously for four hours. All solutions were kept overnight after being stirred for 4 hours at room temperature. Filtered precipitates were annealed at 600°C in an air-cooled muffle furnace.

3.3.3 SnO₂ Nanoparticles:

Tin chloride was dissolved in water and a NaOH solution was added to maintain pH at 9. The result was a yellowish precipitate that was filtered out and annealed at 600°C in an air muffle furnace.

3.3.4 ZnO/SnO₂ Nanoparticles:

Using acetone, an equal quantity of ZnO and SnO₂ was taken and thoroughly ground in a mortar pestle for 2 hours regularly. Pellets of the prepared mixture were made with a pelletizer and kept in a muffle furnace at 600°C for 1 hour.

3.3.5 TiO₂ Nanoparticles:

In a beaker, 7 grams of hexamethylenetetramine is dissolved in 400 millilitres of distilled water and stirred with a magnetic stirrer. Then 8mL of TiCl₄ was added, and the mixture was microwaved three times at 350°C for 5 minutes per time. On a magnetic stirrer, the solution was stirred for one hour. The solution was kept overnight to allow the precipitate to settle. The precipitate was filtered and then annealed for one hour at 400°C.

3.3.6 MoS₂ Nanoparticles:

In a 1:3 ratio, bulk MoS₂ and lithium nitrate were mixed. 50 mL HCl was added to this mixture, and the solution was kept in an ultrasonic bath for 1 hour. Finally, deionized water was used to clean it.

3.3.7 TiO₂/MoS₂ Nanocomposites:

TiO₂ and MoS₂ were mixed in a 2:1 ratio in a mortar pestle and ground for 2 hours daily with acetone. Pellets of the prepared mixture were made in a pelletization unit and kept at 400°C for 1 hour in a muffle furnace.

3.3.8 ZnO/rGO Nanocomposites:

0.5 g of natural graphite was mixed with 11.5 mL concentrated sulphuric acid in a beaker and stirred for two hours. 1.5g potassium permanganate was added to this solution very slowly. After the addition of potassium permanganate, the mixture was heated at room temperature and stirred for one hour. Excess deionized water (DIW) of about 23 mL was added to the beaker and the mixture was heated at 95°C and stirred for one hour. In the end, to terminate the oxidation reactions, 70 mL DIW and 2.5 mL H₂O₂ were added to the mixture. The final suspension was centrifuged and washed with HCl two times and DIW six times and dried in air. GO was reduced by ascorbic acid to form rGO.

The strategy for getting ready ZnO nanoparticles was equivalent to that referenced before. A reasonable measure of Zinc Acetate Dihydrate was mixed in water and NaOH was added dropwise. Precipitation happened when NaOH was added. The entire solution was kept overnight at room temperature. Precipitates were washed, dried and kept in a muffle furnace at 600°C for one hour. At last, to set up the rGO-ZnO, these were blended in a mortar pestle with (CH₃)₂CO and pellets were shaped.

3.3.9 Cu doped Fe₂O₃ Nanoparticles:

For the synthesizing CuFe₂O₄ nanoparticles, Ferric (III) nitrate nonahydrate and Copper (II) nitrate trihydrate (with 1, 4, 7, 8, and 10 per cent doping individually) in required amounts. The sol-gel method was used to create the nanoparticles. In a beaker containing 50 ml of distilled water, 5 g of ferric nitrate was added and stirred at a consistent temperature of 60 degrees Celsius using a magnetic stirrer. Using a thermometer, the temperature rate was maintained constant. Copper nitrate was then added to the same beaker after 1 hour of stirring. The mixture was then stirred for another hour. As a precipitating agent, 1 M NaOH solution was prepared and used.

Precipitation began almost immediately after adding the NaOH solution, and stirring was continued for the next 5 hours after the pH reached around 10. After the stirring, it was cooled to room temperature and filtered. During filtration, the material was washed 3–4 times with distilled water to eliminate unwanted impurities. After that, the reddish-brown product was dried in an oven for around 5 hours at 60 degrees Celsius. After drying, the product's large particles (CuFe_2O_4) were crushed and coarsely powdered. The product's powdered phase was calcined for 3 hours at 600 degrees Celsius in a muffle furnace.

3.3.10: Dye Sensitization By Rose Bengal Dye & Erythrosin B and I-V Studies

ZnO photoanode was prepared as mentioned in the above experiment of ZnO nanorods. ZnO photoanode was immersed in 0.5mM ethanolic solution of rose Bengal and erythrosine B solutions. For dye loading, the electrodes were kept overnight in respective dye solutions. After dye stacking films were washed with ethanol to eliminate the overabundance measure of dye. Then these were exposed to I-V portrayal.

3.4: Sample Characterization

The crystallographic, microstructural, optical, and semiconductor properties of the prepared samples (powders and thin films) were characterised using the following instrumental techniques/methods.

3.4.1: XRD study of crystal phase and microstructure

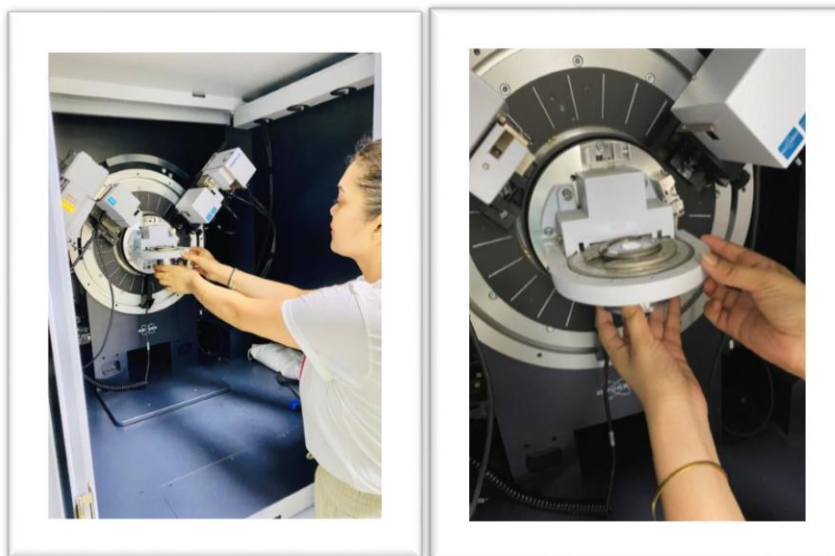


Fig. 3.1: X-ray Diffractometer used in the study

The precise structure and microstructure of glasslike materials are not settled utilizing X-ray diffraction (XRD) examination. At the point when an X-ray beam strikes an example material, it disperses every which way. Most of a molecule's dispersed radiations are offset by other atoms' dissipated radiations. At the point when X-rays hit those crystallographic planes at specific points, they are reinforced instead of obliterated. Diffraction is the term referring to this phenomenon [Cullity and Stock, 2001]. Diffraction occurs when a wave hits a surface with one or more openings that are about the same size as the X-ray wavelength used. Distances of 100-200 pm separate the layers of atoms or ions in crystals. This is the ideal range for causing X-ray diffraction. The number of electrons that an atom contains has a lot to do with its ability to create diffraction patterns. The X-rays' electric field interacts with the cloud of electrons that surrounds an atom. Thousands of such interactions result in the diffraction pattern.

Since large atoms have a large number of electrons, they produce the most powerful patterns. Small atoms with few electrons, such as hydrogen, can have little impact on X-rays (Arora, 2000). Bragg's famous equation (3.1), now known as Bragg's law, demonstrated how diffraction patterns form.

$$\sin\theta = \lambda / 2d_{hkl} \quad (3.1)$$

Here, θ is a large portion of the point between the diffracted bar and the approaching shaft, λ is the frequency of the X-beams, and d_{hkl} is the interplanar dividing between the planes that actuate positive obstruction of the pillar, [Askland 1996]. Here, d_{hkl} is the interplanar dispersing between the planes that prompt positive impedance of the bar and are a large portion of the point between the diffracted bar and the approaching shaft [Askland 1996]. Metal oxide tests (films/powders) are comprised of a few little crystallites, and some of them regularly have (hkl) planes situated at the right point to fulfil Bragg's law [Cullity and Stock, 2001]. This creates a diffracted shaft with a 2θ point to the occurrence bar. A diffractometer utilizes a moving X-beam identifier to record the 2θ points at which the shaft is diffracted, bringing about a diffraction design. The interplanar dividing and personality of the planes that cause diffraction are not set in stone once the X-beam frequency is characterized. Treating the diffraction design as a finger impression is one more approach to utilising X-beam diffraction information. By contrasting an example's diffraction design with a data set of pre-estimated and distinct diffraction designs, an example can be recognized. For the movies and powder tests in this investigation, X-beam diffraction was utilized as a portrayal instrument. Utilizing an X-beam diffractometer with a graphite monochromator and CuK as a radiation source, an X-beam diffraction examination was performed (Bruker AXS D8 Advance, Germany).

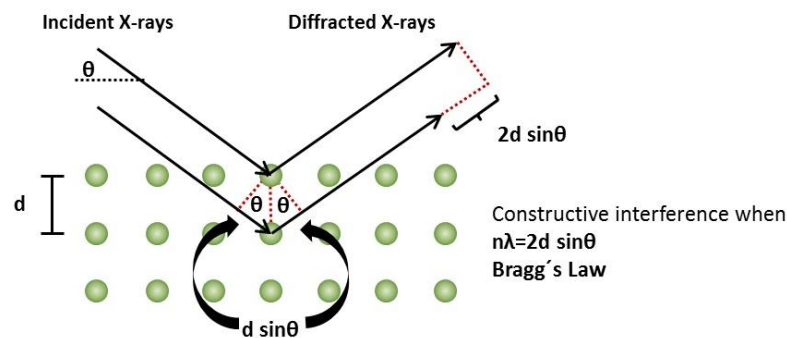


Fig. 3.2: Condition of Bragg's law [https://wiki.anton-paar.com/en/x-ray-diffraction-xrd/]

The average crystallite size in samples was calculated using Scherrer's equation (3.2) and the broadening of X-ray diffraction peaks [Klug and Alexander, 1974; Cullity and Stock, 2001].

$$B=0.9\lambda/ t \text{ Cos } \theta \quad (3.2)$$

where, B is FWHM (full width at the half limit) of the expanded diffraction line on the 2θ scale t normal breadth of crystallite, λ frequency of X-beam and θ the half diffraction point of the centroid.

Even when the crystal size reaches 1000 \AA , all X-ray diffraction lines have a measurable breadth due to factors such as incident beam separation, sample size (in Debye cameras), and X-ray source duration (in diffractometers). As a result, the extra breadth, or broadening, due to the particle size effect alone is denoted by B in equation (3.2). In other words, when the particle size reaches about 1000 \AA , B is zero. The major challenge in determining particle size from line breadth is to determine B from the measured breadth B_M of the diffraction line. Warren's approach is the simplest of the many that have been suggested [Cullity and Stock, 2001]. When the unknown sample is combined with a regular particle size of 1000 \AA , a diffraction line appears that is similar to a line arising from the unknown sample. If B_S is the measured breadth at half the maximum intensity of the line from the standard, the B is given by equation (3.3) [Cullity and Stock, 2001].

$$B^2 = B_M^2 - B_S^2 \quad (3.3)$$

The experimental difficulty of calculating crystallite size from line broadening increases as the size of the crystallite becomes wider. If the crystallite's size is in the range of $0\text{-}500 \text{ \AA}$, the measurements provide a reasonable approximation of its size. A good experimental technique is required to achieve accurate results in the $500\text{-}1000 \text{ \AA}$ range. The observed diffraction data was also utilized to estimate the dislocation density (δ) in the samples. Equation (3.4) was used

$$\delta = 1/t^2, \quad (3.4)$$

XRD measurements are taken with an X-ray diffractometer (Bruker AXS D8 Advance, Germany) at D.E.I (Fig. 3.5), fitted with a graphite monochromator and CuK α as the radiation source, reported crystal phase and microstructural information in the current analysis. Measurements were taken at varying 2θ with a phase size of 0.02 degrees/min with an angular precision of $\sim 0.00^\circ$ and an angular resolution of $> 0.01^\circ$.

3.4.2: Energy-dispersive X-ray spectroscopy (EDX)

The procedure of energy-dispersive X-ray spectroscopy (EDX) helps decide the essential piece of tests. A filter that produces yield beats corresponding in stature to the X-ray photon energy is utilized in blend with a detector tallness analyzer in this strategy. To decrease electrical commotion, the identifier and preamplifier are additionally cooled with fluid nitrogen. Identifiers made of Si (Li) or Si float indicators (SDD) are for the most part utilized. The major idea that every component has a novel nuclear design that takes into account a one-of-a-kind assortment of tops on its X-ray range upholds EDX's portrayal abilities. High-energy light emission particle-like electrons or protons, or light emission beams, are concentrated onto the example being analyzed to prompt the discharge of trademark X-rays from it. Very still, A molecule in the example incorporates ground state (or unexcited) electrons in discrete energy levels or electron shells bound to the core. The occurrence pillar can invigorate an electron in an internal shell, making it be launched out from the shell and leaving an opening in its place. The opening is then loaded up with an electron from an external higher-energy shell, and the energy contrast between the higher-energy shell and the lower-energy shell might be produced as an X-ray. An energy-dispersive spectrometer can assess the degree and energy of X-rays discharged by an example. The essential synthesis of the example is not set in stone since the energy of the X-rays is normal for the distinction in energy between the two shells and of the nuclear design of the material from which they were produced. INCA Penta FET x3 TESCAN was used in connection with energy dispersive X-ray analysis (EDX) at an accelerating voltage of 15 kV and a working distance of 10.27 mm to achieve a localised chemical analysis in this study.



Fig. 3.3: Energy-dispersive X-ray spectroscopy (EDX) used in the study

3.4.3: Surface morphology: SEM analysis

The diffraction of light limits the resolution of optical microscopes to around 1000 diameters magnification. Electron microscopy, then again, utilizes the wave idea of quickly making trip electrons for its potential benefit. Electrons sped up to 10,000 keV may just have a frequency of 0.12 \AA , contrasted with the noticeable light frequency. As a result, electron microscopes can easily achieve magnifications of about 1,000,000, with only spherical and chromatic aberrations limiting their ability to achieve even higher magnifications [Schroder, 1990].

At the moment, the resolution limit of a scanning electron microscope is about 25 \AA . Thus, using a scanning electron microscope to examine a sample, especially films, is expected to reveal the detailed morphological aspects of samples. In a vacuum, the scanning electron microscope produces an electron beam. Electromagnetic condenser focal points collimate the beam, which is then focused by a target focal point and examined across the example surface by electromagnetic diversion loops.



Fig. 3.4: Scanning Electron Microscope used in the study

Collecting secondary electrons emitted by the sample is the primary imaging process. A scintillation material detects secondary electrons by producing light bursts from the electrons. A photomultiplier tube recognizes the light explodes and enhances them. A picture that is strikingly like what might be seen through an optical magnifying lens can be made by connecting the example examine the area with the subsequent sign. [Schroder, 1990] The lighting and shadowing create a very natural-looking surface topography.

3.4.4: Surface topography: AFM analysis

Atomic Force Microscopy is an effective technique for determining the surface profile of thin films (AFM). AFM is based on a straightforward theory. The data is collected by using a mechanical probe to feel the surface. A piezo-electric scanner checks a surface with a molecularly sharp tip and an input system that permits the piezo-electric scanner to keep the tip at a consistent power (to acquire tallness data) or stature (to get

power data) over the example surface. The tips of a cantilever are generally made of Si₃N₄ or Si and stretch down from the end. The optical detection device used by the nanoscope AFM head is based on the tip being connected to the underside of a reflective cantilever.



Fig. 3.5: Atomic Force Microscope used in the study

On the rear of an intelligent cantilever, a diode laser is engaged. The laser bar is redirected off the connected cantilever onto a double component photodiode as the tip examines the outer layer of the example, going all over the shape of the surface. The photodetector analyzes the light forces of the upper and lower photodetectors and changes the distinction over to voltage. The tip will support either a steady power or a consistent stature over the example because of input from the photodiode contrast signal, which is constrained by programming on the gadget. The piezoelectric transducer tracks continuous stature deviation in the steady power mode. The redirection power on the example is estimated in the steady stature mode. During power alignment of the magnifying lens, the checking tip adjustment boundaries should likewise be put in the affectability of the AFM head. The meagre film tests of doped and undoped ZnO were exposed to AFM investigation utilizing an Atomic Force Microscope in this exploration (Nanosurf easyscan Switzerland; Version 1.8). For the entirety of the pictures, the setpoint power was set at 20 μ N for each sweep size of 5 μ m

$\times 5 \mu\text{m}$, which yielded 256×256 information focuses. AFM information was likewise used to ascertain the root mean square unpleasantness of movies.

3.5: Optical characteristics

For hydrogen and oxygen creation, a semiconductor photoelectrode's ability to drive water separating is chiefly directed by its bandgap energy (E_g) and the space of the valence and conduction band edges relative to water redox energy levels (Aroutiounian et al., 2000). Simply a piece of the episode radiation with energy more noteworthy than the bandgap is consumed by the substrate when the semiconductor terminal in a PEC cell is enlightened. This implies that photons with less energy than the bandgap energy are not utilized for energy transformation in a PEC cell. Thus, the semiconductor utilized in PEC cells for energy transformation should have low bandgap energy. Nonetheless, a bandgap that is too little isn't useful because it will bring about lower photovoltage, which will decrease the PEC cell's proficiency considerably further (Nozik, 1978, Gratzel, 2001).

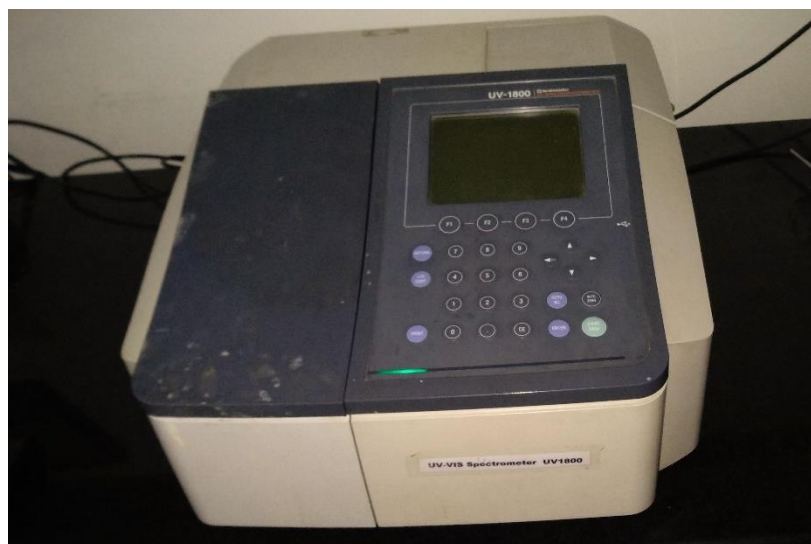


Fig 3.7: UV-Vis spectrometer used for bandgap measurement

The optical absorbance of sample films was determined using UV-Visible Spectrometer (UV -2450, Shimadzu, Japan) in this research. The edge of absorption spectra (Chaudhary et al., 2004) can be used to get a rough understanding of the bandgap energy values.

3.6: Photoelectrochemical (PEC) studies

Samples were subjected to photoelectrochemical (PEC) measurements by using them as working electrodes (WE). The experimentation included the following phases.

3.6.1: Preparation of working electrode (WE)

As mentioned in Section 3.3, the ZnO films were only deposited on 3/4 of the substrate's length. Using silver paint and copper wire, an electrical link was created from the remaining 1/4th length of the substrate. The I-V characteristics of the electrical contact were used to check for Ohmic conduct. After that, the contact and substrate edges were sealed completely with Hysol, a non-transparent and non-conducting epoxy resin (Adhesives Dexter Distributors, Singapore). Following the curing of epoxy working electrodes (WE), they were tested in a PEC cell to see whether they were suitable for water photo splitting. Powder samples were first processed into pellets before being used. In a KBr press, one gramme of sample was pressed at a pressure of 7 tonne cm⁻². To provide mechanical power, the obtained pellets were sintered at 600 °C in air. Using the method described above, an Ohmic electrical contact was formed on one surface of the pellet. When conducting PEC measurements, the other surface (referred to as the front surface) was illuminated.

3.6.2: Current (I) - Potential (V) characteristics: Measurement of photocurrent

In a three-electrode (active, counter, and reference electrodes) configuration electrochemical cell, the I-V characteristics of PEC cells were investigated using the samples prepared in this study as to working electrodes. A quartz window for incoming light was installed in the PEC cell (capacity 100 cm³). To avoid IR heating, a water jacket was placed between the working electrode and the light source. A platinum counter electrode (CE) and a saturated calomel reference electrode were used in association with the semiconductor WE (SCE). The electrolyte was a fluid NaOH arrangement (pH 12), which was cleansed with N₂ for 15-20 minutes not long before each PEC estimation. Utilizing Linear sweep voltammetry (LSV) and a 150 W Xenon Arclight, the cell's I-V attributes were determined in both murkiness and brightening.

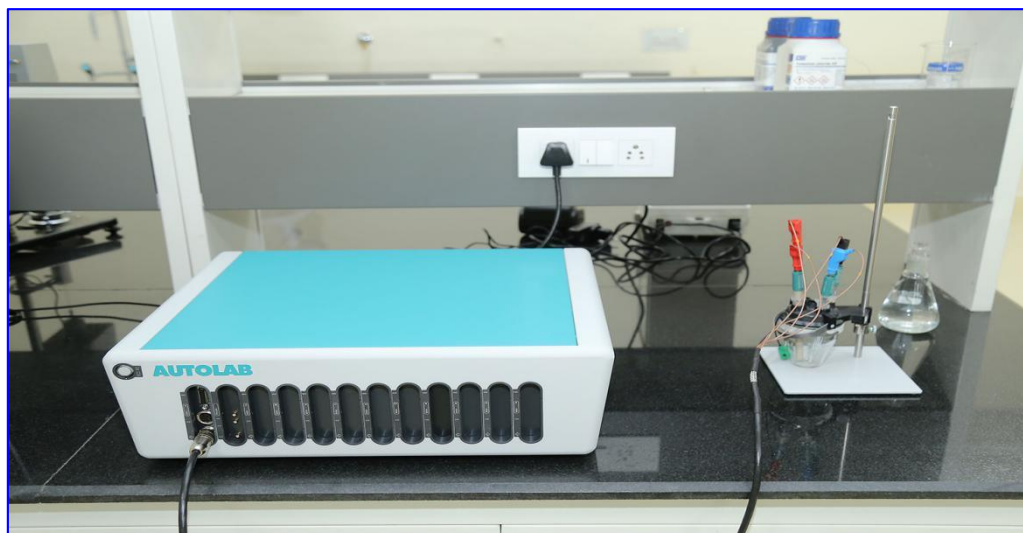


Fig. 3.8: Linear sweep voltammetry

The difference in current observed under illumination and darkness was used to calculate the photocurrent density at a specific bias. Since no other redox couple was present in electrolytic solution besides $\text{OH}^-/\text{H}_2\text{O}$, any large increase in photocurrent could be interpreted as a sign of water photoelectrolysis. Albeit no endeavours were made to gather and investigate advanced gases in this exploration, a particular development of gases as gas rises at the cathode surface was seen under high photocurrent conditions, the strength of which expanded as the photocurrent expanded.

Chapter-4

Results & Discussions

This segment diagrams the results of the new examination. Coming up next are the central matters covered:

- The combination of dainty movies of nanocrystalline ZnO become over ITO plates with different dopants (metal oxides) utilizing sol-gel/turn covering (SG) for PEC water parting is remembered for this examination.
- The investigation of items utilizing XRD, SEM, and AFM uncovered significant microstructural varieties in examples, which adversely affected their PEC execution.
- The study uncovers that the most extreme decrease (or something else) in the bandgap of wide bandgap semiconductors due to doping can't be utilized as the solitary model for deciding their reasonableness for PEC water parting. Extra fundamental microstructural changes are similarly significant and should be expanded for powerful PEC water parting.

4.1 Characterization

The designed samples were subjected to the aforementioned characterizations, which also included crystal phase analysis, microstructural analysis, surface, and optical characteristics.

4.2 ZnO Nanorods

Sample Details					
Precursor	Seed layer	Annealing Temp.	Time	Amount of Ammonia	Sample ID
ZnAc	2	500 °C	6 hr	0 ml	A

Precursor	Seed layer	Annealing Temp.	Time	Amount of Ammonia	Sample ID
ZnAc	2	500 °C	6 hr	5 ml	B
ZnAc	2	500 °C	6 hr	10 ml	C
ZnAc	2	500 °C	6 hr	15 ml	D

- ❖ **XRD:** For microcrystalline structure
- ❖ **AFM:** For Surface topography
- ❖ **SEM:** For surface morphology
- ❖ **EDS:** For chemical composition
- ❖ **UV-Visible Spectroscopy:** For Absorption Maxima and band gap
- ❖ **Dye sensitization:** By Rose Bengal Dye
- ❖ **Current-Voltage Study:** I-V curves by Potentiostat under dark and light, Short circuit current, Open circuit potential

4.2.1- XRD Analysis

For phase and crystalline size measurement, all synthesised samples were subjected to X-ray diffraction. The X-ray diffraction pattern of ZnO nanorods can be seen in Figure 4.1.

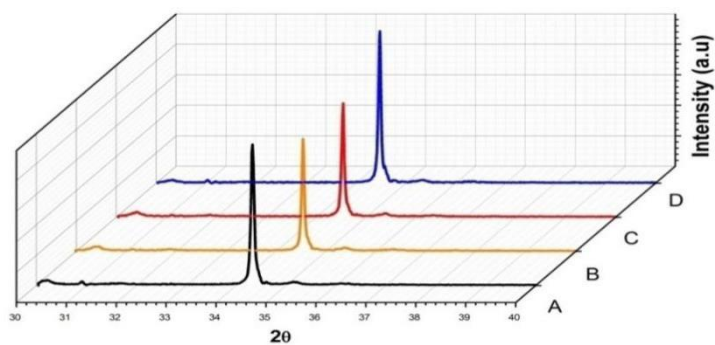


Fig 4.1: X-Ray diffraction pattern of ZnO nanorods

The X-ray diffraction pattern of ZnO nanorods generated in different chemical environments by varying the ammonia content is shown in Figure 5.1. Only one peak at $2\theta = 34.6^\circ$ was found in all of the XRD patterns, which relates to the (002) plane. There were no other significant additional peaks, indicating that nanorods are highly orientated in the (002) plane, which is perpendicular to the substrate. Similar observations were found in all of the samples, demonstrating the method's reliability. However, there is only a slight change in intensity, which could be attributed to crystallinity and nanorod size. The microstructural characteristics of ZnO nanorods are shown in the table below.

Sample ID	Crystalline Size	a	c	c/a
A	64 nm	3.249	5.204	1.6
B	52 nm	3.250	5.206	1.6
C	56 nm	3.250	5.204	1.6
D	72 nm	3.250	5.204	1.6

4.2.2 - UV-Visible Analysis

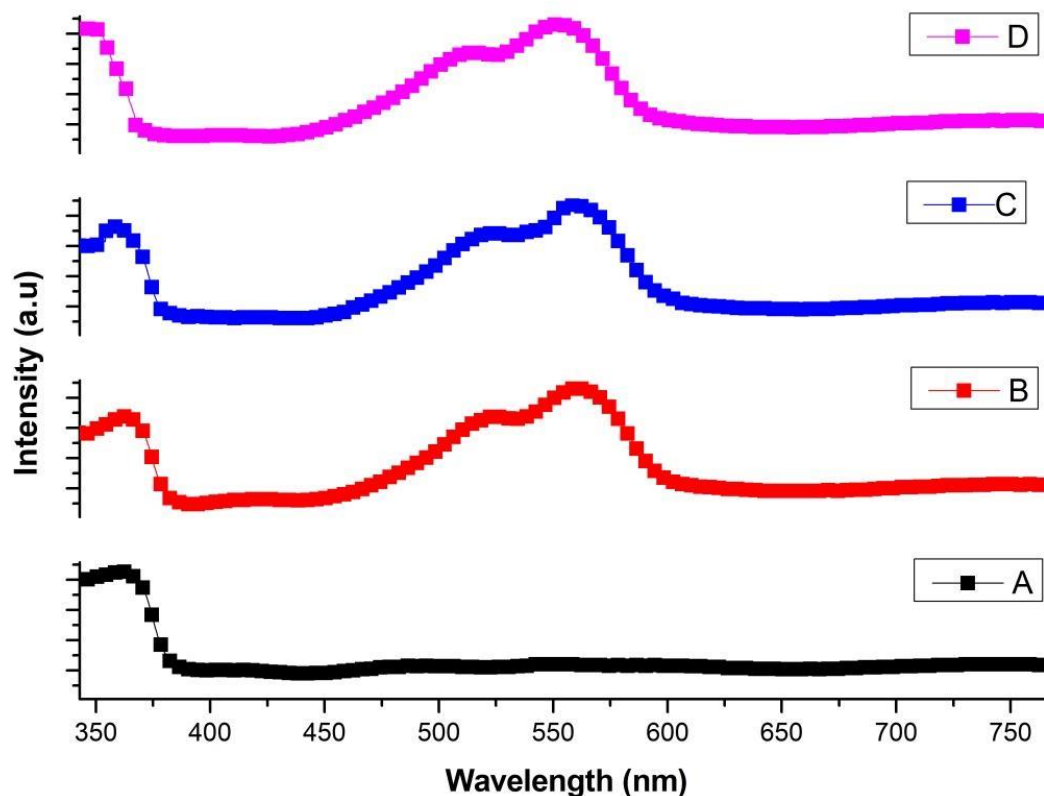
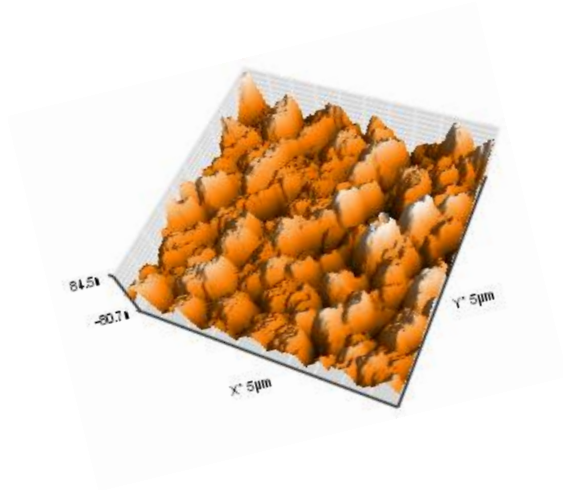


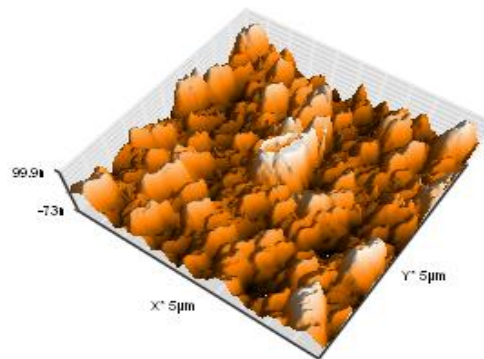
Fig 4.2: Optical Absorption of ZnO nanorods

The absorbance pattern of ZnO nanorods is seen in Figure 4.2. All of the samples have absorption in the 360-385 nm range. However, the optical absorbance of different nanorods varied. Optical absorbance increased as the ammonia content increased. Zinc ion forms a compound with ammonia as more ammonia is added, resulting in increased zinc ion solubility and ZnO nanorod development. Optical absorbance reduced as ammonia concentrations increased. ZnO degrades in high acidic and basic media because it is amphoteric. As a result, lower optical activity may be the result of increased ammonia concentrations. For all of the samples, the calculated Band Gap was 3.2 eV.

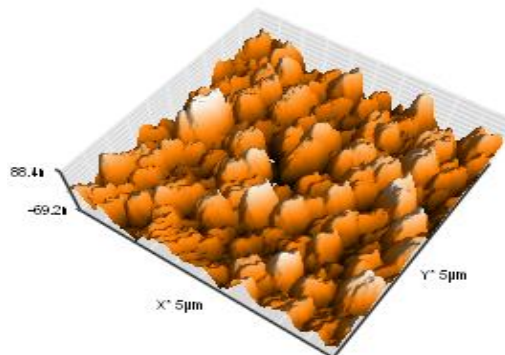
4.2.3 - AFM images



A



B



C

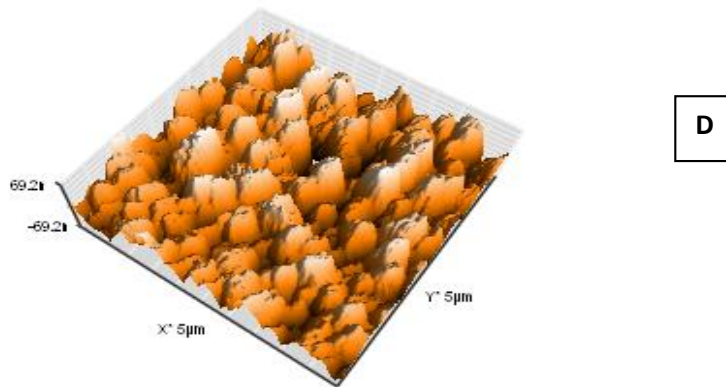


Fig 4.3: AFM images of ZnO nanorods

Figure 4.3 illustrates surface topography using AFM images, which shows a homogeneous dispersion for ZnO nanorods. There were no serious structural flaws discovered. Films were also free from any pinhole.

Sample	RMS Surface roughness
A	56 nm
B	72 nm
C	64 nm
D	78 nm

4.2.4 - SEM images

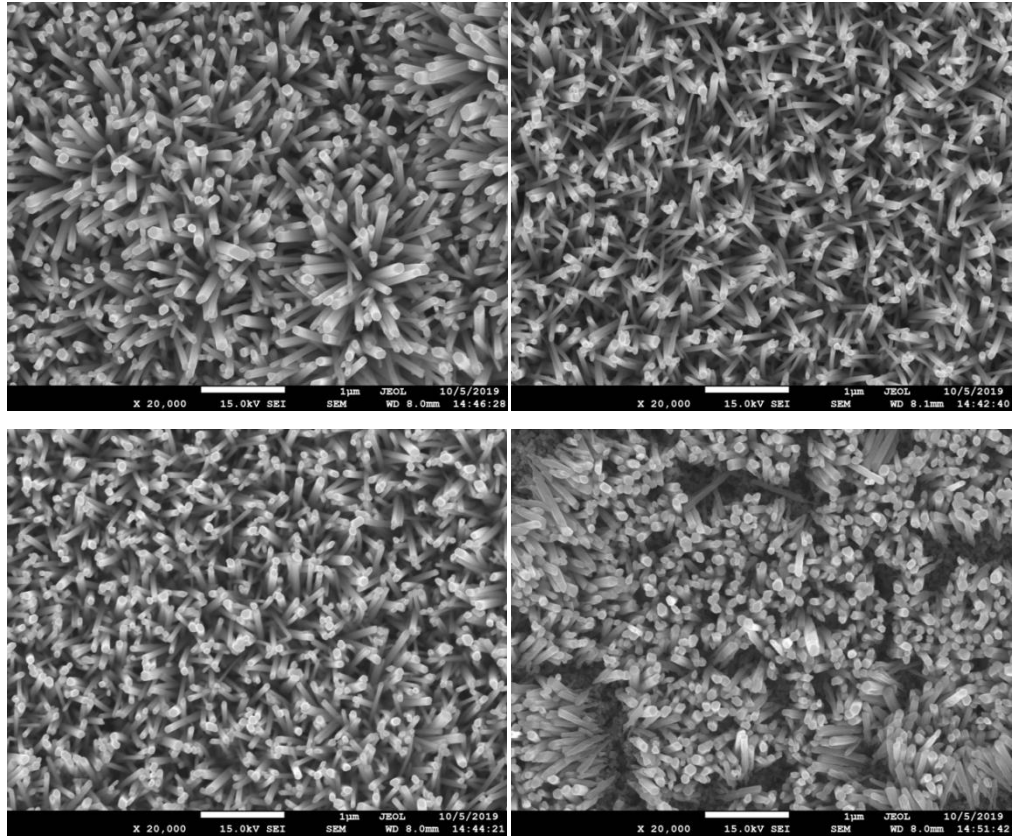


Fig 4.4: Top view of ZnO nanorods

The top view of FE-SEM images can be seen in Figure 4.4. All of the samples have well-shaped nanorods. As the ammonia concentration increased, so did the length and diameter of the nanorods. At greater ammonia concentrations, dense development of nanorods was seen, as well as certain abnormalities. Rods were pointed at lower concentrations of ammonia, but not at greater concentrations.

4.2.4.1 - Side View

Figure 4.5 depicts ZnO nanorods from the side (Sample ID-D). All of the ZnO nanorods are very well aligned along the (002) direction, as seen in the side view of FE-SEM pictures. Perpendicular to the plane, all of the rods are aligned.

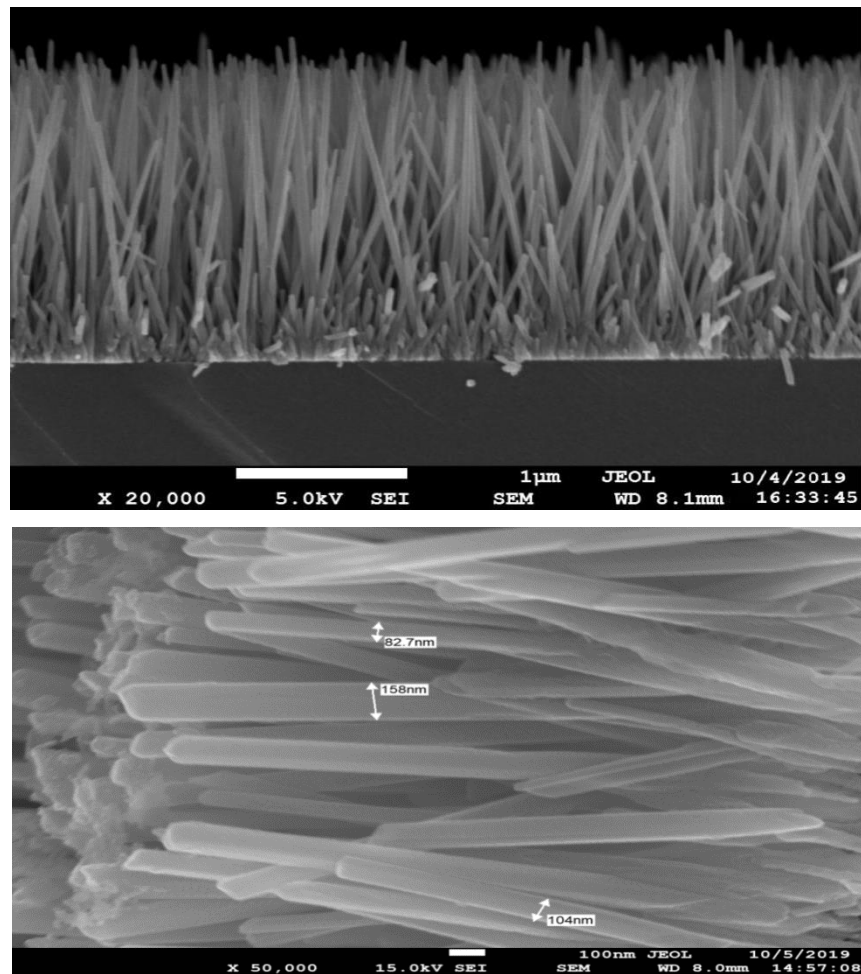


Fig 4.5: Side view of ZnO nanorods

A little bit of degradation can be noticed in the side view of SEM images of nanorods (sample ID-D). Nanorod diameters ranged from 82 to 158 nanometers.

4.2.5 - EDS

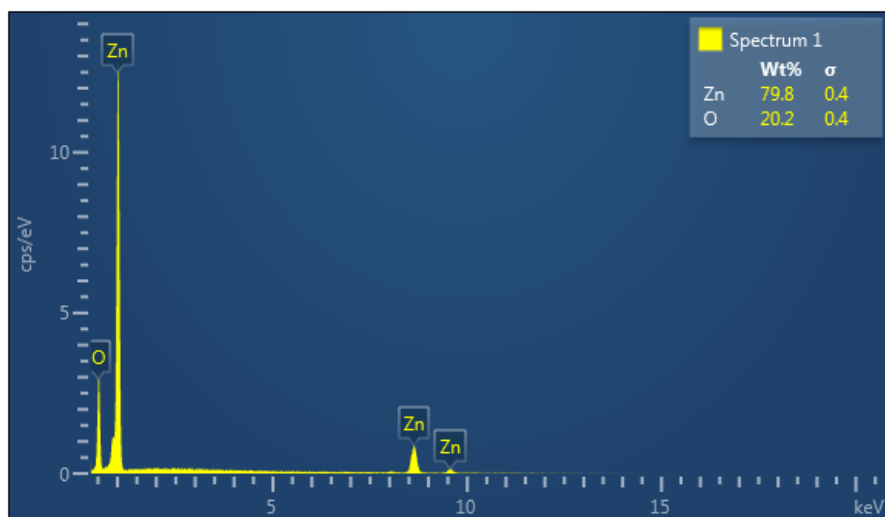


Fig 4.6: Composition details by EDS of ZnO nanorods

The Energy Dispersive X-Ray Spectroscopy had been utilized to investigate the samples. There was no other impurity discovered since the proportion obtained was 79.8% Zn and 20.2% O. This demonstrates that the samples were pure. These findings are in line with the XRD data.

4.2.6 - Dye Sensitization By Rose Bengal Dye and I-V Studies

Except for the band gap, ZnO has all of the desirable characteristics for PEC water splitting. Its band gap is around 3.3 eV, which is in the UV range, and it should be in the visible range for improved PEC efficiency. As a result, dye-sensitized ZnO films were used for PEC. For 24 hours, ZnO nanorods were immersed in a 20 ppm ethanolic Rose Bengal dye solution. Silver paste, copper wire, and epoxy hysol were used to turn the films into functioning electrodes. I-V experiments were carried out using a three-

electrode cell with a ZnO working electrode as anode and a Pt gauze cathode. As a kind of perspective anode, a standard calomel cathode was utilized. The I-V graphs were recorded in both dim and light conditions.

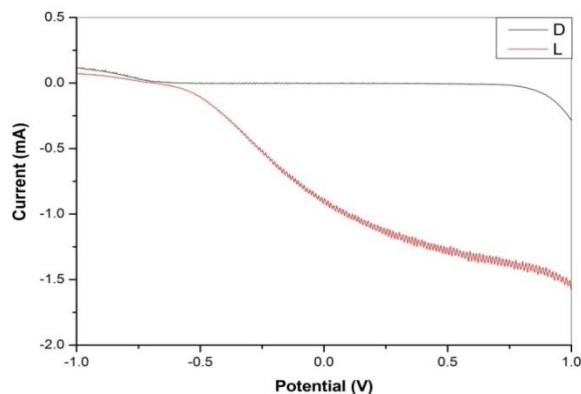


Figure 4.7.1: I-V curves of unsensitised ZnO rods

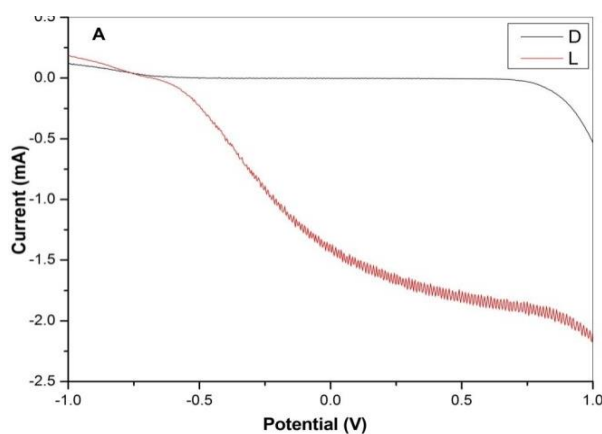


Figure 4.7.2: I-V curves of sensitised ZnO rods (sample A)

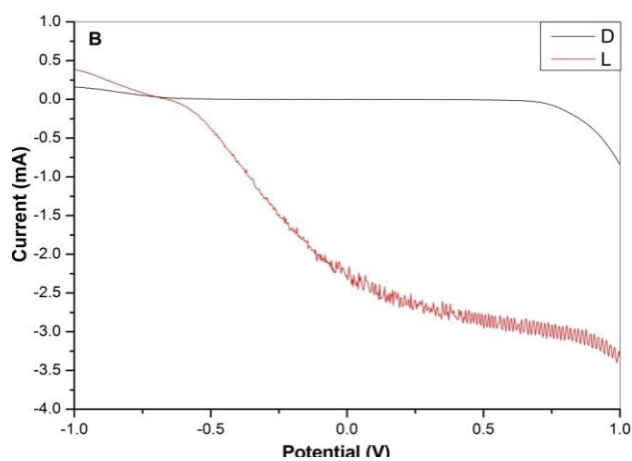


Figure 4.7.3: I-V curves of sensitised ZnO rods (sample B)

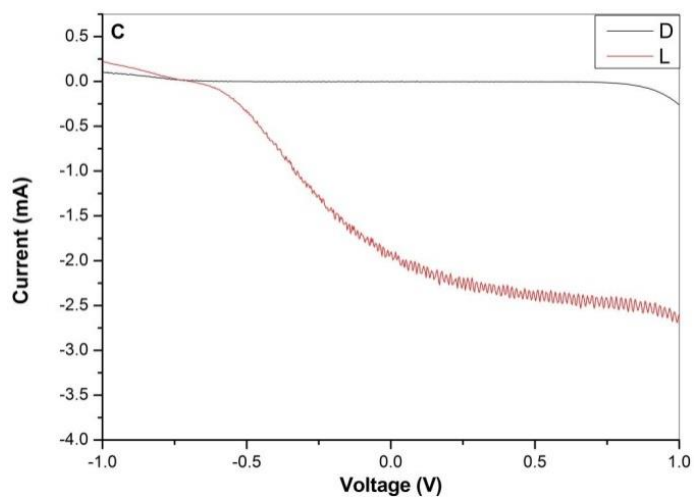


Fig 4.7.4: I-V curves of sensitised ZnO rods (sample C)

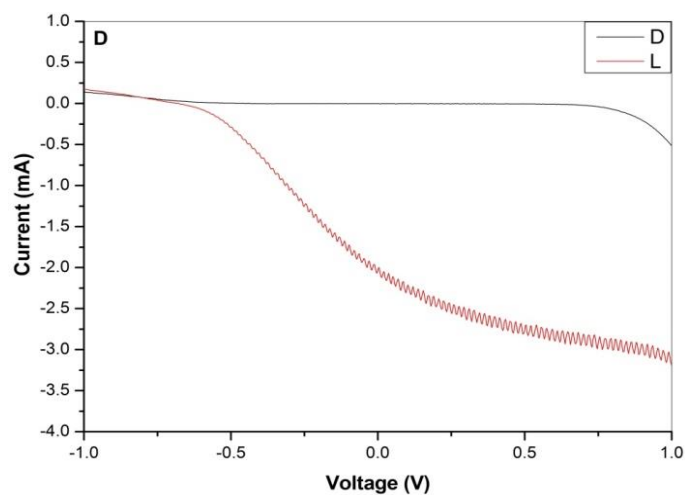


Fig 4.7.5: I-V curves of sensitised ZnO rods (sample D)

As seen in the figures, The dye sensitised ZnO nanorods provided significantly higher photocurrent than the unsensitized ZnO nanorods. With unsensitized ZnO nanorods, a short circuit current (J_{sc}) of 0.89 mA/cm² was observed, which rose considerably after dye sensitization. Increased J_{sc} indicates increased charge carrier production and charge separation. The table below depicts the various I-V characteristics of dye-sensitized ZnO nanorods. In Sample B, the highest photocurrent was measured. A modest

decrease in photocurrent was detected in samples C and D. The intense development of ZnO nanorods may be to blame for this. Gaps between nanorods are critical because they provide additional surface area for a response.

Sample	J_{sc} (mA)	V_{oc} (V)	V_{on} (V)
ZnO P	0.89	- 0.68	- 0.57
A	1.43	- 0.70	- 0.60
B	2.24	- 0.67	- 0.64
C	1.96	- 0.71	- 0.65
D	2.01	- 0.69	- 0.63

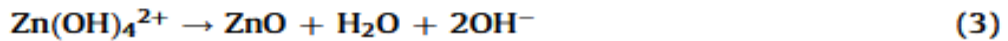
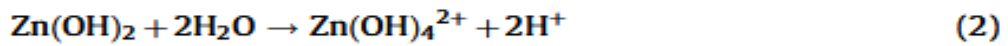
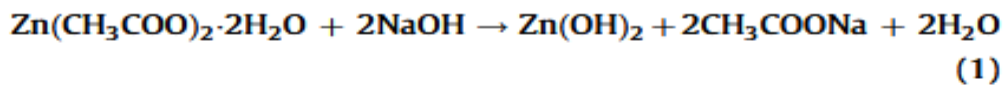
We can finish up on our discoveries that dye-sensitized ZnO nanorods delivered significant photocurrent when illuminated. The shape, size, and orientation of Nanorods, then again, affect the performance of the PEC system, subsequently, the morphology of nanorods should be optimized.

4.3 ZnO Nanoparticles at different pH:

4.3.1 - XRD

Prepared ZnO samples were exposed to X-Ray diffraction analysis, for crystalline structure and phase analysis. The presence of several peaks in the XRD design demonstrated that the samples were polycrystalline. The peaks at 2θ value 31.7, 34.4, 36.2, 47.4, 56.5, 62.8, 66.2, 67.8, 69.0 corresponding to the plane (100), (002), (101), (102), (110), (103), (200), (112) and (201) respectively, and establish the hexagonal wurtzite phase of ZnO. (JCPDS No. PDF 000-005-0664). There was no peak corresponding to any other phase, indicating that the synthesised ZnO is completely free of impurities. The peaks' high intensity also indicates that ZnO nanoparticles are very crystalline. The intensity of the peaks grew as the pH of the solution was raised,

implying that as the pH rose, so did crystallinity. The pH of the solution is significant in Sol-Gel amalgamation because the centralization of H⁺ or OH⁻ particles influences how well the metal-oxygen system polymerizes. Any variety in pH can make metal oxides change their morphology and crystallinity. The precursor concentration, temperature, and annealing temperature all affect the material's characteristics. The mechanism of ZnO production is outlined below.



The consumption of H⁺ ions during the formation of ZnO nanoparticles produces a rise in pH, which leads to deal conditions for ZnO growth. Because Zn(OH)₂ and Zn(OH)₄²⁻ are generated as intermediates in this process, ZnO production is pH sensitive. At higher pH, the positively charged Zn terminated surface attracts a significant amount of OH⁻ ions, forming a strong zinc oxide bond.

By using XRD data and Scherrer's calculation, crystalline size was determined.

$$T = K\lambda/\beta\cos\theta$$

Here, K is the space factor, λ is the wavelength, and β is FWHM in radians.

The calculated crystalline size was 29, 36, 33, and 24 nm for the ZnO prepared at pH 8, 9, 10, 12, respectively.

It was also noticed that as the pH of the peaks increased, the strength of the peaks reduced. According to reports, ZnO has an amphoteric tendency and is unstable at high pH. As a result, a drop in intensity could be linked to a higher pH. (pH 12).

Different microstructural parameters, such as lattice parameter, bond length, and strain, were estimated using XRD data, and their results are listed in the tab.

Table

Sample	a (Å)	c (Å)	c/a	Dislocation density(line ² /m ²)	U	Bond Length(Å)
pH 8	3.1896	5.2084	1.6329	1.18	0.3750	1.9531
pH 9	3.1884	5.2064	1.6329	0.77	0.3750	1.9524
pH 10	3.1870	5.2042	1.6329	0.91	0.3750	1.9516
pH12	3.1858	5.2022	1.6329	1.17	0.3750	1.9508

Variations of lattice parameters, dislocation density and bond length of ZnO nanoparticles synthesized at different pH values.

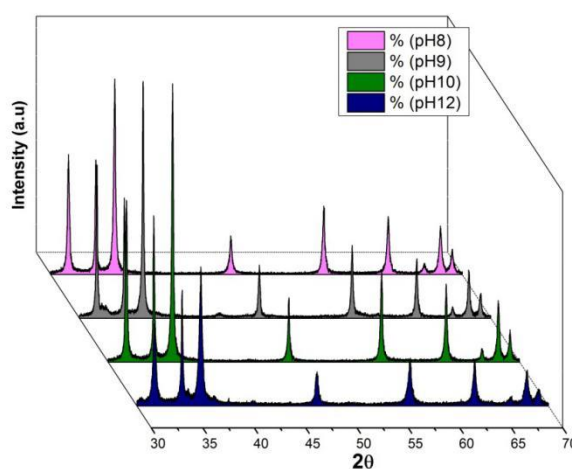


Fig 4.8: X-Ray Diffraction pattern of ZnO Nanoparticles synthesized at different pH values

4.3.2 - UV-Visible Analysis

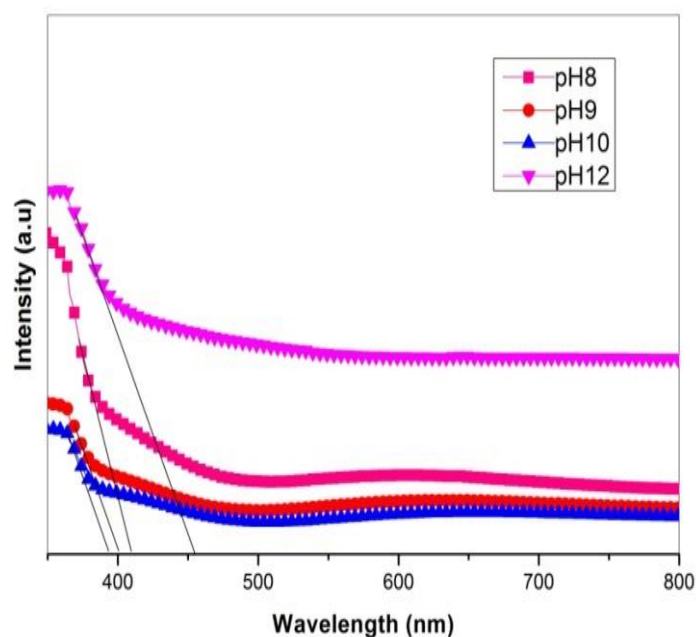


Fig 4.9: Optical Absorption of ZnO Nanoparticles at different pH

UV-Visible Spectroscopy was utilized to determine the absorption edges of nanoparticles to inspect their optical properties. ZnO nanoparticles were found to have a wavelength range of 350-370 nm. As the pH of ZnO nanoparticles increased, rising values of absorption peaks were found. This is because of the way the particle size fundamentally affects the ability of ZnO nanoparticles to retain UV radiation. Since the intrinsic band gap of ZnO is connected with electron transitions from the valence band to the conduction band, pH12 has a

higher absorbance and sharpness than different pHs, and this sharp peak uncovers the monodispersed nature of the nanoparticle's distribution.

4.3.3 - SEM images

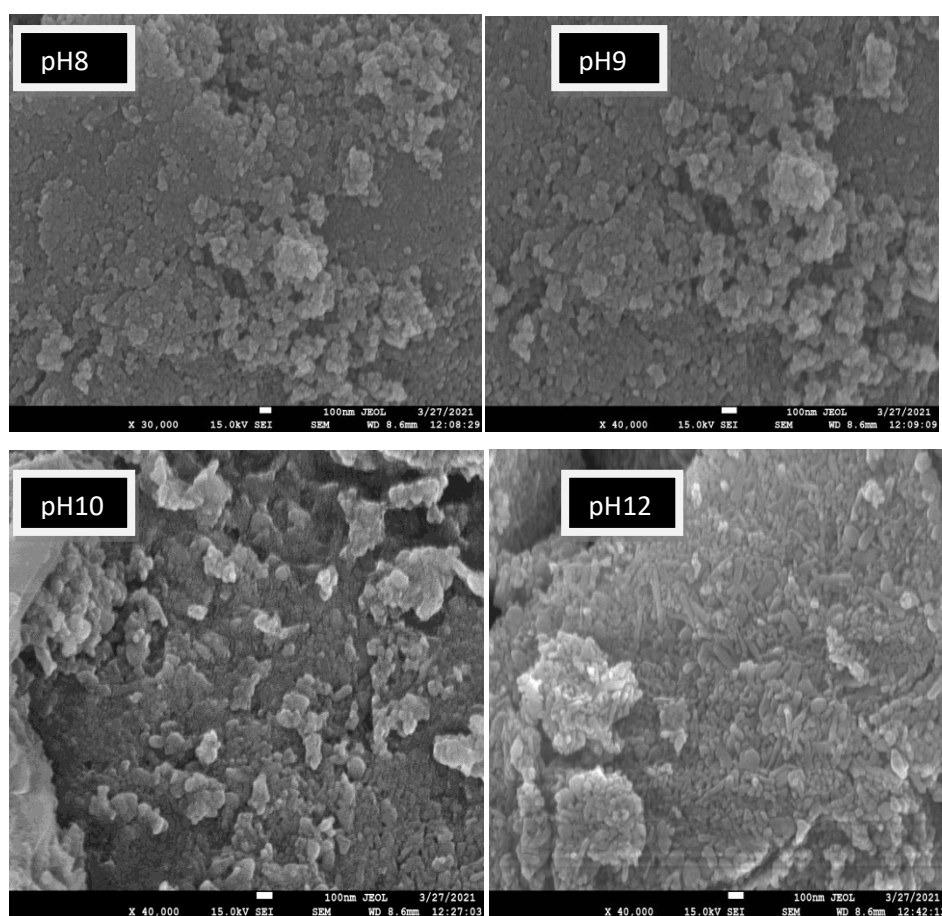


Fig 4.10: FESEM of ZnO powder synthesized at various pH values.

As shown in the image, specimens were analysed by FESEM for surface morphology. There were huge massive particles with a great deal of agglomeration. The essential and basic pHs of Zn(OH)_2 sols during the synthesis process instigated this agglomeration. Particles showed consistency and great nanostructures when the pH was

expanded to alkaline conditions. In any case, as the pH rose, crystallinity crumbled, particularly on account of pH12.

4.3.4 - EDS

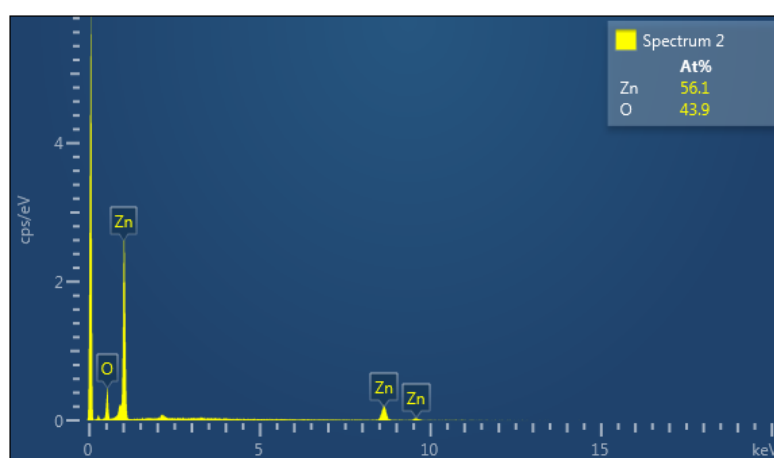


Fig 4.11: EDS of ZnO powder.

The composition of the components in the prepared sample was confirmed by EDS, which revealed 56.1 per cent Zn and 43.9 per cent O. This result indicated that the powder was free of any additional impurities.

4.3.5 - I-V Studies

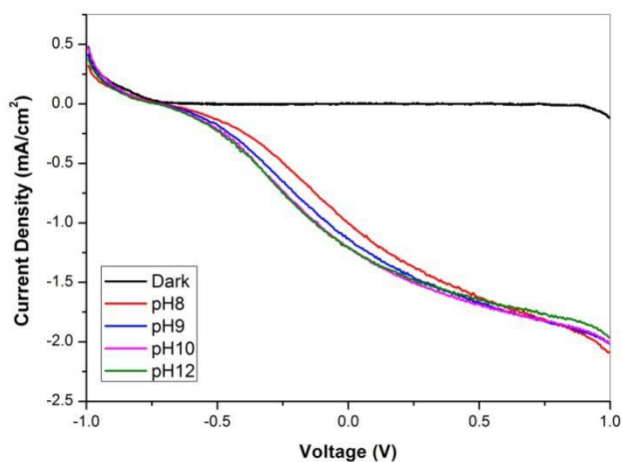


Fig 4.12: I-V curves of ZnO nanoparticles at different pH

I-V Characteristics were recorded by forming three-electrode cells (working electrode, calomel electrode and platinum electrode) in NaOH solution at pH12 by using linear sweep voltammetry. The current-Voltage pattern confirms its n-type nature. Significant charge separation was observed under illumination. As the pH increases to 12, the photocurrent also gets enhanced. At pH10 and pH12, the current density is almost the same. The table below depicts the various I-V characteristics of dye-sensitized ZnO nanorods.

Sample	J _{sc} (mA)	V _{oc} (V)	V _{ON} (V)
pH8	-1.00	-0.70	-0.63
pH9	-1.13	-0.71	-0.66
pH10	-1.20	-0.72	-0.68
pH12	-1.21	-0.72	-0.70

4.4 SnO₂ Nanoparticles:

4.4.1 - XRD

XRD was used to examine tin oxide produced by the sol-gel method. The XRD pattern of a SnO₂ nanoparticle is seen in Figure 4.13. Peaks at 2θ values 26.5, 33.8, 37.9, 38.9, 42.6, 51.7, 54.7, 57.8, 61.8, 62.6, 64.7, 65.9 and 69.2 corresponds to plane (110),(101),(220),(211),(220),(002),(221),(112),(310) and (301) respectively confirms tetragonal cassiterite Tin oxide (JCPDS NO: PDF 01-088-0287). According to the Scherrer formula, the average crystallite size is 22.2 nm, confirming the material's nanometric structure.

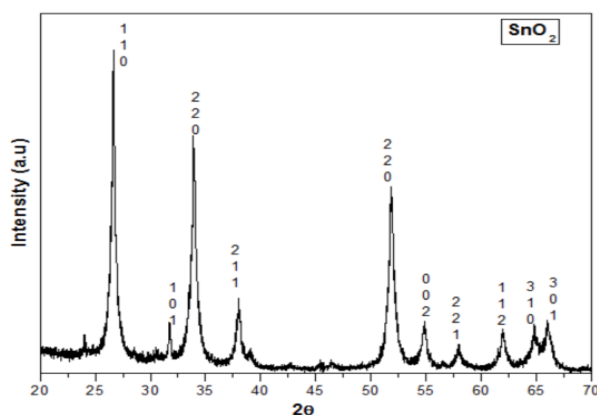
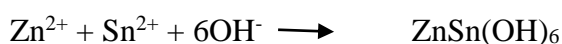


Fig 4.13:X-Ray Diffraction pattern of SnO₂ nanoparticles

4.5 ZnO-SnO₂ Nanocomposite:

4.5.1 - XRD

The XRD pattern of the ZnO-SnO₂ nanocomposite is shown in Fig 4.14. The presence of a few peaks shows that the example is polycrystalline. The hexagonal wurtzite period of ZnO and cassiterite period of SnO₂ are addressed by XRD peaks in the diffraction design, indicating that both phases were restored during solid-state synthesis. The Scherrer formula determines that the average crystallite size is 40nm, confirming the material's nanometric structure. The following equations have been used to represent the chemical reaction steps that lead to the creation of ZnSnO₃ nanocomposite:



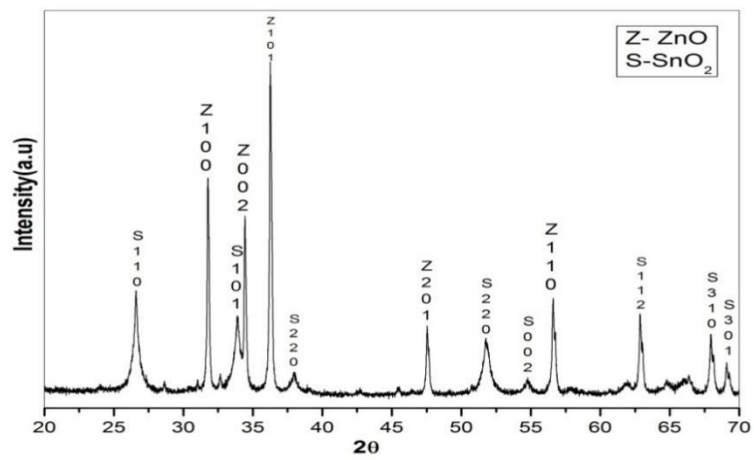


Fig 4.14: X-Ray Diffraction pattern of ZnO-SnO₂ nanocomposite

4.5.2 - UV Visible Analysis

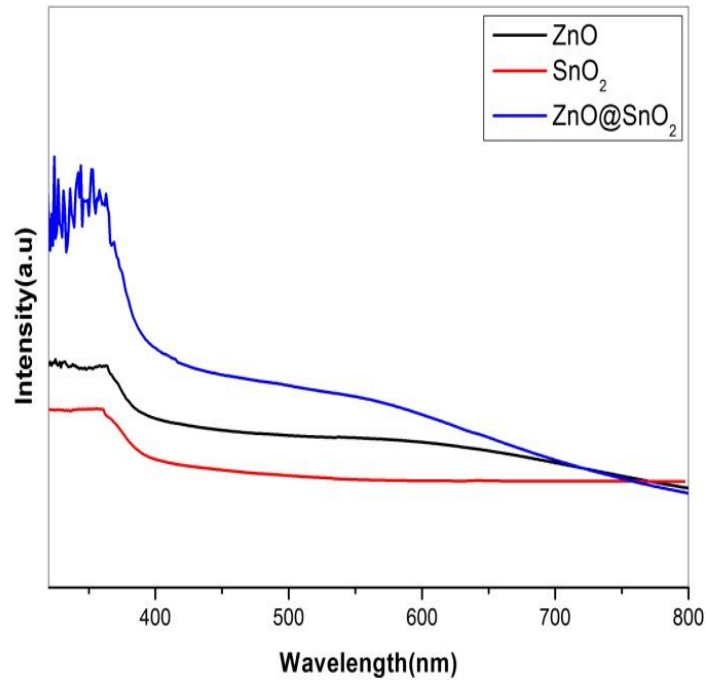


Fig 4.15: Optical Absorption of ZnO@SnO₂ nanoparticles

UV-Visible Spectroscopy was utilized to inspect the optical attributes of ZnO and SnO₂ nanoparticles. The figure portrays the assimilation range. At 350 nm, the assimilation spectra are at their pinnacle, demonstrating that electrons are being photoexcited from the valence band to the conduction band. This also demonstrates that the samples are highly crystalline. When pure ZnO and SnO₂ are mixed, the absorption edge shifts towards the higher wavelength side (redshift), as can be shown.

4.5.3 – SEM images

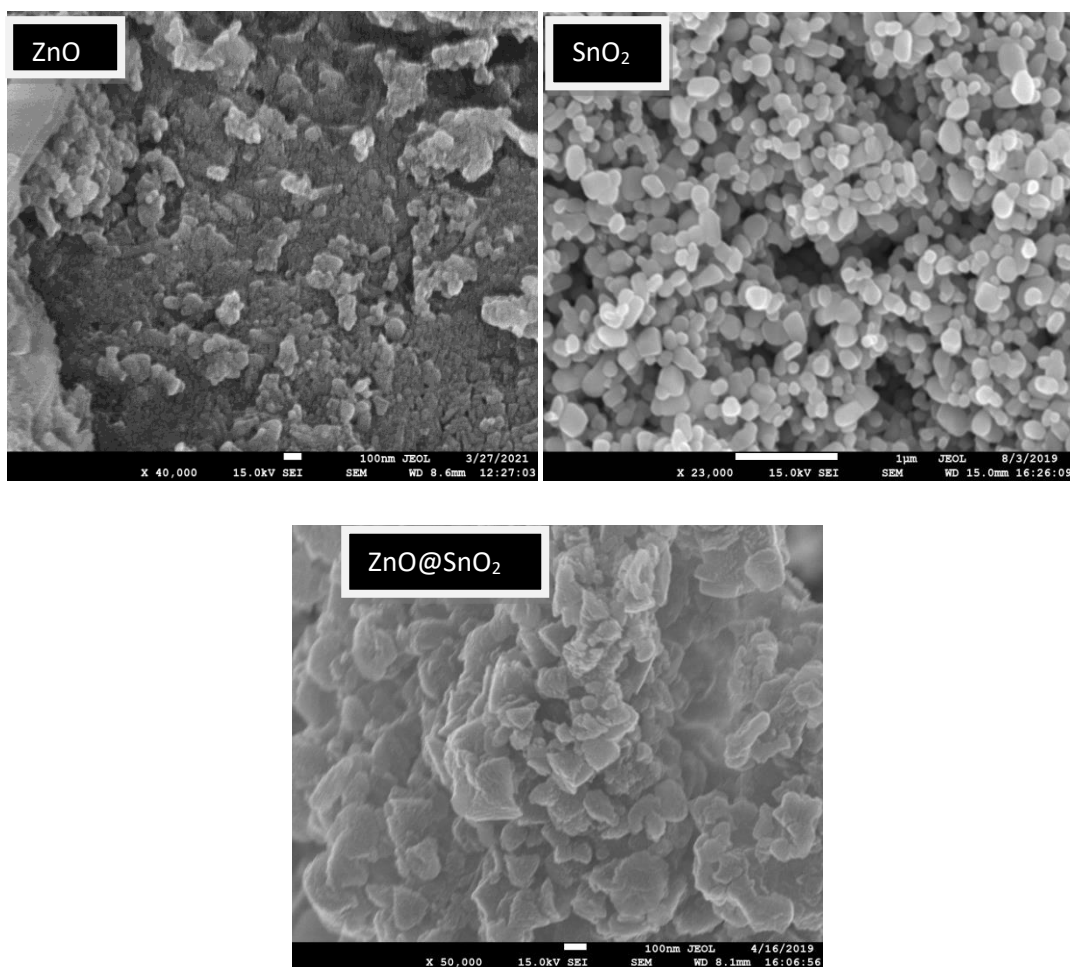


Fig 4.16: FE-SEM images of ZnO@SnO₂ nanoparticles

All of the samples were aggregates of particles whose average sizes looked to be pretty close to those calculated from the XRD patterns, according to FESEM observations provided by the micrographs above. ZnO had a hexagonal shape as shown in the images, but SnO₂ had a sphere-like morphology. The presence of both morphologies was observed in micrographs of ZnO-SnO₂ nanostructures. It was discovered that the layered structure had partially collapsed, resulting in plate-like nanoparticle aggregations.

4.5.4 - EDS

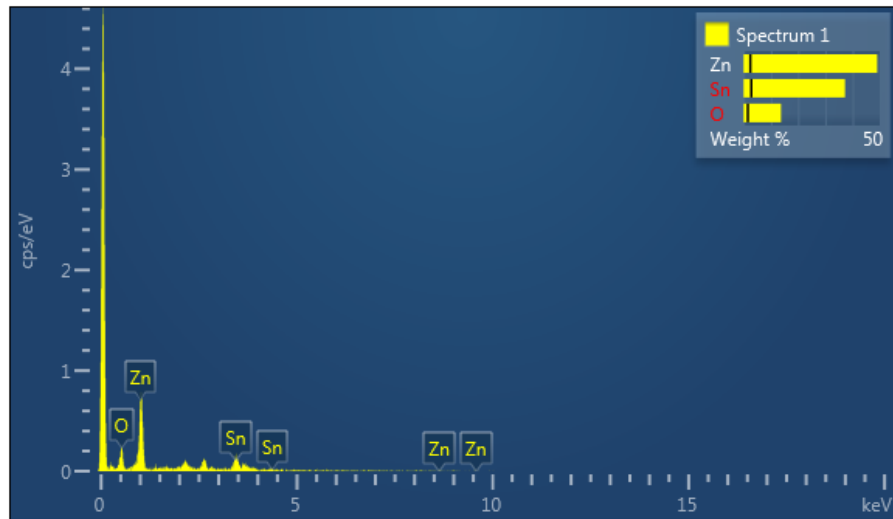


Fig 4.17: Elements of the sample measured by EDS

The energy dispersive spectrometer was used to determine the sample's composition (EDS). The analysis of the prepared sample, which contains the key components zinc, tin, and oxygen, is shown in the figure. According to the results, the sample contained 39.10 per cent zinc, 16.33 per cent tin, and 44.57 per cent oxygen. This result indicated that the powder was free of any additional impurities.

4.5.5 - I-V Analysis

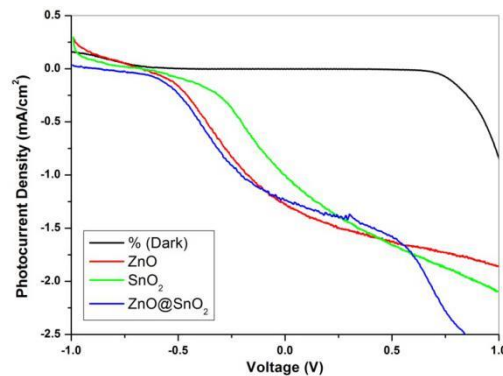


Fig 4.18: I-V curves of ZnO@SnO₂ nanoparticles

I-V Characteristics were recorded by forming three-electrode cells (working electrode, calomel electrode and platinum electrode) in NaOH solution at pH 12 by using linear sweep voltammetry. The current-Voltage pattern confirms its n-type nature. Significant

charge separation was observed under illumination. High photocurrent was observed in the amalgamation of ZnO@SnO₂. A high Short Circuit Current was observed in this case. Open Circuit current also increases in this case. The table below depicts the various I-V characteristics of dye-sensitized ZnO@SnO₂ nanorods.

Sample	J _{SC} (mA)	V _{OC} (V)	V _{ON} (V)
ZnO	-1.27	-0.67	-0.54
SnO ₂	-0.99	-0.67	-0.42
ZnO@SnO ₂	-1.22	-0.87	-0.63

4.6 TiO₂ nanoparticles:

4.6.1 - XRD

A microwave-assisted sol-gel method was used to produce nanostructured TiO₂. Microwave irradiation, unlike traditional approaches, accelerated the reaction time, resulting in adequate precipitation in just 15 minutes. The density of the samples ranged from 3.23 to 3.88 g/cm³, which is lower than the normal density of TiO₂, indicating that TiO₂ is highly porous as synthesised. The X-ray diffraction pattern of TiO₂ annealed at various temperatures is shown in Figure 4.1. Unannealed TiO₂ produced much less intense and broad peaks, showing that TiO₂ is semicrystalline. The XRD peak at 2θ 25.30 matches TiO₂, however, the other peaks are too light to be seen. TiO₂ was annealed at 400°C in the air for enhanced crystallinity. The tetragonal Anatase phase of TiO₂ underwent an exhaustive evolution, and the existence of several peaks suggests that TiO₂ is polycrystalline. Peaks at 2θ 25.35, 37.82, 48.06, 54.08, 55.15, 62.77 and 68.89 corresponding to the planes (101), (004), (200), (105), (211), (204) and (116), respectively confirms the anatase phase of TiO₂ (PDF00-064-0863). No peak corresponded to the rutile or brookite phases of TiO₂.

Scherrer's calculation was used to determine crystal size using FWHM and Integral breadth of XRD peaks, and the values are described in table 1. When compared to unannealed TiO₂, the more intense peaks show that TiO₂ has greater crystallinity because, at higher temperatures, atoms have enough thermal energy to occupy suitable

locations in the crystal lattice, resulting in better crystallisation. Two further low strong peaks were found at $23.6.8^\circ$ and 38.6° corresponding to plane (103) and plane (104) as the annealing temperature was increased to 500°C (112). As the temperature rises, more thermal energy is given to atoms to align them in a stable configuration. In XRD plots, the intensity of the peak corresponding to the plane (101) grew dramatically as the annealing temperature was increased, whereas the intensity of other peaks dropped. This indicates that crystals are orientated along all planes at 400°C , but that when the annealing temperature rises, the orientation of crystals favours the (101) plane. When the annealing temperature was increased to 600°C , a very interesting fact was noticed, namely phase transition. Along with the anatase phase, the existence of the rutile phase was reported when samples were annealed at 600°C . Additional peaks at $20, 27.5^\circ, 36.1, 41.2, 44, 54.5, 56.6,$ and 64.2° correspond to the planes of rutile TiO_2 (110), (101), (111), (210), (211), (220), and (310). (PDF 01-086-0147). In bulk TiO_2 , the rutile phase is more stable, whereas, in sol-gel processed TiO_2 , the anatase phase is preferred. The transition from anatase to rutile occurs at higher temperatures, but it is also dependent on the synthetic circumstances and chemicals used.

At various temperatures, multiple studies reveal anatase to rutile transition. In this investigation, phase transition was seen at a lower temperature than other reported phase transition temperatures. The peak corresponding to the plane (101) has a high intensity relative to other peaks, indicating that the preferred orientation was restored even after the temperature was increased to 600°C . The table below shows microscopic features of samples determined using XRD data (only major peaks are considered). Table 4.2 displays that when the annealing temperature was increased, crystalline size migrated to the higher side, which is consistent with the XRD pattern, which shows that as the annealing temperature was increased, the intensity of major peaks went up due to better crystallinity.

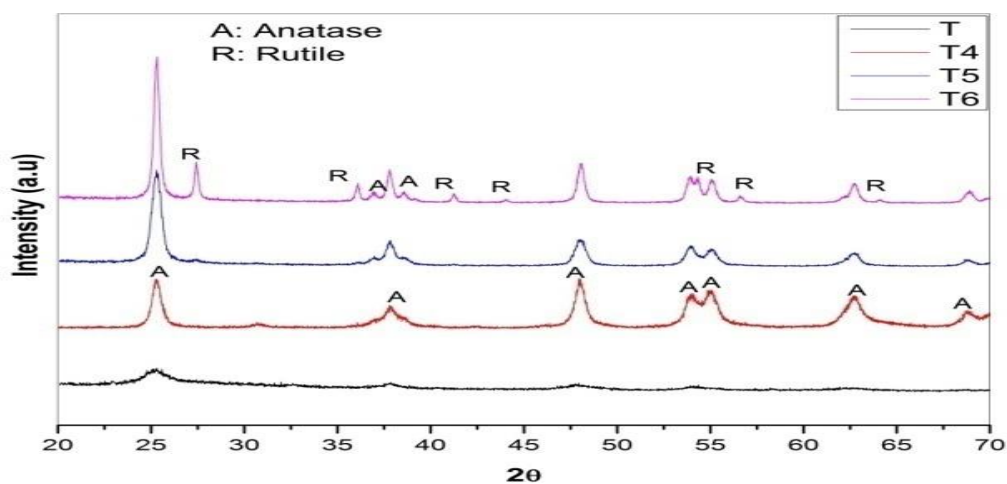


Fig 4.19: X-Ray Diffraction pattern of TiO₂ Nanoparticles at different annealing temperatures

Table: Microscopic details of TiO₂ annealed at different temperature

Sample	Peak position	FWHM	Integra I breadth (IB)	Average Crystalline Size		d spacing	Average Particle size (d.nm)	PDI
				By using FWHM	By using IB			
T	25.3	1.282	1.511	7	6	3.50953	192.4	0.255
	37.8	0.509	0.717	16	12	2.37743		
	47.8	0.737	0.981	12	9	1.89764		
	54.1	0.435	0.686	20	13	1.69152		
	62.8	0.846	0.540	11	17	1.47713		
T4	25.3	0.546	0.667	15	12	3.52350	828.1	0.387
	37.8	0.754	1.043	11	8	2.37501		
	48.0	0.616	0.718	14	12	1.89362		
	62.7	0.972	1.284	11	8	1.47996		

Sample	Peak position	FWHM	Integral breadth (IB)	Average Crystalline Size		d spacing	Average Particle size (d.nm)	PDI
				By using FWHM	By using IB			
T5	25.3	0.582	0.664	14	12	3.51456	734	0.634
	37.8	0.441	0.418	19	20	2.37743		
	47.9	0.680	0.708	13	12	1.89214		
	53.9	0.534	0.610	17	15	1.69687		
	55.0	0.430	0.442	23	23	1.66636		
	62.8	0.732	0.828	14	13	1.48026		
T6	25.3	0.364	0.423	23	19	3.50877	819.6	0.643
	27.4	0.226	0.266	37	31	3.24698		
	36.0	0.233	0.258	36	33	2.48669		
	37.8	0.299	0.332	31	28	2.37690		
	41.3	0.196	0.220	48	43	2.18768		
	48.1	0.415	0.468	23	21	1.89003		
	53.9	-	-	-	-	1.69806		
	55.1	0.352	0.360	28	28	1.66401		
	54.3	-	-	-	-	1.68781		
	62.	0.439	0.580	24	18	1.47993		

4.6.2 – UV Analysis

The absorbance of TiO₂ annealed at different temperatures was recorded using a UV-Visible spectrophotometer to explore the optical characteristics. The absorption curves of various samples are shown in Figure 4.20. In the UV area, all of the samples show significant absorption. Because the band gap is a bulk property, all of the samples have fairly similar maximum values. Optical absorbance, then again, differed as the strengthening temperature was expanded. TiO₂ that had not been annealed had a lower optical absorption, while TiO₂ that had been annealed at a higher temperature had a higher optical absorption.

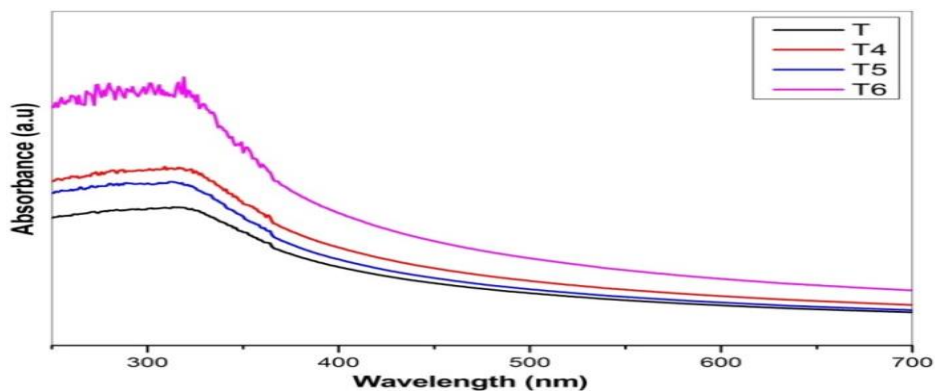


Fig 4.20: Absorbance vs wavelength curves of TiO₂ annealed at different temperature

TiO₂ annealed at 400 and 500 °C showed about the same absorption, however, TiO₂ annealed at 0 degrees Celsius showed significantly greater optical absorption with little redshift than other samples. Improved crystallinity at higher annealing temperatures may be responsible for the increase in optical absorbance. It is well known that as crystalline size increases, the band gap narrows, resulting in a red shift as in sample T6.

The particle size analyser was used in the dynamic light scattering (DLS) research, which relies on the Brownian motion of particles in dispersed solution and calculates the particle size of corresponding material based on light scattering by suspended particles. TiO₂ samples were prepared and dispersed in ethanol before being sonicated for 30 minutes. The table above shows the obtained values of average particle size in d.nm and Polydispersity Index (PDI), as well as the Polydispersity Index (PDI). The size distribution curves produced by the zeta sizer for unannealed TiO₂ and TiO₂ annealed at 600°C are shown in Figures 4.21 and 4.21.1.

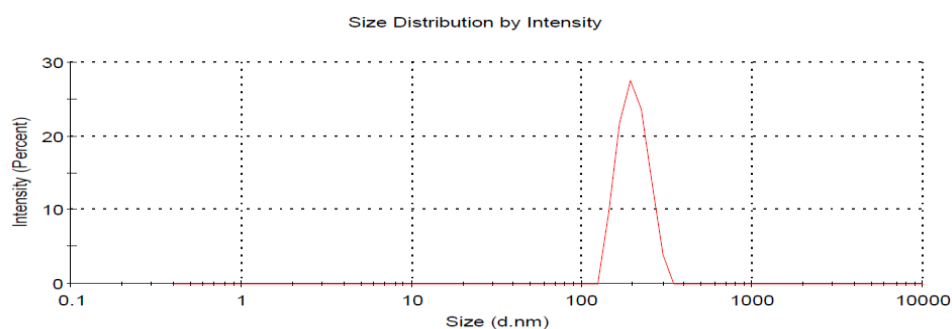


Fig 4.21: Size distribution curve of Unannealed TiO₂ (T)

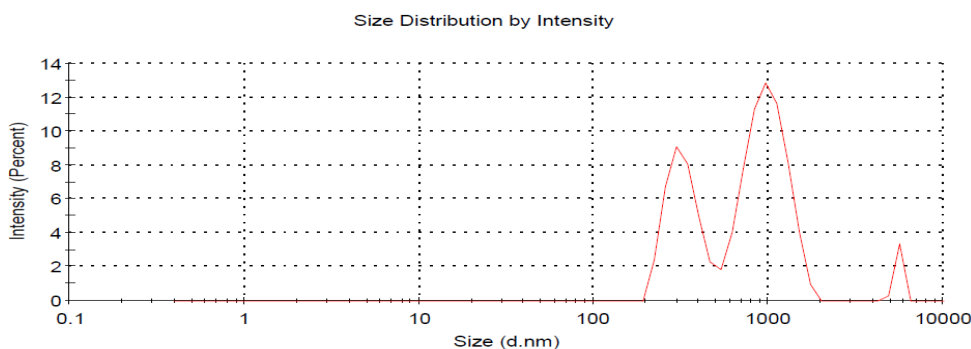


Fig 4.21.1: Size distribution curve of TiO₂ annealed at 600 °C (T6)

4.6.3 – SEM images

To determine the effect of annealing temperature on TiO₂ morphology, samples were examined using an FE-SEM with EDS measurements. FE-SEM pictures of TiO₂ annealed at various temperatures are shown in Figure 4.22. Clusters appear in SEM pictures due to the aggregation of particles with irregular crystalline shapes and sizes in the 20-30 nm range. Clear grain boundaries may be seen in samples annealed at higher temperatures, and the crystalline size matches that determined by XRD. Particles less than 30 nm, with distinct grain boundaries and consistent morphology, can be seen in sample T6.

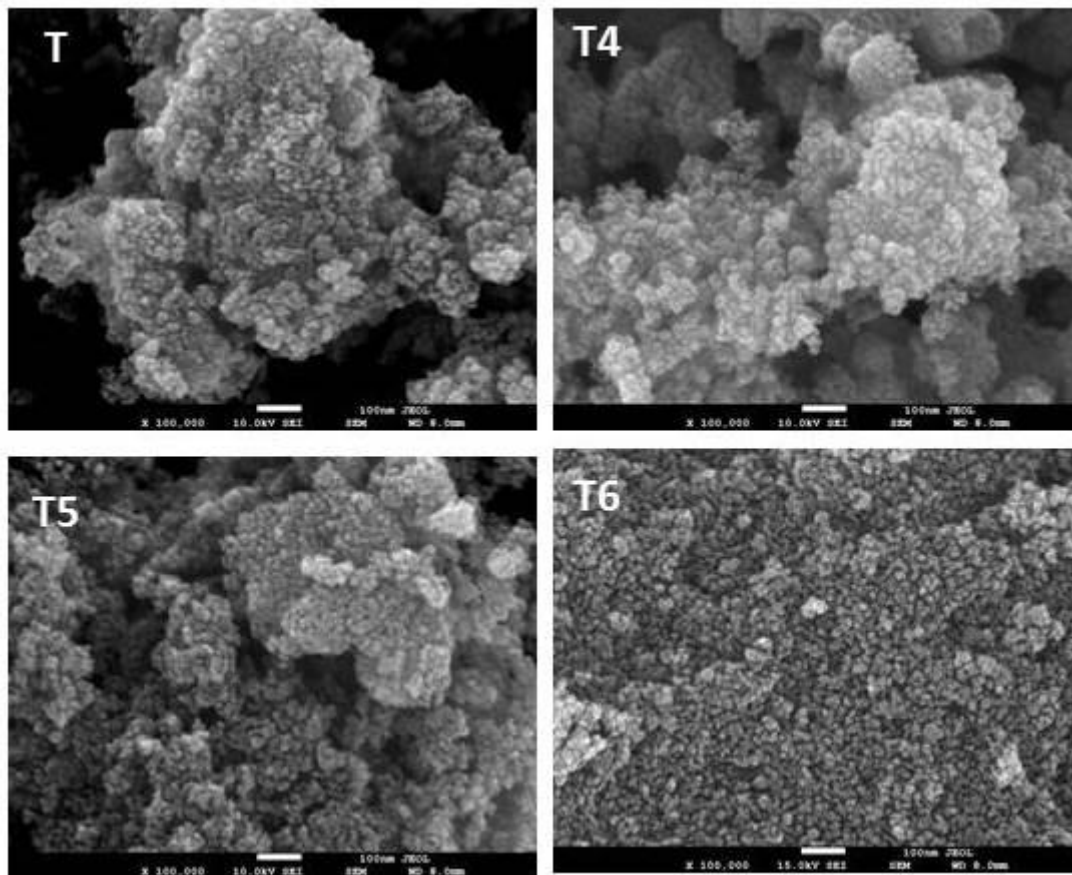


Fig 4.22: FE-SEM images of TiO₂ annealed at different temperature

4.6.4 EDS

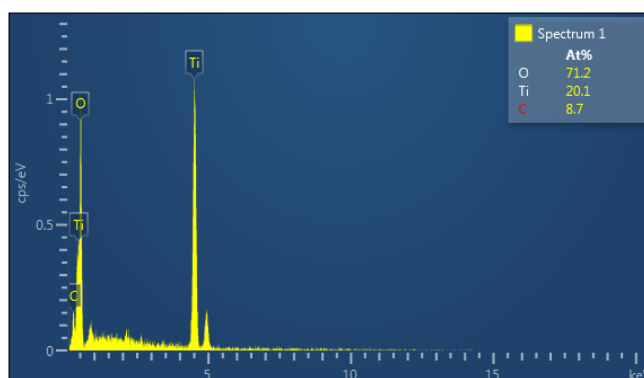


Fig 5.23:EDS measurement of TiO₂ annealed at 600 °C (T6)

Fig 5.23 shows the elemental composition of produced TiO₂ annealed at 600°C, confirming the presence of Titanium and oxygen. Carbon tape was used during the EDS measurement, hence there is an additional peak corresponding to carbon.

4.6.5 - I-V studies

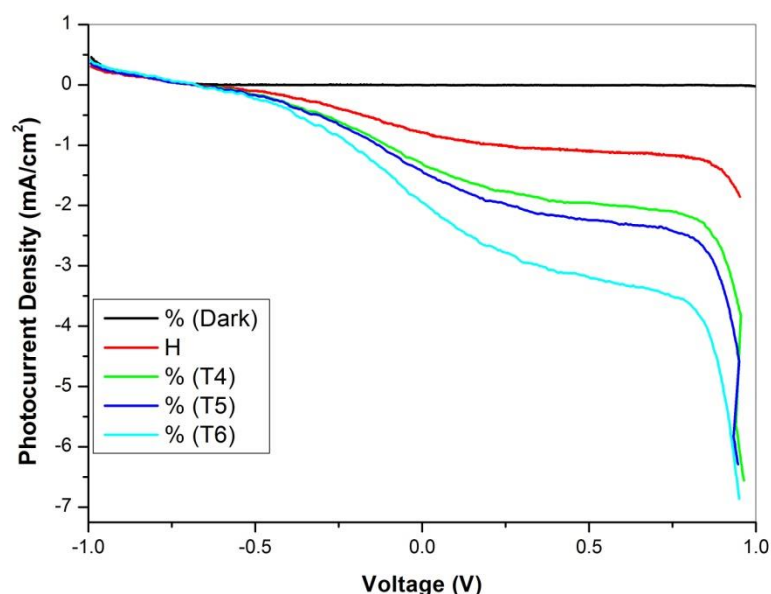


Fig 5.24: I-V curves of TiO₂ annealed at different temperatures

I-V Characteristics were recorded by forming three-electrode cells (working electrode, calomel electrode and platinum electrode) in NaOH solution at pH12 by using linear sweep voltammetry. Current-Voltage pattern confirms n-type nature. Significant charge separation was observed under illumination. High Short Circuit Current J_{sc} was increased from T to T6. T6 have a high photocurrent. The rise in short circuit current may be attributed to the rapid transportation of charge carriers. Open Circuit current density remains similar in all temperatures.

Sample	J_{sc} (mA)	V_{oc} (V)	V_{on} (V)
T	-0.78	-0.69	-0.61

Sample	J_{sc} (mA)	V_{oc} (V)	V_{on} (V)
T4	-1.30	-0.68	-0.63
T5	-1.42	-0.67	-0.65
T6	-1.43	-0.67	-0.66

4.7 TiO₂-MoS₂ nanoparticles:

4.7.1 - XRD

Solid-state synthesis was used to make the TiO₂-MoS₂ nanocomposite. The Anatase phase of TiO₂ and the Molebdenite phase of MoS₂ show extensive evolution in X-Ray diffraction patterns of TiO₂ and TiO₂-MoS₂ which are depicted in Figure 4.25. Peaks at 2θ 24.24, 37.98, 48.10, 54.10, 54.99, 62.79, 68.84 corresponding top planes (101), (004), (200), (105), (211), (204) and (116) confirms the formation of pure tetragonal Anatase phase of TiO₂ (PDF-00-021-1272). It is reported that annealing TiO₂ at 450 °C favours the formation of the anatase phase. Additional peaks at 2θ 14.34, 32.63, 49.77, 58.30 corresponding to planes (002), (100), (105) and 110 belong to Molebdenite phase of MoS₂ (PDF-00-037-1492). However, a minor presence of MoO₃ was also observed.

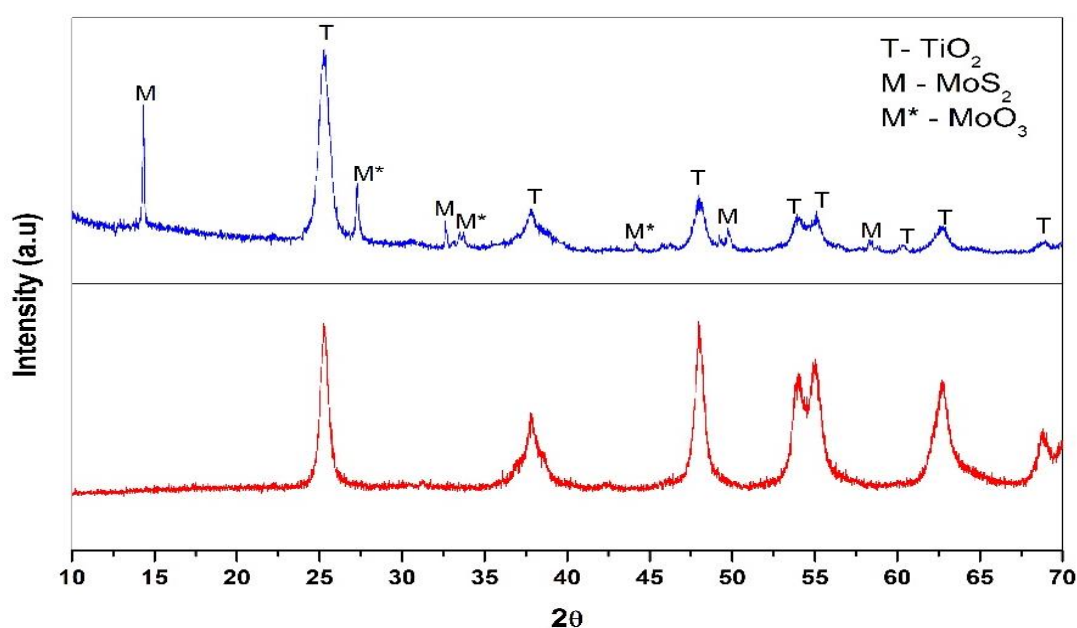


Fig 4.25: X-Ray Diffraction pattern of TiO₂-MoS₂ Nanoparticles

4.7.2 – UV Visible Analysis

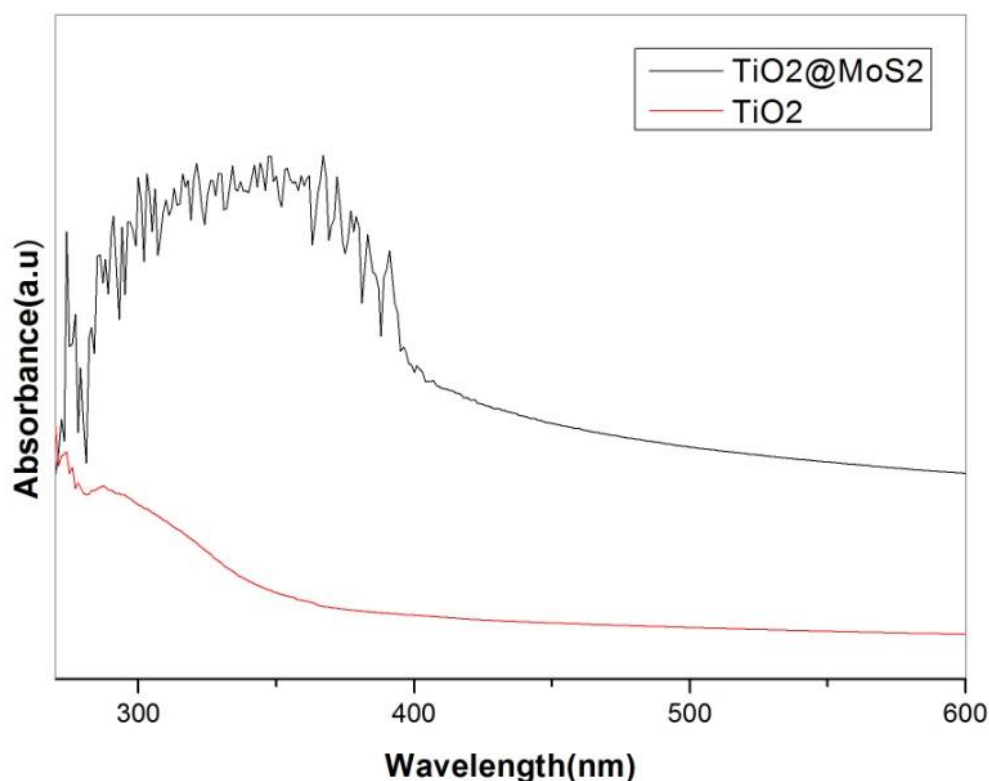


Fig 4.26: UV spectra of TiO₂–MoS₂ nanoparticles

The ultraviolet-visible (UV–Vis) absorption spectra of the samples are shown in Fig 4.26. In the case of bare TiO₂ nanoparticles, the absorption band at 350 nm corresponds to TiO₂'s intrinsic band gap. Light absorption at wavelengths over 400 nm is considerably increased after MoS₂ is introduced. In the visible light band, however, the MoS₂/TiO₂ composites showed significant differences in absorption when compared to pure anatase TiO₂ nanoparticles. All of the materials displayed considerable absorption in visible light after the reduction and deposition processes, with TiO₂/MoS₂ displaying the highest HER activity. The red shift in the combination was seen at the absorption boundaries. This indicates that charge carrier transfer and synergetic modification were crucial in the HER process.

4.7.3 – SEM images

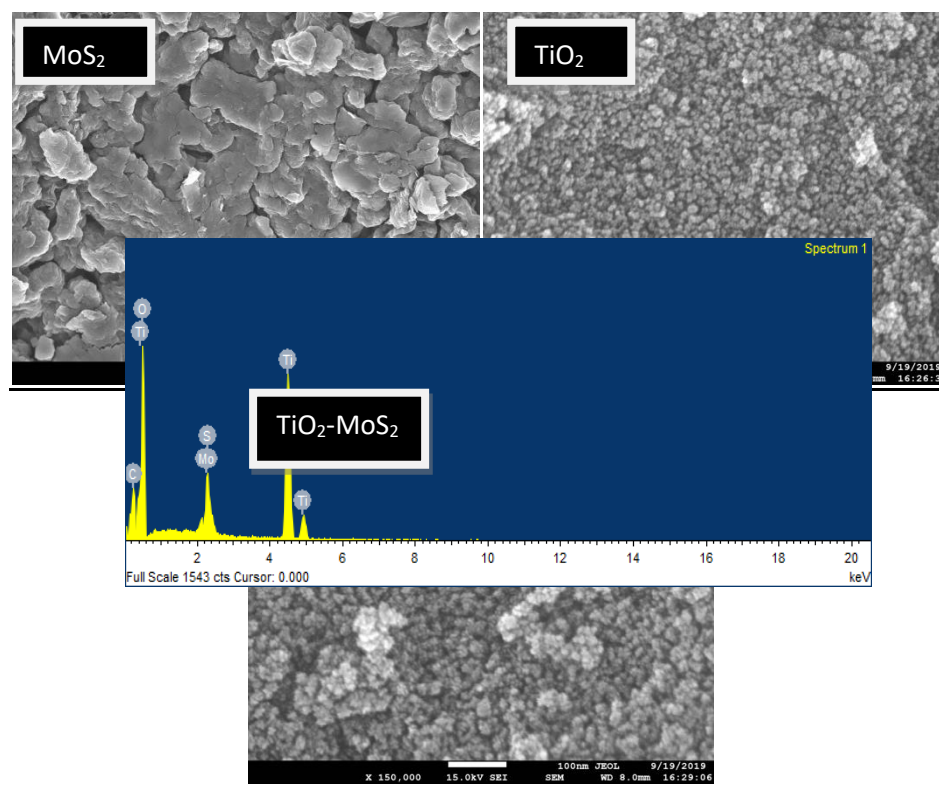


Fig 4.27: FE-SEM images of TiO₂@MoS₂ nanoparticles

Fig 4.27 presented the FESEM images of TiO₂@MoS₂ nanocomposites. TiO₂ displayed dense agglomerations and homogeneous nanocrystalline structures, while MoS₂ showed flake-like structures. It was clear when these were wrapped that the couple of layered MoS₂ nanoparticles framed on the smooth surface of the TiO₂ were straightforward and adaptable.

4.7.4 EDS

Fig 4.28: EDS of TiO₂@MoS₂ nanoparticles

Fig 4.28 shows the elemental composition of produced $\text{TiO}_2@\text{MoS}_2$, confirming the presence of Titanium, Molybdenum, Sulphur, and Oxygen. Carbon tape was used during the EDS measurement, hence there is an additional peak corresponding to carbon.

4.7.5 - I-V Analysis

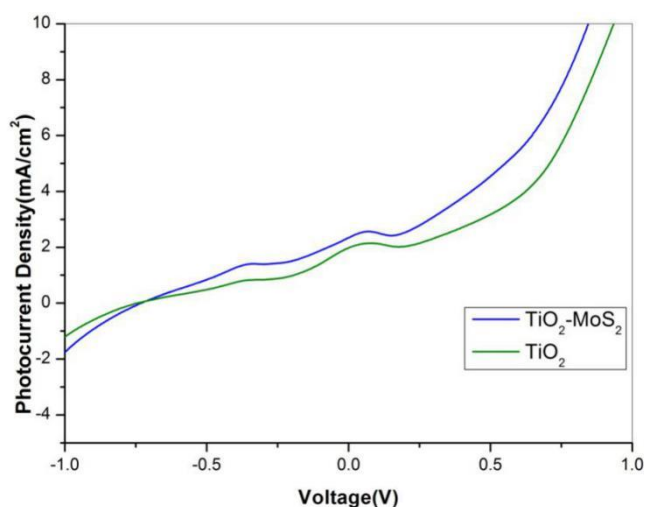


Fig 4.29: I-V curves of TiO_2 - MoS_2 nanocomposites

Sample	J_{sc} (mA)	V_{oc} (V)
TiO_2	2.00	-0.74
$\text{TiO}_2 - \text{MoS}_2$	2.40	-0.73

I-V Characteristics were recorded by forming three-electrode cells (working electrode, calomel electrode and platinum electrode) in NaOH solution at pH12 by using linear sweep voltammetry. Current-Voltage pattern confirms n-type nature. Significant charge separation was observed under illumination. The amalgam of TiO_2 - MoS_2 nanocomposites showed high photocurrent than bare TiO_2 .

4.8 ZnO/Reduced Graphene Oxide Nanocomposites:

4.8.1 - XRD

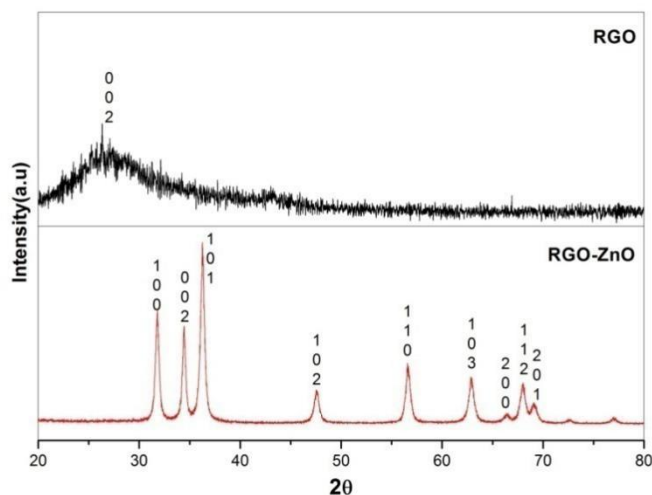


Fig 4.30: X-Ray Diffraction pattern of ZnO/RGO Nanocomposite

The structural features of the sample were investigated using an X-ray diffraction method (Cu K α radiation, $\lambda = 1.5405$, 40 kV, 30 mA). The solubility and dispersibility of graphene oxide in ZnO sol are significant factors in achieving a good composite. The peak in the ZnO-rGO composite's diffraction pattern corresponds to the (002) plane of ZnO's preferred hexagonal wurtzite structure. In the diffraction pattern, there are no peaks of GO or any other impurities. This may be related to the conversion of graphene oxide (GO) into reduced graphene oxide (rGO) during the composite preparation and calcination procedures. The rGO peak in the XRD pattern is relatively broad and weak in comparison to the highly solid peaks of ZnO, therefore it can't be traced completely. OH⁻ ions are required for the production of Zn(OH)₂ nuclei in the sol. The OH groups provided by the amine stabiliser in the sol are primarily responsible for this source. When ZnO solution comes into contact with GO sheets with a large surface area, the necessary OH groups can be derived from the OH groups of the GO sheets in a competitive reaction, resulting in GO sheet reduction. Furthermore, when GO is minimized, functional groups on its surface are eliminated, and by restoring sp² networks, more electrons of carbon atoms are regenerated. As a result, bonding between unpaired electrons and free zinc atoms can be referred to as ZnO's preferred orientation growth. It may be inferred that incorporating modest amounts of GO into ZnO nanoparticles has no significant impact on the structure of zinc oxide and that the

structure is preserved. It can also increase zinc oxide's preferred orientation, which could be considered beneficial. The photogenerated electrons are more efficiently transported and collected through a defined channel when ZnO thin films with preferred orientation growth are used. Any shift in the position of the peaks, on the other hand, could not be identified, disproving the unintentional doping of carbon into the ZnO structure.

4.8.2 - UV Visible Analysis

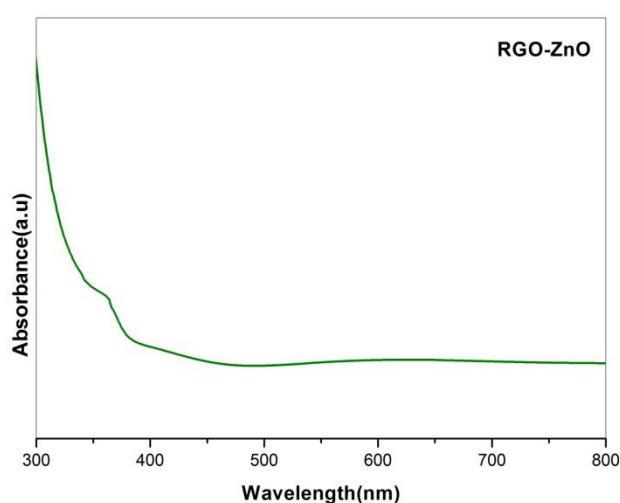


Fig 4.31: Optical Absorption of RGO-ZnO nanoparticles

Fig 4.31 portrays the UV-Vis retention spectra of RGO-ZnO nanoparticles at room temperature. Because electron moves from the valence band to the conduction band, this range uncovers a trademark retention top for RGO+ZnO nanoparticles at 370 nm. The presence of astounding glasslike and pollution-smothered ZnO nanoparticles is demonstrated by this particular assimilation top. The substance association among rGO and ZnO is answerable for a slight redshift in the assimilation edge, as noticed. The commitment of rGO, the expansion in the surface electric charge of the oxides, and the adjustment of the central course of electron-opening pair creation during illumination all add to an increment in absorbance. Accordingly, the presence of RGO in ZnO can support light retention, which is useful for photocatalytic execution.

4.8.3 – SEM images

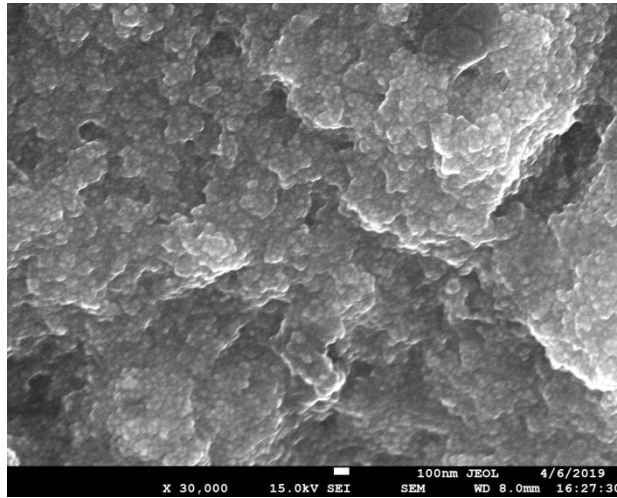


Fig 4.32: FESEM of ZnO-rGO nanocomposites

The FESEM photos of the ZnO-rGO composite show progressive permeable ZnO circles with their permeable construction, which is kept up within any event, when the ZnO/rGO composite is incorporated. ZnO nanoparticles are completely covered and designed on RGO sheets, as can be seen. The expansion of rGO diminished the size and thickness of ZnO nanoparticles.

4.8.4 - EDS

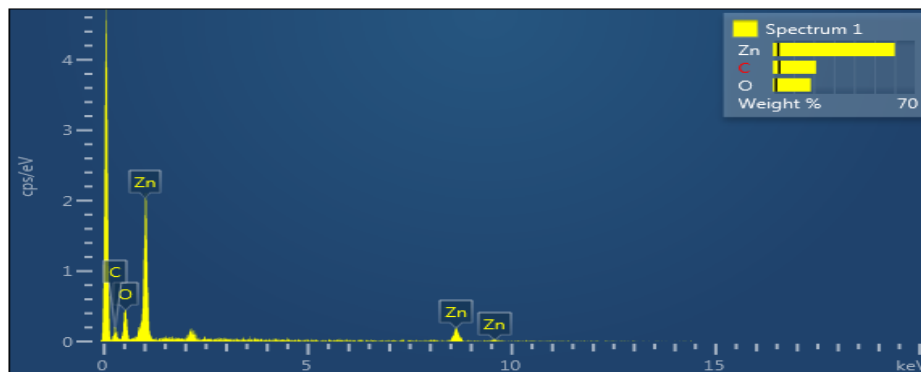


Fig 4.33: I-V curves of TiO₂ annealed at different temperatures

We can confirm the presence of Zinc, Oxygen, and Carbon in the composite through EDS.

4.9 Copper-doped Ferrite Nanoparticles:

4.9.1 - XRD

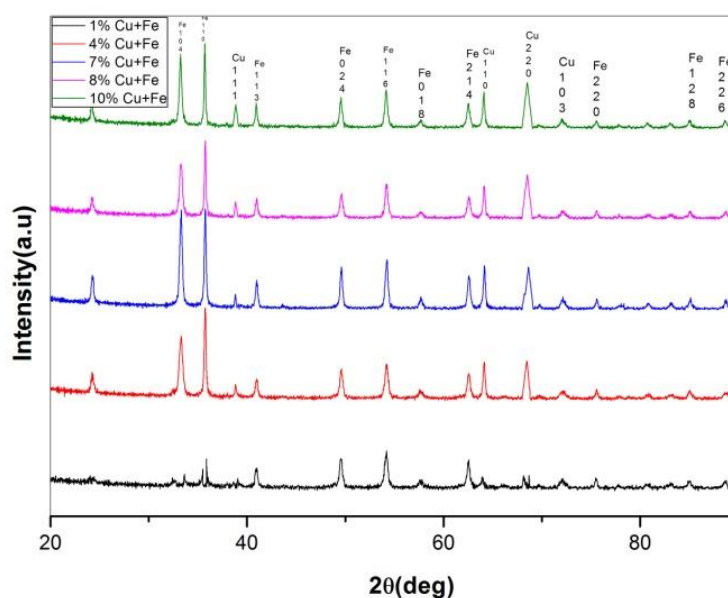


Fig 4.35: X-Ray Diffraction pattern of Copper Ferrite Nanoparticles

To assess the crystal structure and chemical content of the samples, they were produced using the sol-gel process and characterised using X-ray diffraction (XRD). An overall comparison of the four produced patterns is shown in Fig 4.35. The crystalline nature of the CuFe₂O₄ nanoparticles is demonstrated by the strong and crisp reflection peaks in the XRD pattern. It is possible to confirm that the desired CuFe₂O₄ phase is prominent in all of the trials by examining these observations. The peaks at 2θ value 24.50, 33.36, 35.89, 41.15, 49.84, 54.36, 57.63, 62.69, 75.73, 80.99, 88.77 corresponding to the plane (012), (104), (110), (113), (024), (116), (018), (214), (220), (128) and (226) respectively, which confirm the haematite phase of Fe₂O₃ (JCPDS No. PDF 01-007-9926). Moreover, smaller quantities of monoclinic CuO are also detected. The peaks at 2θ values 38.99, 63.97, 68.66, and 72.10 correspond to the plane (111), (110), (220) and (103) respectively, which confirms the formation of CuO (JCPDS No. PDF 03-065-9026). The copper oxide was generated as a result of annealing the samples in air and the presence of oxygen. Higher concentrations favour

the formation of ferrite, which is to be expected. It is feasible to make the main gauge to decide the general immaculateness of the examples if the relative pinnacle power is straightforwardly corresponding to the presence of each stage and the entirety of the examples have been estimated in a similar instrument and under similar conditions. The noticed pattern exactly affirms what thermodynamics predicts: the compound response among CuO and Fe₂O₃ is supported for higher-energy inputs. By and by, as the scale factor, top shape, and unit cell boundaries are accurately changed, the outcomes are thorough with the immaculateness of each example. The ionic radii of Cu²⁺ and Fe³⁺ are 71pm and 63 pm so because of this distinction in ionic radii top moving was normal.

4.9.2 – UV Visible Analysis

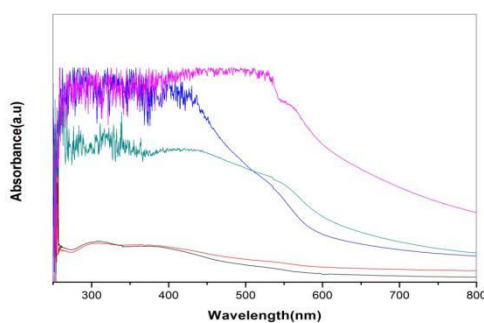


Fig 4.36:Optical absorbance of CuFe₂O₄ nanoparticles.

The UV-Vis assimilation spectra of the CuO doped ferrites nanoparticles at room temperature are displayed in the figure. After the deposition processes, all the samples of CuFe₂O₄ nanoparticles exhibited significant absorption in the visible light, It is observed that prepared samples showed the high HER activity. The absorption edges showed the redshift in the mixture. This suggests that the charge carrier transfer and synergetic modification played important roles in the HER process.

4.9.3 - SEM

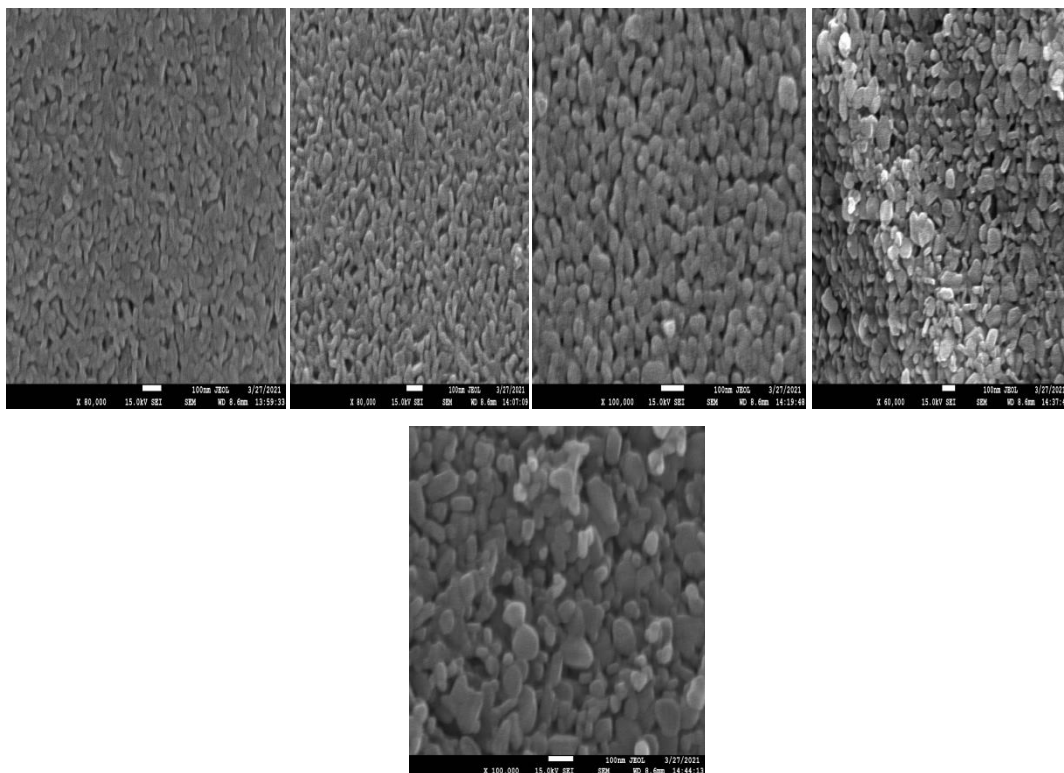


Fig 4.37:FE-SEM images of CuFe_2O_4 nanoparticles.

SEM was used to examine the physical properties of particles to have a better understanding of their morphology. The formation of micrometric clusters by the agglomeration of sub-micrometric particles can be seen in all circumstances. Little particles have been blended, however, because of the great fixation, they go about as building blocks, sintering and delivering bigger agglomerates. With these photos, it's hard to tell how huge the singular little particles are, yet it's clear that they're more modest than $1\ \mu\text{m}$. Furthermore, by looking beneath the enormous totals, one can discover a scattering of particles that are more modest in size than the agglomerates' particles.

4.9.4 - EDS

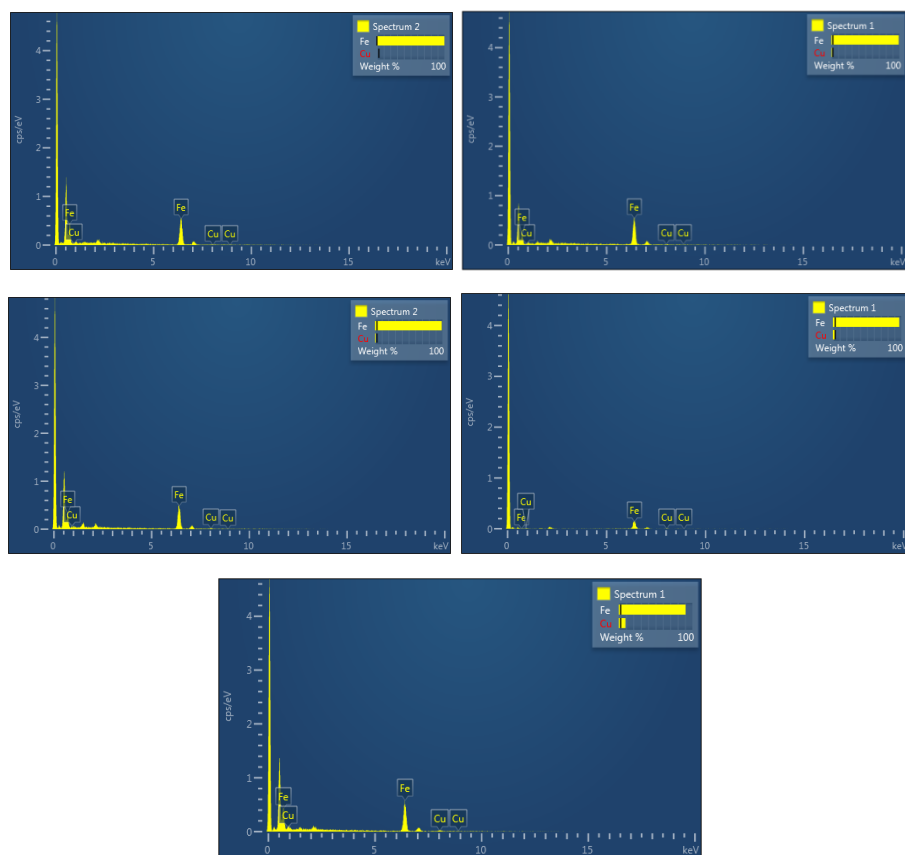


Fig 4.38: Elemental composition of CuFe_2O_4 nanoparticles

Fig 4.37 shows the elemental composition of produced CuFe_2O_4 nanoparticles, confirming the existence of Copper and Iron. Carbon tape was used during the EDS measurement, hence there is an additional peak corresponding to carbon.

4.10 - Dye Sensitization By Rose Bengal Dye & Erythrosin B and I-V Studies

The Rose Bengal dye and Erythrosin B-loaded ZnO nanoparticles were prepared and investigated. Dyes act as a photocatalyst for electron transitions from the surface into the conduction band.

4.10.1 – UV Visible Analysis

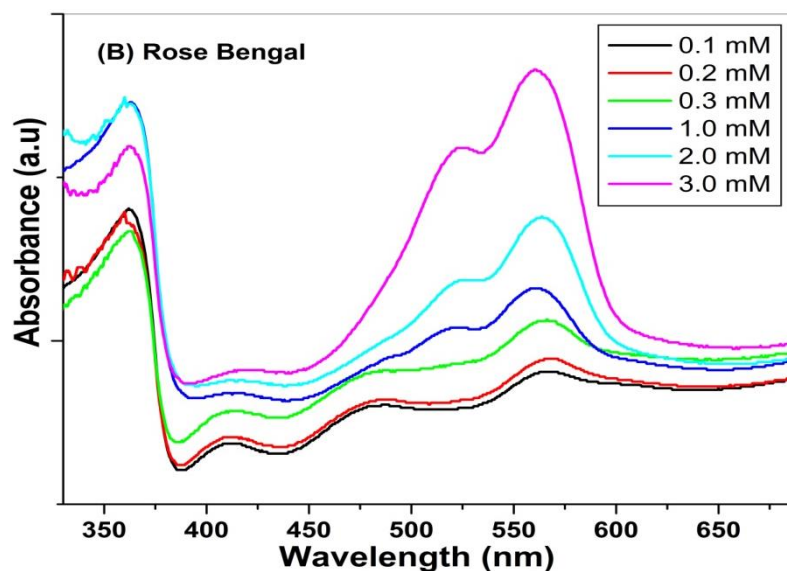
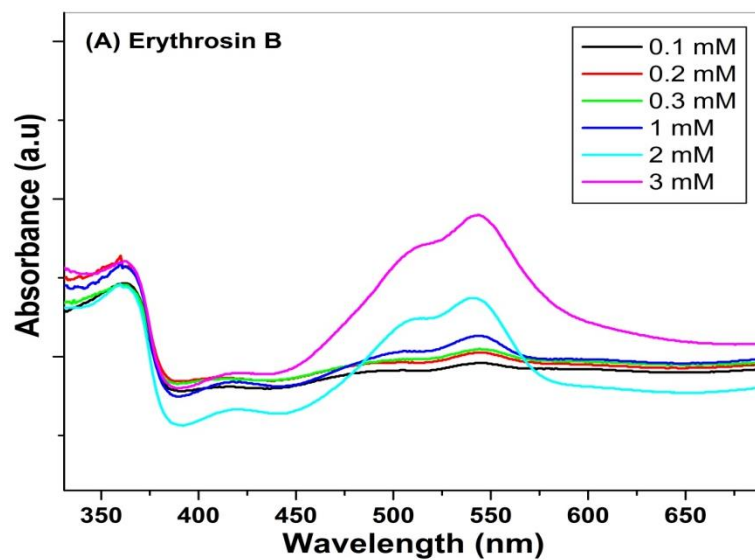


Fig 4.39: Absorbance curve of dye-loaded ZnO films with (A) Erythrosin B (B) Rose Bengal

In both cases, ZnO optical absorption is visible at about 360 nm. Absorption in the case of Erythrosin B was significant at ~550 nm while in the case of Rose Bengal it was seen around 575 nm.

4.10.2 – IV studies

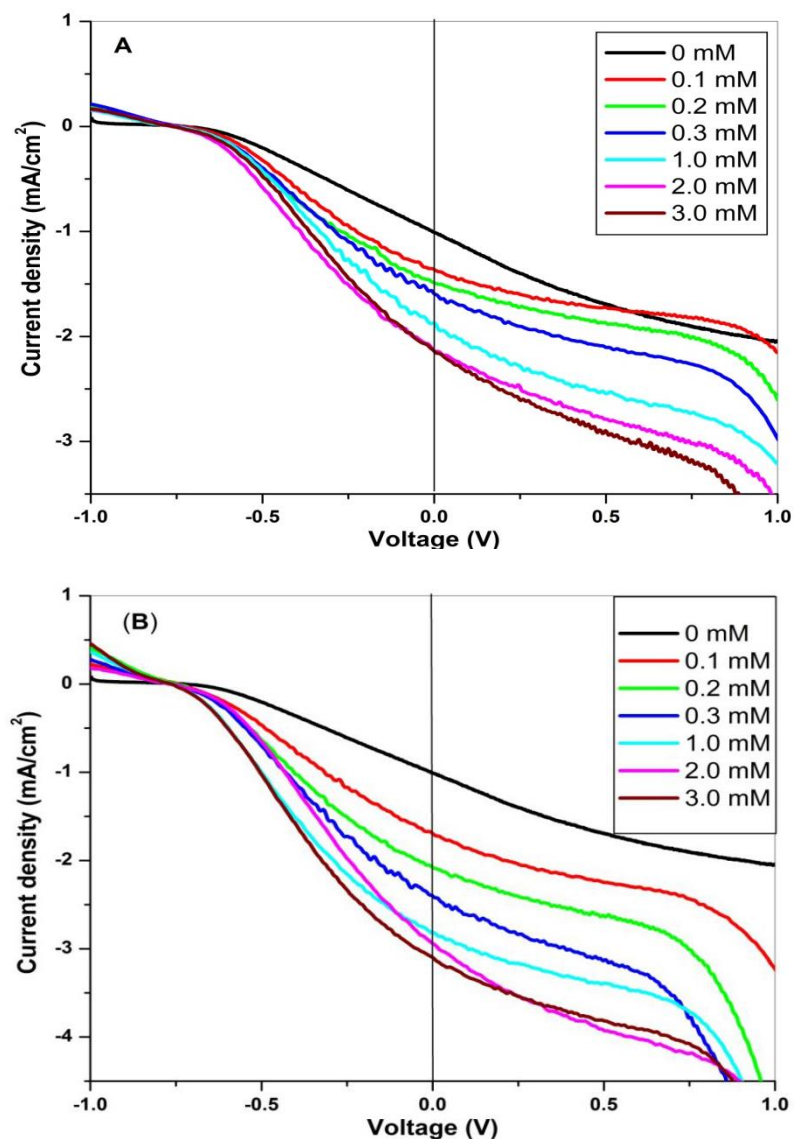


Fig 4.40: Observed IV curves of ZnO loaded with the dye of different concentrations with (A) Erythrosin B and (B) Rose Bengal

All the samples showed significant photocurrent density. At higher concentrations of dyes, saturation in photocurrent was observed. In the case of Erythrosin B, at a higher current, more saturation was observed. In the case of Rose Bengal, effective charge separation was observed may be due to stronger optical absorption in the visible region.

4.10.3 Open circuit potential and short circuit current

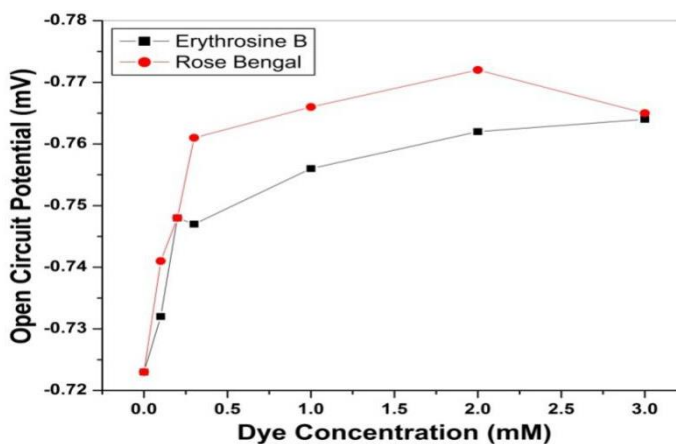
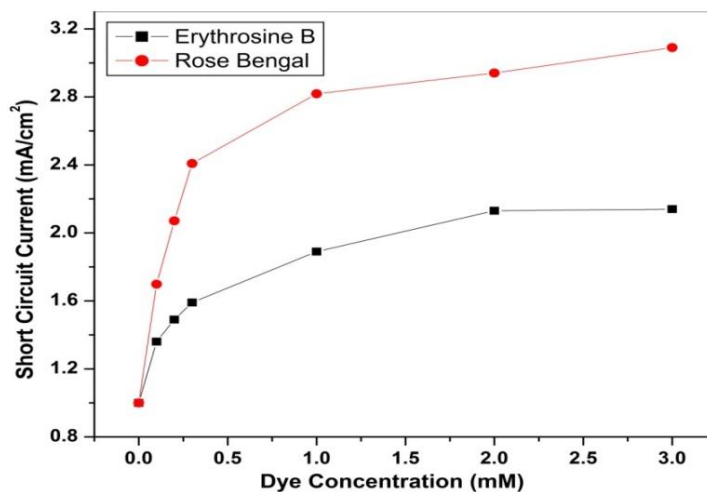


Fig 4.41: Obtained open circuit potential and short circuit current with ZnO films loaded with different concentrations of dyes.

As concentration increases, the short circuit also rises with it. Rose Bengal dye showed a significantly higher short circuit current than the Erythrosin B. While in the case of open circuit potential, the material was the same and just the dye was modified, no significant effect was seen.

This comparative study showed that Rose Bengal dye-loaded ZnO exhibit more photocurrent than ZnO with Erythrosin B dye.

Chapter-5

Conclusion

- ❖ This contemporary analysis deals with the generation of hydrogen from solar energy by the photoelectrochemical splitting of water. Much of the work in this area has remained focused on the materials (i.e. semiconductors) that can be

used as photoelectrodes. Several new dimensions have been added in recent years to this research and one such significant change in the approach is the idea of using nanomaterials (for efficient PEC splitting of water), which is being investigated with a lot of optimism and hope. The main interest in nanomaterials on this issue is generated from the following facts: (i) their enhanced surface that may yield a large area of contact with the electrolyte and may enable absorption of light; (ii) their altered band gap and band edge positions that may again critically affect the absorption of light and generation of charge carriers; and (iii) their altered microstructure and surface morphology (which would so depend upon the preparatory protocol/conditions employed) that may vary their electrical conduction property and/or charge carrier life time and mobility.

- ❖ The research presented in this thesis exhibited in the First chapter is related to the background and development of the use of renewable energies especially hydrogen as a fuel. The second chapter deals with the literature survey related to our topic of research. The third chapter is all about experiments performed and instrumentation used in the present thesis work. In the fourth chapter, all the characterization part is profoundly discussed.

ZnO Nanorods

- ❖ The X-ray diffraction pattern of ZnO nanorods generated in different chemical environments by varying the ammonia content shows only one peak at 34.6° was found in all of the XRD patterns, which relates to the (002) plane. There were no other significant additional peaks, indicating that nanorods are highly orientated in the (002) plane, which is perpendicular to the substrate. Similar observations were found in all of the samples, demonstrating the method's reliability. However, there is only a slight change in intensity, which could be attributed to crystallinity and nanorod size.
- ❖ All of the samples have absorption in the 360-385 nm range. However, the optical absorbance of different nanorods varied. Optical absorbance increased

as the ammonia content increased. Zinc ion forms a compound with ammonia as more ammonia is added, resulting in increased zinc ion solubility and ZnO nanorod development. Optical absorbance reduced as ammonia concentrations increased. ZnO degrades in high acidic and basic media because it is amphoteric. As a result, lower optical activity may be the result of increased ammonia concentrations. For all of the samples, the calculated Band Gap was 3.2 eV.

- ❖ There were no serious structural flaws discovered in AFM images. Films were also free from any pinhole.
- ❖ The top view of FE-SEM images displayed all of the samples have well-shaped nanorods. As the ammonia concentration increased, so did the length and diameter of the nanorods. At greater ammonia concentrations, dense development of nanorods was seen, as well as certain abnormalities. Rods were pointed at lower concentrations of ammonia, but not at greater concentrations. All of the ZnO nanorods are very well aligned along the (002) direction, as seen in the side view of FE-SEM pictures. Perpendicular to the plane, all of the rods are aligned.
- ❖ Energy Dispersive X-Ray Spectroscopy had been utilized to analyse the samples. There could have been no other impurity found since the extent acquired was 79.8% Zn and 20.2 per cent O. This exhibits that the samples were unadulterated.

We can finish up on our findings that dye-sensitised ZnO nanorods delivered significant photocurrent when illuminated. The shape, size, and orientation of nanorods, on the other hand, affect the performance of the PEC system, subsequently, the morphology of nanorods should be optimized.

ZnO Nanoparticles at different pH

- ❖ The peaks' high intensity indicates that ZnO nanoparticles are very crystalline. The intensity of the peaks grew as the pH of the solution was raised, implying that as the pH rose, so did crystallinity. The pH of the arrangement is significant in the Sol-Gel union because the grouping of H⁺ or OH⁻ particles influences how well the metal-oxygen structure polymerizes. The utilization of H⁺ particles during the arrangement of ZnO nanoparticles produces an ascent in pH, which prompts bargain conditions for ZnO development. Since Zn(OH)₂ and Zn(OH)₄ are created as intermediates in this interaction, ZnO creation is pH delicate. At higher pH, the decidedly charged Zn-ended surface draws in a lot of OH⁻ particles, shaping a solid zinc oxide bond. It was additionally seen that as the pH of the pinnacles expanded, the strength of the pinnacles decreased. As per reports, ZnO has an amphoteric propensity and is unsound at high pH. Subsequently, a drop in force could be connected to a higher pH. (pH 12).
- ❖ ZnO nanoparticles were found to have a wavelength range of 350-370 nm. As the pH of ZnO nanoparticles increased, rising values of absorption peaks were found. This is because of the way that the molecule size altogether affects the capacity of ZnO nanoparticles to assimilate UV radiation. pH12 has a higher absorbance and sharpness than other pHs, and this sharp peak reveals the monodispersed nature of the nanoparticle distribution.
- ❖ There were large bulky particles with a lot of agglomeration in FESEM images of the samples. The fundamental pHs of Zn(OH)₂ sols during the blend interaction incited this conglomeration. Particles showed consistency and great nanostructures when the pH was expanded to soluble conditions. Nonetheless, as the pH rose, crystallinity crumbled, particularly on account of pH12.
- ❖ The composition of the components in the prepared sample was confirmed by EDS, which revealed 56.1 per cent Zn and 43.9 per cent O. This result indicated that the powder was free of any additional impurities.

- ❖ As the pH increases to 12, the photocurrent also gets enhanced.

SnO₂ Nanoparticles

- ❖ According to the Scherrer formula, the average crystallite size is 22.2 nm, confirming the material's nanometric structure.

ZnO-SnO₂ Nanocomposite

- ❖ The presence of a few peaks in its XRD design shows that the sample is polycrystalline. The hexagonal wurtzite phase of ZnO and cassiterite phase of SnO₂ are addressed by XRD peaks in the diffraction structure, showing that the two stages were reestablished during the strong state blend. The Scherrer formula establishes that the normal crystallite size is 40nm, affirming the material's nanometric structure.
- ❖ UV-Visible Spectroscopy was utilized to look at the optical properties of ZnO and SnO₂ nanoparticles. The figure portrays the absorption spectrum. At 350 nm, the absorption spectra are at their peak, showing that electrons are being photoexcited from the valence band to the conduction band. This additionally exhibits that the samples are exceptionally crystalline. When pure ZnO and SnO₂ are blended, the absorption edge shifts towards the higher frequency side (redshift), as can be shown.
- ❖ The presence of the two morphologies was seen in micrographs of ZnO-SnO₂ nanostructures. It was found that the layered design had to some extent imploded, bringing about plate-like nanoparticle collections.
- ❖ The analysis of the prepared sample, which contains the key components zinc, tin, and oxygen, is shown in the figure. According to the results, the sample contained 39.10 per cent zinc, 16.33 per cent tin, and 44.57 per cent oxygen.

TiO₂ nanoparticles

- ❖ Unannealed TiO₂ produced much less intense and broad peaks, showing that TiO₂ is semicrystalline. The XRD peak at 2θ 25.30 matches TiO₂, however, the other peaks are too light to be seen. When compared to unannealed TiO₂, the more intense peaks show that TiO₂ has greater crystallinity because, at higher temperatures, atoms have enough thermal energy to occupy suitable low cations in the crystal lattice, resulting in better crystallisation. The transition from anatase to rutile occurs at higher temperatures, but it is also dependent on the synthetic circumstances and chemicals used. When the annealing temperature was increased, crystalline size migrated to the higher side, which is consistent with the XRD pattern, which shows that as the annealing temperature was increased, the intensity of major peaks went up due to better crystallinity.
- ❖ In the UV area, all of the samples show significant absorption. Because the band gap is a bulk property, all of the samples have fairly similar maximum values. Optical absorbance, contrarily, varied as the annealing temperature was increased. TiO₂ that had not been annealed had a lower optical absorption, while TiO₂ that had been annealed at a higher temperature had higher optical absorption. Improved crystallinity at higher annealing temperatures may be responsible for the increase in optical absorbance. It is well known that as crystalline size increases, the band gap narrows, resulting in a red shift as in sample T6.
- ❖ The particle size analyser was used in the dynamic light scattering (DLS) research, which relies on the Brownian motion of particles in dispersed solution and calculates the particle size of corresponding material based on light scattering by suspended particles. TiO₂ samples were prepared and dispersed in ethanol before being sonicated for 30 minutes.
- ❖ Clusters appear in SEM pictures due to the aggregation of particles with irregular crystalline shapes and sizes in the 20-30 nm range. Clear grain

boundaries may be seen in samples annealed at higher temperatures, and the crystalline size matches that determined by XRD. Particles less than 30 nm, with distinct grain boundaries and consistent morphology, can be seen in sample T6.

- ❖ The elemental composition of produced TiO_2 was annealed at 600°C , confirming the presence of Titanium and oxygen. Carbon tape was used during the EDS measurement, hence there is an additional peak corresponding to carbon.

TiO₂-MoS₂ nanoparticles

- ❖ Solid-state synthesis was used to make the TiO_2 - MoS_2 nanocomposite. The Anatase phase of TiO_2 and the Molebdenite phase of MoS_2 show extensive evolution in XRaydiffraction patterns of TiO_2 and TiO_2 - MoS_2 . Additional peaks belong to the Molebdenite phase of MoS_2 . However, a minor presence of MoO_3 was also observed.
- ❖ In the case of bare TiO_2 nanoparticles, the absorption band at 350 nm corresponds to TiO_2 's intrinsic band gap. Light absorption at wavelengths over 400 nm is considerably increased after MoS_2 is introduced. In the visible light band, however, the $\text{MoS}_2/\text{TiO}_2$ composites showed significant differences in absorption when compared to pure anatase TiO_2 nanoparticles. All of the materials displayed considerable absorption in visible light after the reduction and deposition processes, with $\text{TiO}_2/\text{MoS}_2$ displaying the highest HER activity. The red shift in the combination was seen at the absorption boundaries. This indicates that charge carrier transfer and synergetic modification were crucial in the HER process.
- ❖ TiO_2 displayed dense agglomerations and homogeneous nanocrystalline structures, while MoS_2 showed flake-like structures. It was obvious when these were wrapped that the few-layered MoS_2 nanoparticles cast on the smooth surface of the TiO_2 were transparent and flexible.

- ❖ The elemental composition of produced $\text{TiO}_2@\text{MoS}_2$, confirms the presence of Titanium, Molybdenum, Sulphur, and Oxygen. Carbon tape was used during the EDS measurement, hence there is an additional peak corresponding to carbon.

ZnO/Reduced Graphene Oxide Nanocomposites

- ❖ The top in the ZnO-rGO composite's diffraction pattern relates to the (002) plane of ZnO's favoured hexagonal wurtzite structure. In the diffraction pattern, there are no peaks of GO or some other impurities. It's conceivable that this is identified with the transformation of graphene oxide (GO) into diminished graphene oxide (rGO) during the composite planning and calcination procedures. The rGO top in the XRD design is moderately wide and frail in contrast with the exceptionally strong pinnacles of ZnO, along these lines it can't be followed totally.
- ❖ Due to electron moves from the valence band to the conduction band, this range uncovers a trademark assimilation top for RGO+ZnO nanoparticles at 370 nm. The presence of superb glasslike and pollutant-smothered ZnO nanoparticles is demonstrated by this unmistakable retention top. Compound association among rGO and ZnO is answerable for a slight redshift in the retention edge, as noticed. Subsequently, the presence of RGO in ZnO can help light retention, which is useful for photocatalytic execution.
- ❖ The FESEM of the ZnO-rGO composite show various levelled permeable ZnO circles with their permeable design, which is kept up with in any event when the ZnO/rGO composite is blended. ZnO nanoparticles are completely covered and brightened on RGO sheets, as can be seen. The expansion of rGO decreased the size and thickness of ZnO nanoparticles.

Copper doped ferrites nanocomposites

- ❖ The translucent nature of the CuFe_2O_4 nanoparticles is exhibited by the solid and fresh reflection tops in the XRD design. It is feasible to affirm that the ideal CuFe_2O_4 stage is unmistakable in the entirety of the preliminaries by analyzing these perceptions. The copper oxide was produced because of strengthening the examples in air and the presence of oxygen. Higher fixations favour the arrangement of ferrite, which is not out of the ordinary. It is feasible to make the first gauge to decide the general immaculateness of the examples if the relative pinnacle power is straightforwardly corresponding to the presence of each stage and the entirety of the examples have been estimated in a similar instrument and under similar conditions.
- ❖ The arrangement of micrometric bunches by the agglomeration of sub-micrometric particles can be found in all conditions. Little particles have been incorporated, yet because of the great focus, they go about as building blocks, sintering and creating bigger agglomerates. With the SEM photos, it's hard to tell how huge the singular little particles are, however, it's clear that they're more modest than 1 μm . Moreover, by looking beneath the enormous totals, one can discover a scattering of particles that are more modest in size than the agglomerates' particles.

Dye Sensitization By Rose Bengal Dye & Erythrosin B and I-V Studies

- ❖ The Rose Bengal dye and Erythrosin B-loaded ZnO nanoparticles were prepared and investigated. Dyes acts as a photocatalyst for electron transitions from the surface into the conduction band.
- ❖ In both cases, ZnO optical absorption is visible at about 360 nm.
- ❖ Absorption in the case of Erythrosin B was significant at ~550 nm while in the case of Rose Bengal it was seen around 575 nm.

- ❖ All the samples showed significant photocurrent density.
- ❖ At higher concentrations of dyes, saturation in photocurrent was observed.
- ❖ In the case of Erythrosin B, at a higher current, more saturation was observed.
- ❖ In the case of Rose Bengal, effective charge separation was observed may be due to stronger optical absorption in the visible region.
- ❖ As conc. increases, the short circuit also rises with it.
- ❖ Rose Bengal dye showed a significantly higher short circuit current than the Erythrosin B.
- ❖ Because the material was the same and just the dye was modified, no significant effect was seen in the case of open circuit potential.

Table : Comparative Analysis of the values of short circuit current and open circuit current values of prepared nanomaterials.

- ❖ As a result, we may conclude that the Rose Bengal dye's influence on the ZnO photoanode resulted in **higher Short Circuit Current** than the other experimental work performed.

SAMPLE	J_{SC} (mA/cm²)	V_{OC}(V)
ZnO Nanorods	0.81	-0.60
Dye sensitized ZnO Nanorods	2.01	0.71
ZnO nanoparticles with different pH	-1.21	-0.72
ZnO+SnO₂	-1.22	-0.87
TiO₂	-1.43	-0.67
TiO₂+MoS₂	2.40	-0.74
Erythrosin B + ZnO photoanode	2.0	-0.76
Rose Bengal + ZnO photoanode	3.2	-0.76

REFERENCES

- Abe R, Sayama K, Domen K and Arakawa H (2001), A new type of water splitting system composed of two different TiO₂ photocatalysts (anatase, rutile) and a I₃⁻/I⁻ shuttle redox mediator, Chern Phys Lett, 344, 339 - 344.

- Abn C H, Han W S, Kong B Hand Cho H K (2009), Ga-doped ZnO nanorod arrays grown by thermal evaporation and their electrical behavior, *Nanotechnology*, 20, 15601-15603.
- Abothe J (1990), Behaviour of sprayed CdS photoelectrodes etched with ammonia solution, *Sernicond. Sci. Technol*, 5, 752.
- Agarwal D C, Kumar A, Khan S A, Kabiraj D, Singh F, Tripathi A, Pivin J C, Chauhan R Sand Avasthi D K (2006), SHI induced modification of ZnO thin films: Optical and structural studies, *Nucl. Instr. Meth. Phys. Res. B.*, 244, 136-140.
- Ahn K S, Deutsch T, Yan Y, Jiang C-S, Perkins C L, Turner J, and Al-Jassim M (2007), Synthesis of band-gap-reduced p-type ZnO films by Cu incorporation, *Journal of Applied Physics*, 102, 023517.
- Ahn K S, Shet S, Deutsch T, Jiang C S, Yan Y, Al-Jassim M and Turner J (2008), Enhancement of photoelectrochemical response by aligned nanorods in ZnO thin films, *Journal of Power Sources*, 176, 387-392.
- Ajayi F F, Chae K J, Kim K Y, Choi M and Kim I S (2009), Photocurrent and photoelectrochemical hydrogen production with tin porphyrin and platinum nanowires immobilized with nafion on glassy carbon electrode, *International Journal of Hydrogen Energy*, 34, 110-114.
- Allam N K, Poncheri A J and El-Sayed M A (2011), Vertically oriented Ti-Pd mixed oxynitride nanotube arrays for enhanced photoelectrochemical water splitting, *ACS Nano*, 5, 5056-5066.
- Alpuche-A viles M A and Wuv Y (2009), Photoelectrochemical Study of the Band Structure of Zn₂SnO₄ Prepared by the Hydrothermal Method, *J Am. Chern. Soc.*, 131, 3216-3242.
- Amouyal E (1995), Photochemical production of hydrogen and oxygen from water : A review and state of the art, *Solar Ener Mat. And Solar Cells*, 38, 249-276.
- Arora G D (2000), *Crystallography and Crystal Structure*, 1st edition, Sarup and Sons, New Delhi, India.

- Aroutiounian V M, Ghoolinian M Z and Tributsch H (2000), Fractal model of a porous semiconductor, *Applied Surface Science*, 162-163, 122-132.
- Arumugam M (2011), Photovoltaic Performance of ZnO Nanosheets Solar Cell Sensitized with Beta-Substituted Porphyrin, *Journal of Nanomaterials*, 2011, Article ID 301873 - 9 pp.
- Asenjo B, Chaparro A M, Gutierrez M T, Herrero J and Klaer J (2008), Study of CuInS₂/ZnS/ZnO solar cells, with chemically deposited ZnS buffer layers from acidic solutions, *Solar Energy Materials and Solar Cells*, 92, 302-306.
- Ashrafi A (2008), Pulsed laser deposited stoichiometric ZnO thin films, *App. Surf Science*, 255, 2342- 2346.
- Ashrafi A and Jagadish C (2007), Review of zincblende ZnO: Stability of metastable ZnO phases, *J Appl. Phys.*, 102, 071101-1 - 071101-12.
- Askland D R (1996), *The Science and Engineering of Materials*, Third Edition, London, Chapman & Hall, 854.
- Atzmuller R, Schaak G and Becker C R (1996), Quantum confinement effects above the fundamental band gap in HgTe/Hg_{0.3}Cd_{0.7} Te heterostructures studied by resonant Raman scattering near the E₁ edge, *Phys. Rev. B*, 54, 16907-16918.
- Badawy W A (1997), Preparation, electrochemical, photoelectrochemical and solid-state characteristics of indium-incorporated TiO₂ thin films for solar cell fabrication, *Journal of Materials Science*, 32, 4979 - 4984.
- Bahadur Land Rao T N (1992), Photoelectrochemical studies of cobalt-doped ZnO sprayed thin film semiconductor electrodes in acetonitrile medium, *Sol. Energy Mater. Sol. Cells*, 27, 347-360 .
- Bajorowicz, B., Kobylański, M.P., Gołbiewska, A., Nadolna, J., A. and Malankowska, A.; Quantum dot-decorated semiconductor micro-and nanoparticles: A review of their synthesis, characterization and application in photocatalysis.; *Advances in colloid and interface science*, 2018, (256), 352-372.

- Bak T, Nowotny J, Rekas M and C.C. Sorrell (2002), Photo-electrochemical hydrogen generation from water using solar energy. Materials-related aspects, International Journal of Hydrogen Energy, 27,991 - 1022.
- Balamurugan B, Mehta B R, Avasthi D K, Singh F, Arora A K, Rajalakshmi M, Raghavan G, Tyagi A K and Shivprasad S M (2002), Modifying the nanocrystalline characteristics-structure, size, and surface states of copper oxide thin films by highenergy heavy-ion irradiation, J. Appl. Phys., 92, 3304 - 3307.
- Bamwenda G R, Tsubota S, Nakamura T and Haruta M (1995), Photoassisted hydrogen production from a water ethanol solution: a comparison of activities of Au-TiO₂ and PtTiO₂, J Photochem Photobio! A: Chern, 89 (2), 177 - 89.
- Bandara J and Pradeep U W (2006), Effect of Cathode thickness on the performance of the cell Lil PAN:EC:PC:LiCF₃S₀₃/PPy:DBS, Sri Lankan Journal ofPhysics, 7, 23-28.
- Bao D H, Gu H Sand Kuang A X (1998), Sol-gel-derived c-axis oriented ZnO thin films, Thin Solid Films, 312, 37-39.
- Bard A J and Faulkner L R (2001), Electrochemical Methods, Fundamentals and Applications, Second Edition, New York, John Wiley & Sons .
- Bard A J and Faulkner L R (2001), Electrochemical Methods, Fundamentals and Applications, Second Edition, New York, John Wiley & Sons.
- Bard, A. J., & Fox, M. A. (1995). Artificial photosynthesis: solar splitting of water to hydrogen and oxygen. Accounts of Chemical Research, 28(3), 141-145.
- Barpuzary D, Khan Z, Vinothkumar N, De M and Qureshi M (2012), Hierarchically grown urchinlike CdS@ZnO and CdS@Ah03 heteroarrays for efficient visible-lightdriven photocatalytic hydrogen generation, 1. Phys. Chern. C, 116, 150-156.

- Bartlett, A. A. (1986). Sustained availability: A management program for nonrenewable resources. *American Journal of Physics*, 54(5), 398-402.
- Bauer C, Boschloo G, Mukhtar E and Hagfeldt A (2004), Ultrafast relaxation dynamics of charge carriers relaxation in ZnO nanocrystalline thin films, *Chem. Phys. Lett.*, 387,176- 181.
- Belhocine-Nemmar F, Hatem M Band Boughias O (2010), Temperature Effect on the Organic Solar Cells Parameters, *World Academy of Science, Engineering and Technology*. 64.
- Benemann J R (1997), Feasibility analysis of photobiological hydrogen production, *International Journal of Hydrogen Energy*, 22, 979 - 987.
- Benouis C E, Sanchez-Juarez A and Aida M S (2007), Physics Properties Comparison Between Undoped ZnO and AZO, ZnO Doped Thin Films Prepared By Spray Pyrolysis, 1. *Applied Sciences*, 7,220 - 225 .
- Beranek R, Macak J M, Gartner M, Meyer K and Schmuki P (2008), Enhanced visible light photocurrent generation at surface-modified TiO₂ nanotubes, *Electrochimica acta*, 54, 2640-2646. Berger T, Lana-Villarreal T, Monllor-Satoca D and Gomez R (2008), Thin Films of Rutile Quantum-size Nanowires as Electrodes: Photoelectrochemical Studies, *J Phys.Chem. C*, 112, 15920-15928.
- Bhat S V and Deepak F L (2005), Tuning the bandgap of ZnO by substitution with Mn²⁺,Co²⁺ and Ni²⁺, *Solid State Communications*, 135,345- 347.
- Bilgen E (2001), Solar hydrogen from photovoltaic electrolyzer system, *Energy Conversion and Management*, 42, 1047-1057.
- Bjorkstbn U, Moser J and Gratzel M (1994), Photoelectrochemical Studies on Nanocrystalline Hematite Films, *Chem. Mater.*, 6, 858-863.
- Bolton, J. R. (1996). Solar photoproduction of hydrogen: a review. *Solar energy*, 57(1), 37-50.

- Bozleea B J and Exarhos G J (2000), Preparation and characterization of gold and ruthenium colloids in thin zinc oxide films, *Thin Solid Films*, 377-378,1-7.
- Bratin P and Tomkiewicz M 1982 *Photoelectrochemistry: Fundamental Processes and Measurement Techniques* vol. 82-3 ed. W L Wallace, A J Nozik, S K Deb and R H Wilson (Pennington, NJ: Electrochemical Society) pp 704-14.
- British Petroleum (2003), *Statistical Review of World Energy*.
- Butler M A (1977), Photoelectrolysis and physical properties of the semiconducting electrode W03, *J Appl. Phys.*, 48, 1914- 1920.
- Byrne J A, Eggins B R, Linquette-Mailley S and Dunlop P S M, The effect of hole acceptors on the photocurrent response of particulate TiO₂ anodes, *Analyst*, 1998, 123,2007- 2012.
- Caglar M, Ilican S, Caglar Y and Yalcuphanoglu F (2009), Electrical conductivity and optical properties of ZnO nanostructured thin film, *Applied Surface Science*, 255, 4491 -4496.
- Cetinorgu E, Goldsmith Sand Boxman R L (2006), Air annealing effects of the optical properties of ZnO-SnO₂ thin films deposited by a filtered vacuum arc deposition system, *Semicond. Sci. Technol.*, 21, 364- 369.
- Chandra S (1985), *Photoelectrochemical solar cells*. New York: Gordon and Breach, p. 98.
- Chandra S (1985), *Photoelectrochemical solar cells*. New York: Gordon and Breach, p.98. <https://www.fchea.org/>
- Chang C and Kuo E (2010), Light-trapping effects and dye adsorption of ZnO hemisphere -array surface containing growth-hindered nanorods, *Colloids and Surfaces A: Physicochemical and Engineering Aspects*, 363, 22-29.
- Chaudhary Y S, Agrawal A, Shrivastav R, Satsangi V and Dass S (2004), A study on the photoelectrochemical properties of copper oxide thin films, *Int. J. Hydrogen Energy*, 29, 131-136.

- Chaudhary Y S, Agrawal A, Shrivastav R, Satsangi V and Dass S (2004), A study on the photoelectrochemical properties of copper oxide thin films, *Int. J. Hydrogen Energy*, 29, 131-136.
- Chemelewski W D, Hahn N T and Mullins C B (2012), Effect of Si Doping and Porosity on Hematite's (α -Fe₂O₃) Photoelectrochemical Water Oxidation Performance, *J. Phys. Chem. C*, 116, 5255-5261.
- Chen D, Zhang H, Hu S and Li J (2008), A novel composite polymer electrolyte containing room-temperature ionic liquids and heteropolyacids for dye-sensitized solar cells, *J. Phys. Chem. C*, 112, 117-122.
- Chen Wei, Qiu Y, Zhong Y, Won K S and Yang S (2010), High-Efficiency DyeSensitized Solar Cells Based on the Composite Photoanodes of SnO₂ Nanoparticles/ZnO Nanotetrapods, *J. Phys. Chem. A*, 114, 3127- 3138.
- Chen Z, Jaramillo T F, Deutsch T G, Kleiman-Shwarsctein A, Forman A J, Gaillard N, Garland R, Takanabe K, Heske C, Sunkara M, McFarland E W, Domen K, Miller E L, Turner J A and Dinh H N (2010), Accelerating materials development for photoelectrochemical hydrogen production: Standards for methods, definitions, and reporting protocols, *J. Mater. Res.*, 25, 3-16.
- Chena W, Wang J and Wang M-R (2007), Influence of doping concentration on the properties of ZnO:Mn thin films by sol-gel method, *Vacuum*, 81, 894-898.
- Cheng S, Fu W, Yang H, Zhang L, Ma J, Zhao H, Sun M and Yang L (2012), Photoelectrochemical Performance of Multiple Semiconductors (CdS/CdSe/ZnS) Cosensitized TiO₂ Photoelectrodes, *J. Phys. Chem. C*, 116, 2615- 2621.
- Cheng Wand Ma X (2009), Structural, optical and magnetic properties of Fe-doped ZnO, *Journal of Physics: Conference Series*, 152, 012039.
- Chien C H, Chiou S H, Guo G Y and Yao Y D (2004), Electronic structure and magnetic moments of 3d transition metal-doped ZnO, *Journal of Magnetism and Magnetic Materials*, 282, 275- 278.

- Chikoidze E, Dumont Y, Jomard F and Gorochov O (2007), Electrical and optical properties of ZnO:Mn thin films grown by MOCVD, *Thin Solid Films*, 515 8519- 8523 .
- Cho I S, Chen Z, Fonnan A J, Kim D R, Rao P M, Jaramillo T F and Zheng X (2011), Branched TiO₂ Nanorods for Photoelectrochemical Hydrogen Production, *Nano Lett.*, 11, 4978-4984.
- Choi W Y, Tennin A and Hoffmann M R (1994), The Role of Metal Ion Dopants in Quantum-Sized TiO₂: Correlation between Photoreactivity and Charge Carrier Recombination Dynamics, *J. Phys. Chem.*, 98, 13669-13679.
- Coleman V A, Buda M, Tan H H, Jagadish C, Phillips M R, Koike K, Sasa S, Inoue M and Yano M (2006), Observation of blue shifts in ZnO/ZnMgO multiple quantum well structures by ion-implantation induced intermixing, *Semicond. Sci. Technol.*, 21, L25-L28.
- Connolly, J. (Ed.). (2012). *Photochemical conversion and storage of solar energy*. Elsevier.
- Coskun C, Look D C, Farlo G C and Sizelove J R (2004), Radiation hardness of ZnO at low temperatures, *Semicond. Sci. Technol.*, 19,752-754.
- Cullity B D and Stock S R (2001), *Elements of X-Ray Diffraction*, Third Edition, New Jersey: Prentice-Hall, Inc.
- Currao A (2007), Photoelectrochemical Water Splitting, *Chimia*, 61, 815-819
- Deng R, Zou Y and Tang H (2008), Correlation between electrical, optical properties and Ag²⁺ centers of ZnO:Ag thin films, *Physico B*, 403, 2004-2007.
- Diebold U, Koplitz L V and Dulub O (2004), Atomic-scale properties of low-index ZnO surfaces, *App. Surf. Science*, 237, 336-342.
- Dincer I (2002), Technical, environmental and exergetic aspects of hydrogen energy systems, *international Journal (of Hydrogen Energy*, 27 (3), 265-285.

- Djemal G, Muller N, Lachish U and Cahen D (1981), Photoelectrochemical cells using polycrystalline and thin film MoS₂/sub 2/ electrodes, *Solar Energy Mater.*, 5, 403 - 416.
- Dotan H, Sivula K, Gratzel M, Rothschild A and Warren S C (2011), Probing the photoelectrochemical properties of hematite (α-Fe₂O₃) electrodes using hydrogen peroxide as a hole scavenger, *Energy Environ. Sci.*, 4, 958-964.
- energy.gov 2021; fuelcell.pdf 2004
- Farley N R S, Staddon C R, Zhao L, Edmonds K W, Gallagher B and Gregory D H (2004), Sol-gel formation of ordered nanostructured doped ZnO films, *J. Mater. Chem.*, 14, 1087-1092.
- fchea.org
- Feng X (2004), Electronic structures and ferromagnetism of Cu- and Mn-doped ZnO, *J. Phys.: Condens. Matter*, 16, 4251-4259.
- Feng, X., Shankar, K., Varghese, O. K., Paulose, M., Latempa, T. J., & Grimes, C. A. (2008). Vertically aligned single crystal TiO₂ nanowire arrays grown directly on transparent conducting oxide coated glass: synthesis details and applications. *Nano letters*, 8(11), 3781-3786.
- Fichou D, Pouliquen J, Kossanyi J, Jakani M, Campet G and Claverie J (1985), Extension of the photoresponse of semiconducting zinc oxide electrodes by 3d-impurities absorbing in the visible region of the solar spectrum, *J Electroanal Chem*, 188, 167-168.
- Fiddes A J C, Durose K and Brinkman A W (1996), Preparation of ZnO films by spray pyrolysis, *J. Cryst. Growth*, 159, 210 - 213.
- Final report by Hawaii Natural Energy Institute, University of Hawaii-Manoa and Sen tech, Inc. Bethesda, Maryland.
- Flickyngerova S, Skriniarova J, Netrvalova M, Kovac J, Novotny I, Sutta P and Tvarozek V (2010), Surface modification of doped ZnO thin films, *Applied Surface Science*, 256, 5606-5609.
- Fretwell R and Douglas P (2002), Nanocrystalline-TiO₂-Pt photoelectrochemical cells UV induced hydrogen evolution from aqueous solutions of alcohols, *Photochem. Photobiol. Sci.*, 1, 793- 798.

- Fu-Chun Z, Zhi-Yong Z, Wei-Hu Z, Jun-Feng Y and Jiang-Ni Y (2009), First-Principles study on magnetic properties of V-Doped ZnO nanotubes, *Chin. Phys. Lett.*, 26, 016105-016109.
- Fujishima A and Honda K (1972), Electrochemical photolysis of water at a semiconductor electrode, *Nature*, 238, 37-38.
- Fukumura T, Toyosaki H and Yamada Y (2005), Magnetic oxide semiconductors, *Semicond. Sci. Technol.*, 20, S 1 03-S III.
- Gao Y and Nagai M (2006), Morphology evolution of ZnO thin films from aqueous solutions and their application to solar cells, *Langmuir*, 22, 3936 -3940.
- Garcia-Belmonte G (2010), Temperature dependence of open-circuit voltage in organic solar cells from generation-recombination kinetic balance, *Solar Energy Materials & Solar Cells*, 94, 2166-2169.
- Gartner W W (1959), Depletion-Layer photo effects in semiconductors, *Phys. Rev.*, 116, 84-90.
- Genovese M P, Lightcap I V and Kamat P V (2012), Sun-Believable Solar Paint. A Transformative One-Step Approach for Designing Nanocrystalline Solar Cells, *ACS Nano*, 6, 865-872.
- Ghosh, D., Devi, P., & Kumar, P. (2020). Modified p-GaN microwells with vertically aligned 2D-MoS₂ for enhanced photoelectrochemical water splitting. *ACS Applied Materials & Interfaces*, 12(12), 13797-13804.
- Ghosh, N. G., Sarkar, A., & Zade, S. S. (2021). The type-II nn inorganic/organic nano-heterojunction of Ti³⁺ self-doped TiO₂ nanorods and conjugated co-polymers for photoelectrochemical water splitting and photocatalytic dye degradation. *Chemical Engineering Journal*, 407, 127227.
- Ghosh R, Paul G K and Basak D (2005), Effect of thermal annealing treatment on structural, electrical and optical properties of transparent sol-gel ZnO thin films, *Materials Research Bulletin*, 40, 1905-1914.
- Gomez M, Rodriguez J, Tingary S, Hagfeldt A, Lindquist S E and Granquist C G (1999), Photoelectrochemical effect in dye sensitized,

- sputter deposited Ti oxide films: The role of thickness-dependent roughness and porosity, *Sol Energy Mater Sol Cells*, 59, 277-287.
- Gomez M, Rodriguez J, Tingary S, Hagfeldt A, Lindquist S E and Granquist C G (1999), Photoelectrochemical effect in dye sensitized, sputter deposited Ti oxide films: The role of thickness-dependent roughness and porosity, *Sol Energy Mater Sol Cells*, 59, 277-287.
 - Gratzel M (2001), Photoelectrochemical cells, *Nature*, 414, 338-344.
 - Green M A (1992), *Solar Cells*, Kensington: The University of New South Wales, 274.
 - Grimes C A, Varghese O K and Ranjan S (2008), *Light Water Hydrogen: The Solar Generation of Hydrogen by Water Photoelectrolysis*, ISBN: 978-0-387-33198-0, Springer.
 - Grundmann M, Wenckstern H V, Pickenhain R, Nobis T, Rahm A and Lorenz M (2005), Effects of oxygen-gas flow rate on lattice dynamics and microstructure for Ga-doped ZnO thin films, *Superlattices and Microstructures*, 38, 317- 328.
 - Guillen E, Casanueva F, Anta J A, Vega-Poot A, Oskam G, Alcantara G, FernandezLorenzo C. and Martin-Calleja J (2008), Photovoltaic performance of nanostructured zinc oxide sensitised with xanthene dyes, *Journal of Photochemistry and Photobiology A:Chemistry*, 200, 364-370.
 - Guo, J., Li, Y., Li, S., Cui, X., Liu, Y., Huang, W., & Zhang, X. (2020) One-step fabrication of TiO₂/graphene hybrid mesoporous film with enhanced photocatalytic activity and photovoltaic performance. *Chinese Journal of Catalysis*; 41(8), 1208-1216.
 - Guo, X., Guangxun Z., Qing L., Huaiguo X., and Huan P.; Non-noble metal-transition metal oxide materials for electrochemical energy storage; *Energy Storage Materials*, 2018,(15),171-201.
 - Gupta M, Sharma V, Shrivastava J, Solanki A, Singh A P, Satsangi V R, Dass Sand Shrivastav R (2009b), Preparation and characterization of nanostructured ZnO thin films for photoelectrochemical splitting of water, *Bull. Mater. Sci*, 32, 23-30

- Gupta M, Shrivastava J, Sharma V, Solanki A, Singh A P, Satsangi V R, Dass Sand Shrivastav R (2009a), Enhanced Photoelectrochemical Activity of 120 MeV Ag⁹⁺ Irradiated Nanostructured Thin Films of ZnO for Solar-Hydrogen Generation via Splitting of Water, *Advanced Materials Research*, 67, 95-102.
- Gür, T. M., Bent, S. F., & Prinz, F. B. (2014). Nanostructuring materials for solar-to-hydrogen conversion. *The Journal of Physical Chemistry C*, 118(37), 21301-21315.
- Gust D, Moore T A and Moore A L (2009), Solar fuels via Artificial Photosynthesis, *Accounts of Chemical Research*, 42(12),1890-1898.
- Hagfeldt A and Gratzel M (1995), Light-induced redox reactions III nanocrystalline systems, *Chem. Rev.*, 95, 49-68.
- Halvorsen B, Kverndokk Sand Torvanger A (1989), Global, Regional and National Carbon Dioxide Emissions 1949-86 - Documentation of a LOTUS Database", Working Paper 59/89, Centre for Applied Research, Oslo.
- Hamedani H A, Allam N K, Garmestani Hand El-Sayed M A (2011), Electrochemical fabrication of strontium-doped TiO₂ nanotube array electrodes and investigation of their photoelectrochemical properties, *J. Phys. Chem. C*, 115, 13480-13486.
- Han J, Mantas P Q and Senos A M R (2002), Defect chemistry and electrical characteristics of undoped and Mn-doped ZnO, *Journal of the European Ceramic Society*, 22, 49- 59.
- Han J, Mantas P Q, Senos A M R (2001), Effect of Al and Mn doping on the electrical conductivity of ZnO, *Journal of the European Ceramic Society*, 21 , 1883-1886.
- Han J, Shen M and Cao W (2003), Hopping conduction in Mn-doped ZnO, *Applied Physics Letters*, 82.
- Han, J., & Liu, Z. (2021). Optimization and modulation strategies of zinc oxide-based photoanodes for highly efficient photoelectrochemical water splitting. *ACS Applied Energy Materials*, 4(1), 1004-1013.

- Harvey P R, Rudham R and Ward S (1983), Photocatalytic oxidation of liquid alcohols and binary alcohol mixtures by rutile, 1. Chem. Soc. Faraday Trans., 79, 2975-2981.
- He H, Cai W, Lin Y and Chen B (2010), Surface decoration of ZnO nanorod Arrays by electrophoresis in the Au colloidal solution prepared by laser ablation in water, Langmuir, 26, 8925-8932.
- Heidt, L. J. (1951, July). Non-biological photosynthesis. In Proceedings of the American Academy of Arts and Sciences (Vol. 79, No. 4, pp. 228-235). American Academy of Arts & Sciences.
- Heller A, (1981), Conversion of sunlight into electric power, Acc. Chem. Res. , 14, 154-162
- Hlaing W M, Saraf L V, Engelhard M H, Shutthanandan V, Bergman L, Huso J and McCluskey M D (2009), Suppression of conductivity in Mn-doped ZnO thin films, Journal of Applied Physics, 105,013715.
- Hng H H and Chan P L (2009), Cr2O3 doping in ZnO-O.5 mol% V2O5 S varistor ceramics, Ceramics International, 35, 409-413.
- Hoang S, Guo S, Hahn N T, Bard A J and Mullins C B (2012), Visible Light Driven Photoelectrochemical Water Oxidation on Nitrogen-Modified TiO2 Nanowires, Nano Lett. , 12,26-32.
- Hodes G (2001), Electrochemistry of Nanomaterials, Weinheim, Wiley-VCH.
- Holladay J D, Hu J, King D L and Wang Y (2009), An Overview of Hydrogen Production Technologies, Catalysis Today, 139,244-260.
- Hotchandani Sand Kamat P V (1992), Charge-transfer processes in coupled semiconductor systems. Photochemistry and photoelectrochemistry of the colloidal cadmium sulfide-zinc oxide system, 1. Phys. Chem. 96,6834-6839.
- Hou D L, Ye X J, Meng H J, Zhou H J, Li X L, Zhen C M and Tang G D (2007), Magnetic properties of Mn-doped ZnO powder and thin films, Materials Science and Engineering, B 138, 184-188.
- Hsi C S, Houg B, Houb B Y, Chen G J and Fuc S L (2008), Effect of Ru addition on the properties of Al-doped ZnO thin films prepared by radio

- frequency magnetron sputtering on polyethylene terephthalate substrate, Journal of Alloys and Compounds, 464,89-94.
- Hsieh P T, Chen Y C, Kao K S, Lee M S and Cheng C C (2007), The ultraviolet emission mechanism of ZnO thin film fabricated by sol- gel technology, Journal of the European Ceramic Society, 27, 3815- 3818.
 - <https://chembam.com/definitions/nanotechnology>
 - http://solarcellcentral.com/solar_page.html
 - <https://www.bmw.com/en/innovation/how-hydrogen-fuel-cell-cars-work.html>
 - <https://www.businesstoday.in/auto/story/nitin-gadkari-drives-indias-first-hydrogen-powered-car-to-parliament-327937-2022-03-30>
 - <https://economictimes.indiatimes.com/industry/renewables/indias-top-carmaker-sees-hydrogetn-as-interesting-alternative/articleshow/84982089.cms>
 - <https://www.energy.gov/node/28747/#useful>
 - https://www.kngac.ac.in/elearning-portal/ec/admin/contents/2_18K4CSAP3
 - <https://www.radiation-dosimetry.org/what-is-electron-donor-and-electron-acceptor-definition>
 - <https://www.sarthaks.com/883212/elucidate-the-formation-of-a-n-type-and-p-type-semiconductors>
 - Hu Y M, Chen Y T, Zhong Z X, Yu C C, Chen G J, Huang P Z, Chou W Y, Chang J and Wang C R (2008), The morphology and optical properties of Cr-doped ZnO films grown using the magnetron co-sputtering method, Applied Surface Science, 254,3873-3878.
 - Huang X, Coffey J L , Paramo J A and Strzhemechny Y M (2010), Dual wavelength Emissive ZnO tetrapods: Effects of erbium/gennaniul11 surface modification, Cryst. Growth Des., 10 (1),32- 35.
 - Huang, X., Zhang, R., Gao, X., Yu, B., Gao, Y., & Han, Z. G. (2021). TiO₂-rutile/anatase homojunction with enhanced charge separation for photoelectrochemical water splitting. International Journal of Hydrogen Energy.

- Ievtushenko A, Lashkarev G, Lazorenko V, Karpyna V, Sichkovskiy V, Kosyachenko L, Sklyarchuk V, Sklyarchuk O, Bosy V, Korzhinski F, Ulyashin A, Khranovskyy V and Yakimova R (2008), Ultraviolet detectors based on ZnO:N thin films with different contact structures, *Acta Physica Polonica A*, 114, 1123-1129.
- Ilican S, Caglar Y, Caglar M and Demirci B (2008), Polycrystalline indium-doped ZnO thin films: preparation and characterization, *J. Optoelectronics Advanced Materials*, 10, 2592 - 2598.
- Inamdar A I, Mujawar S H, Ganesan V and Patil P S (2008), Surfactant-mediated growth of nanostructured ZnO thin films via electrodeposition and their photoelectrochemical performance, *Nanotechnology*, 19, 325706-325710.
- Inamdar A I, Sonavane A C, Sharma S K, Inamdar P S (2010), Nanocrystalline zinc oxide thin films by novel double pulse single step electrodeposition, *Journal of Alloys and Compounds*, 495, 76-81.
- Ingler Jr W B and Khan SUM (2004), Photoresponse of spray pyrolytically synthesized magnesium-doped iron (III) oxide (P-Fe₂O₃) thin films under solar simulated light illumination, *Thin Solid Films*, 461, 301- 308.
- Innocenti M, Cattarin S, Loglio F, Cecconi T, Seravalli G and Foresti M L (2004), Ternary cadmium and zinc sulfides: composition, morphology and photoelectrochemistry *Electrochim. Acta*, 49 (8), 1327-1337.
- Innocenti M, Cattarin S, Loglio F, Cecconi T, Seravalli G and Foresti M L (2004), Ternary cadmium and zinc sulfides: composition, morphology and photoelectrochemistry *Electrochim. Acta*, 49 (8), 1327-1337.
- International Energy Agency, (2002 b) *World Energy Outlook* · 14
- Irzh A, Genish I, Klein L, Solovyov L A and Gedanken A (2010), Synthesis of ZnO and Zn nanoparticles in microwave plasma and their deposition on glass slides, *Langmuir*, 26 (8), 5976-5984.
- Jabeen, U., Adhikari, T., Shah, S. M., Pathak, D., Kumar, V., Nunzi, J. M., & Mushtaq, A.; Synthesis, characterization and photovoltaic

- applications of noble metal—doped ZnS quantum dots ; Chinese Journal of Physics, 2019, (58), 348-362.
- Jakani M, Campet G, Claverie J, Fichou D, Pouliquen J, and Kossanyi J (1985), Photoelectrochemical properties of zinc oxide doped with 3d elements, *J. Solid State Chemistry*, 56, 269-277.
 - Jang H J, Park C J and Kwon H S (2009), Photoelectrochemical Analysis of the Effects of pH and Sulfate Ions on the Structure and the Composition of the Passive Film Formed on Fe-20Cr-15Ni Alloy, *Met. Mater. Int.*, 15, 57-62.
 - Janotti A and Van de Walle C G (2009), Fundamentals of zinc oxide as a semiconductor, *Rep. Prog. Phys.*, 72, 126501 - 126529.
 - Jayanthi K, Chawla S, Sood K N (2009), Chhibara M and Singh S, Dopant induced morphology changes in ZnO nanocrystals, *Applied Surface Science*, 255, 5869- 5875.
 - Jayaraj M K, Antony A and Ramachandran M (2002), Transparent conducting zinc oxide thin film prepared by off-axis rf magnetron sputtering, *Bull. Mater. Sci.*, 25, 227-230.
 - Jayatissa A H (2003), Preparation of gallium-doped ZnO films by oxidized ZnS films, *Semicond. Sci. Technol.*, 18, L27- L30.
 - Jeong S H, Lee S B and Boo J H (2004), The insert of Zinc Oxide thin film in Indium Tin Oxide anode for organic electro luminescence devices, *Current Appl. Phys.*, 4, 655-658.
 - Jeong S H, Park B N, Lee S B and Boo J H (2007 a), Metal-doped ZnO thin films :Synthesis and characterizations, *Surface & Coatings Technology*, 201, 5318-5322.
 - Jeong S H, Park B N, Yoo D G and Boo J H (2007 b), Al-ZnO thin films as transparent conductive oxides : Synthesis, characterization, and application tests ,*J. Korean Phys. Society*, 50, 622-625.
 - Jia W, Monge K, Xu Wand Katiyar R (2002), Spectroscopy of pure and Eu³⁺ doped ZnO, *Integrated Ferroelectrics*, 42, 357-363.
 - Jiang, H., Chen, Y., Li, L., Liu, H., Ren, C., Liu, X., & Tian, G. (2020). Hierarchical ZnO nanorod/ZnFe₂O₄ nanosheet core/shell nanoarray

- decorated with PbS quantum dots for efficient photoelectrochemical water splitting. *Journal of Alloys and Compounds*, 828, 154449.
- Jin W, Lee I K, Kompch A, Dorfier U and Winterer M (2007), Chemical vapor synthesis and characterization of chromium doped zinc oxide nanoparticles, *Journal of the European Ceramic Society*, 27, 4333-4337.
 - Jin W, Lee I K, Kompch A, Dorfier U and Winterer M (2007), Chemical vapor synthesis and characterization of chromium doped zinc oxide nanoparticles, *Journal of the European Ceramic Society*, 27,4333-4337.
 - Joy J., Jinu M., and Soney C. G.; Nanomaterials for photoelectrochemical water splitting–review. ;*International Journal of Hydrogen Energy*, 2018,(14), 4804-4817.
 - Klug H P and Alexander L E (1974), X-ray diffraction procedures for polycrystalline and amorphous materials, New York, Wiley.
 - Kathirvel P, Manoharan D, Mohan S M and Kumar S (2009), pectral investigations of chemical bath deposited zinc oxide thin films - Ammonia gas sensor, *J Optoelectron Biomed Mater*, 1, 25-33 .
 - Kaur R, Singh A V and Meill-a R M (2004), Development of highly transparent and conducting yttrium doped ZnO film: Role of sol-gel stabilizers, *Mater. Sci Pol.*, 22, 201-209.
 - Kavan, L. (2019). Conduction band engineering in semiconducting oxides (TiO₂, SnO₂): Applications in perovskite photovoltaics and beyond. *Catalysis Today*, 328, 50-56.
 - Ke, J., He, F., Wu, H., Lyu, S., Liu, J., Yang, B., ... & Ostrikov, K. (2021). Nanocarbon-enhanced 2D photoelectrodes: a new paradigm in photoelectrochemical water splitting. *Nano-Micro Letters*, 13(1), 1-29.
 - Kennedy J H, Shinar R and Ziegler J D (1980), a Fe₂O₃ photoanodes doped with silicon, *J. Electrochem. SOC*, 127,2307 -2309.
 - Khan SUM and Akikusa J (1999), Photoelectrochemical Splitting of Water at Nanocrystalline n-Fe₂O₃ Thin-Film Electrodes, *J. Phys. Chern. B*, 103, 7184-7189 .

- Khan SUM and Bockris J (1984), A model for electron transfer at the illuminated p-type semiconductor-solution interface, *J. Phys. Chem.*, 88, 2504-2515.
- Khan SUM and Bockris J O M (1984), A model for electron transfer at the illuminated p-type semiconductor-solution interface, *J. Phys. Chem.*, 88, 2504-2515.
- Khan SUM and Sultana T (2003), Photoresponse of n-TiO₂ thin film and nanowire electrodes, *Solar Energy Mater. Solar Cells*, 76, 211-221.
- Khan SUM and Zhou Z Y (1993), Photoresponse of undoped and iodine-doped iron oxide thin film electrodes, *J Electroanal. Chem.*, 357 (1-2), 407-420.
- Khan SUM, Al-Shahry M and Ingler W B (2002), Efficient Photochemical Water Splitting by a Chemically Modified n-TiO₂, Jr., *Science*, 297, 2243 - 2245.
- Khan, S. U., & Akikusa, J. (1998). Stability and Photoresponse of Nanocrystalline n-TiO₂ and n-TiO₂/Mn₂O₃ Thin Film Electrodes during Water Splitting Reactions. *Journal of the Electrochemical Society*, 145(1), 89.
- Khan, S. U., & Akikusa, J. (1999). Photoelectrochemical splitting of water at nanocrystalline n-Fe₂O₃ thin-film electrodes. *The Journal of Physical Chemistry B*, 103(34), 7184-7189.
- Khaselev, O., & Turner, J. A. (1998). A monolithic photovoltaic-photoelectrochemical device for hydrogen production via water splitting. *Science (New York, N.Y.)*, 280(5362), 425-427.
- Kim H, Kim J, Kim W and Choi W (2011), Enhanced Photocatalytic and Photoelectrochemical Activity in the Ternary Hybrid of dS/TiO₂/W₀₃ through the Cascadal Electron Transfer, *J Phys. Chem. C*, 115, 9797-9805.
- Kim I S, Jeong E K, Kim D Y, Kumar M and Choi S Y (2009), Investigation of p-type behavior in Ag-doped ZnO thin films by E-beam evaporation, *App. Surj Science*, 255, 4011--4014.

- Kim K J and Park Y R (2004), Optical investigation of Zn_{1-x}Fe_xO films grown on Al₂O₃(0001) by radio-frequency sputtering, *J. Appl. Phys.*, 96, 4150 - 4153.
- Kim K T, Kim G H, Woo J C and Kim C I (2008), Characteristics of Nickel-doped Zinc Oxide thin films prepared by sol-gel method, *Surface & Coatings Technology*, 202, 5650- 5653.
- Kim S K, Jeong S Y and Cho C R (2003), Structural reconstruction of hexagonal to cubic ZnO films on PtTi/SiO₂/Si substrate by annealing, *App/. Phys. Lett.*, 82, 562-564.
- Kim T H, Jeong S H, Kim I S, Kim S S and Lee B T (2005), Magnetron sputtering growth and characterization of high quality single crystal Ga-doped n-ZnO thin films, *Semicond. Sci. Technol.*, 20, L43-L46.
- Kim Y S, Tai W P and Shu S J (2005), Effect of preheating temperature on structural and optical properties of ZnO thin films by sol- gel process, *Thin Solid Films*, 491 , 153 - 160.
- Ko S H, Lee D, Kang H W, Nam K H, Yeo J Y, Hong S J, Grigoropoulos C P and Sung H J (2011), Nanoforest of Hydrothermally Grown Hierarchical ZnO Nanowires for a High Efficiency Dye-Sensitized Solar Cell, *Nano Lett.*, 11, 666-671.
- Koca A and Sahin M (2002), Photocatalytic hydrogen production by direct sun light from sulfide/sulfite solution, *International Journal of Hydrogen Energy*, 27, 363 - 367.
- Kocha S S and Turner J A (1996), Impedance analysis of surface modified Ga₂O₃/In₂O₃/aqueous electrolyte interface, *Electrochimica Acta*, 41, 1295-1304.
- Kotay S M and Das D (2008), Biohydrogen as a renewable energy resource – prospects and potential. *International Journal of Hydrogen Energy*, 33, 258-63.
- Kozuka H, Takahashi Y, Zhao G and Yoko T (2000), Preparation and photoelectrochemical properties of porous thin films composed of submicron TiO₂ particles, *Thin Solid Films*, 358, 172-179.

- Kreith, F., & West, R. (2004). Fallacies of a hydrogen economy: a critical analysis of hydrogen production and utilization. *J. Energy Resour. Technol.*, 126(4), 249-257.
- Kresse G, Du1ub 0 and Diebold U (2003), Competing stabilization mechanism for the polar ZnO(OO0l)-Zn surface, *Phys. Rev. B*, 68, 245409-1 - 245409-15 .
- Krishna R, Baranwal V, Katharria Y S, Kabiraj D, Tripathi A, Singh F, Khan S A, Pandey A C and Kanjilal D (2006), Nanostructure formation on zinc oxide film by ion bombardment, *Nucl. Instr. Meth. Phys. Res. B*, 244, 78-80.
- Krol R V D, Liang Y and Schoonman J (2008), Solar hydrogen production with nanostructured metal oxides, 1. *Mater. Chern.*, 18,2311-2320.
- Kronawitter C x , Vayssieres L , Shen S, Guo L, Wheeler D A ,Zhang J Z, Antoun B R and Mao S S (2011), A perspective on solar-driven water splitting with all-oxide hetero- nanostructures, *Ene. Environ. Sci .*, 4,3889-3899.
- Krunks M, Katerski A, Dedova T, Acik 10 and Mere A (2008), Nanostructured solar cell based on spray pyrolysis deposited ZnO nanorod array, *Solar Energy Materials and Solar Cells*, 92,1016-1019.
- Kucheyev S 0, Biener J, Wang Y M, Baumann T F, Wu K J, Buuren T V, Hamza A V, Satcher J H, Elam J Wand Pellin M J (2005), Atomic layer deposition of ZnO on ultralow-density nanoporous si lica aerogel monoliths, *Appl. Phys. Lett.*, 86, 083108-1 -083108-3.
- Kumar S S, Rajendran K, Banerjee S, Chini T K and Sengodan V (2008), Influence of Mn doping on the micro structure and optical property of ZnO, *Materials Science in Semiconductor Processing*, 11 , 6- 12.
- Kumar P., Kumar A.; Hydrogen Generation Via Photoelectrochemical Splitting of Water; In: Martínez L., Kharissova O., Kharisov B. (eds) *Handbook of Ecomaterials*. Springer, 2018,1-38.

- Kumar S G and Devi L G (2011), Review on Modified TiO₂ Photocatalysis under UV/Visible Light: Selected Results and Related Mechanisms on Interfacial Charge Carrier Transfer dynamics, *J Phys. Chem. A*, 115, 13211-13241.
- Kumara G R R A, Murakami K, Shimomura M, Velauthamurty K, Premalal E V A, Rajapakse R M G and Bandara H M N (2010), Electrochemical impedance and X-ray photoelectron spectroscopic analysis of dye-sensitized liquid electrolyte based SnO₂/ZnO solar cell, *Journal of Photochemistry and Photobiology A: Chemistry*, 215, 1-10.
- Kyesmen, P. I., Nombona, N., & Diale, M. (2021). Heterojunction of nanostructured α -Fe₂O₃/CuO for enhancement of photoelectrochemical water splitting. *Journal of Alloys and Compounds*, 863, 158724.
- Lee H J, Kim S K, Cho C R, Kim S J and Jeong S Y (2005), Influence of impurities on the structural and magnetic properties in ZnO, *Journal of the Korean Physical Society*, 46, S34 - S38.
- Lee J H and Park B O (2003), Transparent conducting ZnO:Al, In and Sn thin films deposited by the sol-gel method, *Thin Solid Films*, 426, 94-99.
- Lee J H, Lee D G, Park J I and Kim J Y (2010), Bio-hydrogen production from a marine brown algae and its bacterial diversity, *Korean Journal of Chemical Engineering*, 27 (1), 187-192.
- Lee K, Nam W S and Han G Y (2004), Photocatalytic water-splitting in alkaline solution using redox mediator. 1 :Parameter study, *International Journal of Hydrogen Energy*, 29, 1343 - 1347.
- Lee S G, Lee S W and Lee H I (2001), Photocatalytic production of hydrogen from aqueous solution containing CN⁻ as a hole scavenger, *Appl Catal A: Gen*, 207, 173 - 181.
- Lee W, Mane R S, Lee S H and Han S H (2007), Enhanced photocurrent generations in RuL₂(NCS)₂/di-(3-aminopropyl)-viologen self-assembled on 11120) nanorods, *Electrochemistry Communications*, 9, 1502-1507.

- Lee W, Min S K, Cai G, Mane R S, Ganesh T, Koo G, Chang J, Baek S J, Lee S H and Han S H (2008), Polymer-sensitized photoelectrochemical solar cells based on watersoluble polyacetylene and p-In₂S nanorods, *Electrochimica Acta*, 54, 714-719.
- Leea J B, Leea H J, Seob S H and Parka J S (2001), Characterization of undoped and Cu-doped ZnO films for surface acoustic wave applications, *Thin Solid Films*, 398-399, 641-646.
- Lewis N S (1990), Mechanistic studies of light-induced charge separation at semiconductor/liquid interfaces, *Acc. Chem. Res.*, 23, 176.
- Lewis N S and Nocera D G (2006), Powering the planet: Chemical challenges in solar energy utilization, *Proc. Natl. Acad. Sci. U. S. A.*, 103, 15729-15735.
- Li C Z, Choi W B and Chuang C H (2008), Size effects on the photoelectrochemical activities of single wall carbon nanotubes, *Electrochimica Acta*, 54, 821-828.
- Li C., Jayaraman B., Nam H. K., and Joong H. L.; Hierarchical Zn–Co–S nanowires as advanced electrodes for all solid state asymmetric supercapacitors.; *Advanced Energy Materials*, 2018,(8) .
- Li G R, Qu D L, Zhao W X and Tong Y X (2007), Electrochemical deposition of (Mn,Co)-codoped ZnO nanorod arrays without any template, *Electrochemistry Communications*, 9, 1661-1666.
- Li H, Cheng C, Li X, Liu J, Guan C, Tay Y Y and Fan H J (2012), Composition-Graded Zn_xCd_{1-x}Se@ZnO Core-Shell Nanowire Array Electrodes for Photoelectrochemical Hydrogen Generation, *J Phys. Chem. C*, 116, 3802-3807.
- Li Y and Zhang J Z (2010), Hydrogen Generation from Photoelectrochemical Water Splitting based on Nanomaterials, *Laser & Photon. Rev.*, 4, 517-528.
- Liang J, Wu H, Chen N and Xu T (2005), Annealing effect on electrical properties of high-k MgZnO films on silicon., *Semicond. Sci. Technol.*, 20, L15- L19.

- Licht S (2005), Thermochemical solar hydrogen generation, *Chem. Commun.*, 4635-4646.
- Licht, S., & Peramunage, D. (1990). Efficient photoelectrochemical solar cells from electrolyte modification. *Nature*, 345(6273), 330-333.
- Licht, S., Wang, B., Mukerji, S., Soga, T., Umeno, M., & Tributsch, H. (2000). Efficient solar water splitting, exemplified by RuO₂-catalyzed AlGaAs/Si photoelectrolysis. *The Journal of Physical Chemistry B*, 104(38), 8920-8924.
- Lin S S and Huang J L (2004), Effect of thickness on the structural and optical properties of ZnO films by r.f. magnetron sputtering, *Surf Coat. Technol.*, 185,222-227
- Lin Y C, Hohn K L and Stagg-Williams S M (2007), Hydrogen generation from methanol oxidation on supported Cu and Pt catalysts: Effects of active phases and supports, *Applied Catalysis A: General*, 327 (2), 164–172.
- Ling Y, Wang G, Wheeler D A, Zhang J Z and Li Y (2011), Sn-Doped Hematite Nanostructures for Photoelectrochemical Water Splitting, *Nano Lett.*, 11,2119 - 2125.
- Liu D. and Kamat P V (1993), Photoelectrochemical behavior of thin cadmium selenide and coupled titania/cadmium selenide semiconductor films, *J Phys. Chem.*, 97, 10769-10773.
- Liu Z, Jin Z, Li Wand Qiu J (2005), Preparation of ZnO porous thin films by sol-gel smethod using PEG template, *Materials Letters*, 59, 3620 - 3625.
- Liu Z, Li J, Ya J, Xin Y and Jin Z (2008), Mechanism and characteristics of porous ZnO films by sol- gel method with PEG template, *Materials Letters*, 62, 1190-1193.
- Lokhande C D and Pawar S H (1982), Effect of temperature on the performance of the PEC cells formed with chemically deposited CdS films, *Solar Energy Mater.*, 7, 313 -318.

- Lonkar, S. P., Pillai, V., & Abdala, A. ; Solvent-free synthesis of ZnO-graphene nanocomposite with superior photocatalytic activity; *Applied Surface Science*, 2019, (465), 1107-1113.
- Look D C (2005), Electrical and optical properties of p-type ZnO, *Semicond. Sci. Technol.*, 20, S55-S61.
- Loste, J., Jose M., Laurent B., Helene G., and Maud S.; Transparent polymer nanocomposites: An overview on their synthesis and advanced properties.; *Progress in Polymer Science*, 2018.
- Low W., Poi S. K., Siew S. L., Chiu W. S., and E R. E.; Recent development of mixed transition metal oxide and graphene/mixed transition metal oxide based hybrid nanostructures for advanced supercapacitors.; *Journal of Alloys and Compounds*, 2018.
- Lu L, Li R, Fan K and Pen G T (2010), Effects of annealing conditions on the photoelectrochemical properties of dye-sensitized solar cells made with ZnO nanoparticles, *Solar Energy*, 84, 844-853.
- Luo L, Zhang Y, Mao S S and Lin L (2006), Sol-Gel synthesis of polycrystalline ZnO and ZnS fibers, *Sensors and Actuators A*, 127,201-206.
- Luo W, Li Z, Yu T and Zou Z (2012), Effects of Surface Electrochemical Pretreatment on the Photoelectrochemical Performance of Mo-Doped BiVO₄. *J Phys. Chem. C*, 116,5076-5081.
- Lupan O , Guerin V M, Tiginyanu I M, Ursaki V V, Chow L, Heinrich Hand Pauporte T (2010), Well-aligned arrays of vertically oriented ZnO nanowires electrodeposited on ITO-coated glass and their integration in dye sensitized solar cells, *Journal of Photochemistry and Photobiology A: Chemistry*, 211, 65 -73.
- Lupan O , Shishiyanu S, Ursaki V, KhallafH, Chow L, Shishiyanu T, Sontea V, Monaco E and Railean S (2009), Synthesis of nanostructured Al-doped zinc oxide films on Si for solar cells applications, *Solar Energy Materials and Solar Cells*, 93, 1417-1422.
- Maeda Y, Kawana Y, Kawamura K, Hayami S, Sugihara S, and Okai T (2005), Hydrogen gas evolution from water included in a silica gel

- cavity and on metal oxides with GAMMA-ray irradiation, *J Nuc! and Radiochem. Sci.*, 6, 131-134.
- Maeda, K., Teramura, K., Lu, D., Takata, T., Saito, N., Inoue, Y., & Domen, K. (2006). Photocatalyst releasing hydrogen from water. *Nature*, 440(7082), 295-295.
 - Maiti UN, Ghosh P K, Nandy Sand Chattopadhyay K K (2007), Effect of Mn doping on the optical and structural properties of ZnO nano/micro-fibrous thin film synthesized by sol-gel technique, *Physica, E*, 387,103-108.
 - Marlinda, A. R., Yusoff, N., Sagadevan, S., & Johan, M. R. (2020). Recent developments in reduced graphene oxide nanocomposites for photoelectrochemical water-splitting applications. *International Journal of Hydrogen Energy*, 45(21), 11976-11994.
 - Martín-Gamboa, M.; Iribarren, D.; Dufour, J. ; Environmental impact efficiency of natural gas combined cycle power plants: A combined life cycle assessment and dynamic data envelopment analysis approach ; Elsevier. *Science of The Total Environment*.2018,(615), 29-37.
 - Maruska H P and Ghosh A K (1978), Photocatalytic decomposition of water at semiconductor electrodes, *Solar Energy*. 20, pp.1A3-.458. Pergamon Press.
 - Maruyama T (1998), Copper oxide thin films prepared from copper dipivaloylmethanate and oxygen by chemical vapor deposition, *Jpn. J Appl. Phys.*, 37, 4099-4102.
 - Mathew X, Bansal A, Turner IA, Dhere R, Mathews N.R. and Sebastian P.I, Photoelectrochemical Characterization of Surface Modified CdTe for Hydrogen Production, *Journal of New Materials for Electrochemical Systems* 5, 149-154 (2002)
 - Matsuoka K, Iriyama Y, Abe T, Matsuoka M and Ogumi Z (2005), Electro-oxidation of methanol and ethylene glycol on platinum in alkaline solution: Poisoning effects and product analysis, *Electrochim. Acta*, 51, 1085-1090.

- McCann J F, Kazacos M and Hancman D (1981), Temperature dependence for the power outputs of n-CdSe liquid junction cells, *Nature*, 289, 780 - 782.
- Meyer B K, Sann J, Hofmann D M, Neumann C and Zeuner A (2005), Shallow donors and acceptors in ZnO ,*Semicond. Sci. Technol.*, 20, S62-S66.
- minihydrogen.com
- Misho R H and Murad W A (1992), Band gap measurements in thin films of hematite Fe₂O₃, pyrite FeS₂ and troilite FeS prepared by chemical spray pyrolysis, *Sol. Energy Mater. Sol. Cells*, 27, 335-341.
- Miyake Hand Kozuka H (2005), Photoelectrochemical Properties of Fe₂O₃-Nb₂O₅ Films Prepared by Sol-Gel Method.*J. Phys. Chem. B*, 109,17951-17956.
- Mohapatra S K, K. S. Raja, V. K. Mahajan, and M. Misra (2008), Efficient Photoelectrolysis of Water using TiO₂ Nanotube Arrays by Minimizing Recombination Losses with Organic Additives, *J. Phys. Chem. C*, 112, 11007-11012.
- Mondal A, Basu R, Das Sand Nandy P (2010), Increased quantum efficiency in hybrid photoelectrochemical cell consisting of thionine and zinc oxide nanoparticles, *Journal of Photochemistry and Photobiology A: Chemistry*, 211, 143-146.
- Moreno M S, Kasama T, Dunin-Borkowski R E, Cooper D, Midgley P A, Steren L B, Duhalde Sand Vignolo M F (2006), Local study of the magnetism of Co-doped ZnO thin films,*J. Phys. D: Appl. Phys.*, 39, 1739-1742.
- Morrison S R (1980), *Electrochemistry at semiconductor and oxidized metal electrodes*. New York: Plenum Press, 1-401.
- Morrison S R (1980), *Electrochemistry at semiconductor and oxidized metal electrodes*.New York: Plenum Press, 1-401.
- Mridha Sand Basak D (2006), Investigation of a p-CuO/n-ZnO thin film heterojunction for H₂ gas-sensor applications, *Semicond. Sci. Technol.*, 21, 928-932.

- Mu, J., Teng, F., Miao, H., Wang, Y., & Hu, X. (2020). In-situ oxidation fabrication of 0D/2D SnO₂/SnS₂ novel Step-scheme heterojunctions with enhanced photoelectrochemical activity for water splitting. *Applied Surface Science*, 501, 143974.
- Muller Nand Cahen D (1983), Photoelectrochemical solar cells: Temperature control by cell design and its effects on the performance of cadmium chalcogenide-polysulphide systems, *Solar Cells*, 9,229 - 245.
- Musat V, Rego A M, Monteiro R and Fortunato E (2008), Microstructure and gas-sensing properties of sol- gel ZnO thin films, *Thin Solid Films*, 516, 1512- 1515.
- Natu G and Wu Y (2010), Photoelectrochemical Study of the Ilmenite Polymorph of CdSnO₃ and Its Photoanodic Application in Dye-Sensitized Solar Cells, *J. Phys. Chem. C*,114,6802-6807
- Navale S C, Ravi V and Mulla I S (2009), Investigations on Ru doped ZnO: Strain calculations and gas sensing study, *Sensors and Actuators B*, 139,466-470.
- Nga, K.H.; Minggwa, L.J.; Mark-ee, W.F.; Mohammad, K.F.; HjJumali, M.H.; Kassimab, M.B. ; A new method for the fabrication of a bilayer WO₃/Fe₂O₃ photoelectrode for enhanced photoelectrochemical performance; *J.Matter.Res.Bull*,2018,(98), 47-52.
- Noack V and Eychmuller A (2002), Annealing of nanometer-sized Zinc Oxide Particles, *Chem. Mater.*, 14, 1411-1417.
- Norris B J, Anderson J, Wager J F and Keszler D A (2003), Spin-coated zinc oxide transparent transistors, *J. Phys. D: Appl. Phys.*, 36, L105-L107.
- Nowotny J (1994), In: Nowotny J, editor. *Science of ceramic interfaces II*. Amsterdam: Elsevier., p 1. · 4, 21
- Nowotny J, Sorrell C C, Sheppard L Rand Bak T (2005a), Solar-hydrogen:Environmentally safe fuel for the future, *International Journal o./HjJdrogen Energy*, 30,521 - 544.
- Nowotny, J., Bak, T., Chu, D., Fiechter, S., Murch, G. E., & Veziroglu, T. N. (2014). Sustainable practices: solar hydrogen fuel and education

- program on sustainable energy systems. *International journal of hydrogen energy*; 39(9), 4151-4157.
- Nozik A J (1978), Photoelectrochemistry: Applications to solar energy conversion, *Annu. Rev. Phys. Chem.*, 29,189-194.
 - Nozik, A J and Memming R (1996), Physical Chemistry of Semiconductor-Liquid Interfaces. *J. Phys. Chem.*, 100, 13061 - 13078.
 - Nunes P, Fortunato E, Tonello P, Braz Fernandes F, Vilarinho P, Martins Rand Ohi J (2005), Hydrogen energy cycle: An overview, *J. Mater. Res.*, 20, 3180-3187.
 - Ohta T (2000), Preliminary theory of mechano-catalytic water-splitting, *Int. J. Hydrogen Energy*, 25, 287-293.
 - Ohyama M, Kouzuka Hand Yoko T (1997), Sol-gel preparation of ZnO films with extremely preferred orientation along (002) plane from zinc acetate solution, *Thin Solid Films*, 306 (1), 78-85.
 - Oriel-Instruments (1999), *Book of Photon Tools*,. p. 1-3. · 4, 21
 - Ozgur U, Alivov Y I, Liu C, Teke A, Reshchikov M A, Dogan S, Avrutin V, Cho S J and Morkoc H (2005), A comprehensive review of ZnO materials and device, *J Appl. Phys.*, 98,041301-1 - 041301-103.
 - Pagni O, Sornhlahlo N N, Weichsel C and Leitch A W R (2006), Electrical properties of ZnO thin films grown by MOCVD, *Physico B*, 376-377, 749 - 751.
 - Pandey B, Ghosh S, Srivastava P, Avasthi D K, Kabiraj D and Pivin J C (2008), Synthesis and characterization of Ni-doped ZnO: A transparent magnetic semiconductor,*Journal of Magnetism and Magnetic Materials*, 320, 3347-3351.
 - Pankove J I (1971), *Optical Processes in Semiconductors*, Englewood Cliffs, New Jersey, Prentice-Hall, Inc.
 - Paraguay D F, Morales J, Estrada L W, Andrade E and Miki-Yoshida M (2000), Influence of Al, In, Cu, Fe and Sn dopants in the microstructure of zinc oxide thin films obtained by spray pyrolysis, *Thin Solid Films*, 366, 16.

- Park K, Xi J, Zhang Q, and Cao G (2011), Charge Transport Properties of ZnO Nanorod Aggregate Photoelectrodes for DSCs, *J Phys. Chem. C*, 115,20992-20999
- Park S H, Chang J H, Ko H J, Minegishi T, Park J S, Im I H, Ito M, Oh D C, Cho M W and Yao T (2008), Lattice deformation of ZnO films with high nitrogen concentration, *Appl. Surf Sci.*, 254, 7972-7975.
- Park T E, Kim D C, Kong B Hand Cho H K (2004), Structural and optical properties of ZnO thin films grown by RF magnetron sputtering on Si substrates , *J Korean Phys. Soc.*, 45, S697-S700.
- Parthasarathy M, Ramgir N S, Sathe B R, Mulla I Sand Pillai V K (2007), Surface-state-mediated electron transfer at nanostructured ZnO multipod/electrolyte interfaces, *J Phys. Chem. C*, 111, 13092-13102.
- Patil P S, Lokhande C D and Pawar S H (1989), Effect of temperature on photoelectrochemical properties of n-Fe₂O₃/KOH cells, *J Phys. D: Appl. Phys.*, 22, 550-554.
- Paul G K, Ghosh R, Bera S K, Bandyopadhyay S, Sakurai S. and Akimoto K (2008), Deep level transient spectroscopy of cyanide treated polycrystalline p-Cu₂O/n-ZnO solar cell, *Chemical Physics Letters*, 463, 117-120.
- Pearton S J, Norton D P, Ip K, Heo Y Wand Steiner T (2005), Recent progress in processing and properties of ZnO, *Progress in Materials Science*, 50,293- 340.
- Peng S Q, Peng Y J, Li Y X, Lu G X and Li S B (2009), Photocatalytic hydrogen generation using glucose as electron donor over Pt/Cd_xZn_{1-x}S solid solutions, *Res Chem Intermed*, 35(6-7), 739-749.
- Persat A, Suss M E and Santiago J G (2009), Basic principles of electrolyte chemistry for microfluidic electrokinetics. Part II: Coupling between ion mobility, electrolysis, and acid- base equilibria, *Lab Chip*, 9,2454-2469.
- Podila R, Queen W, Nath A, Jeverson T A, Aline L S, Fazzio A, Gustavo M D, He J, Shiou J H, Malcolm J Sand Apparao M R (2010), Origin of

- FM Ordering in Pristine Micro- and Nanostructured ZnO, *Nano Lett.*, 10, 1383-1386.
- Poznyak S K, Kokorin A I, Kulak A I (1998), Effect of electron and hole acceptors on the photoelectrochemical behaviour of nanocrystalline microporous TiO₂ electrodes, *J. Electroanal. Chem.*, 442,99-105.
 - Qifeng Z, Dandeneau C S, Zhou X and Cao G (2009), ZnO Nanostructures for DyeSensitized Solar Cells, *Adv. Mater.*, 21, 4087 - 4108.
 - Qiu D J, Wua H Z, Fengc A M, Laob Y F, Chena N B and Xu TN (2004), Annealing effects on the microstructure and photoluminescence properties of Ni-doped ZnO films, *Applied Surface Science*, 222, 263-268.
 - Qu, Wanjun, Hui Hong, and Hongguang Jin ; A spectral splitting solar concentrator for cascading solar energy utilization by integrating photovoltaics and solar thermal fuel. ; *Applied Energy*,2019 (248) ,162-173.
 - Quintana M, Marinado T, Nonomura K, Boschloo G and Hagfeldt A (2009), Organic chromophore-sensitized ZnO solar cells: Electrolyte-dependent dye desorption and bandedge shifts, *Journal of Photochemistry and Photobiology A: Chemistry*, 202, 159-163.
 - Radecka M, Rekas M, Trenczek-Zajac A and Zakrzewska K (2008), Importance of the band gap energy and flat band potential for application of modified TiO₂ photoanodes in ater photolysis, *Journal of Power Sources*, 181,46- 55.
 - Ranjan, R., Kumar, M., & Sinha, A. S. K. (2019). Development and characterization of rGO-supported CdSMoS₂ photoelectrochemical catalyst for splitting water by visible light. *International Journal of Hydrogen Energy*, 44(31), 16176-16189.
 - Raoufi D and Raoufi T (2009), The effect of heat treatment on the physical properties of sol- gel derived ZnO thin films, *Applied Surface Science*, 255, 5812-5817.

- Reddy, I. N., Reddy, C. V., Sreedhar, A., Cho, M., Kim, D., & Shim, J. (2019). Effect of plasmonic Ag nanowires on the photocatalytic activity of Cu doped Fe₂O₃ nanostructured photoanodes for superior photoelectrochemical water splitting applications. *Journal of Electroanalytical Chemistry*, 842, 146-160.
- Reddy, C. V., Reddy, I. N., Akkinapally, B., Reddy, K. R., & Shim, J. (2020). Synthesis and photoelectrochemical water oxidation of (Y, Cu) codoped α -Fe₂O₃ nanostructure photoanode. *Journal of Alloys and Compounds*, 814, 152349.
- Rhodes C L, Lappi S, Fischer D, Sambasivan S, Genzer J and Franzen S (2008), Characterization of monolayer formation on aluminum-doped zinc oxide thin films, *Langmuir*, 24, 433-440.
- Richter A P, John R L and Bing Z (2010), Size and wavelength dependence of the charge-transfer contributions to surface-enhanced raman spectroscopy in Ag/PATP/ZnO Junctions, *J. Phys. Chem. C*, 114, 1610-1614.
- Riha S C, Fredrick S J, Sambur J B, Liu Y, Prieto A L and Parkinson B A (2011), Photoelectrochemical Characterization of Nanocrystalline Thin-Film CU₂ZnSnS₄ Photocathodes, *Applied Materials and Interfaces*, 3, 58 - 66.
- Riha S C, Fredrick S J, Sambur J B, Liu Y, Prieto A L and Parkinson B A, Photoelectrochemical Characterization of Nanocrystalline Thin-Film CU₂ZnSnS₄ Photocathodes, *Applied Materials and Interfaces*, 3 (1), 58-66.
- Roeb M, Sattler C, Kluser R, Monnerie N, Oliveira L D, Konstandopoulos A G, Agrafiotis C, Zaspalis V T, Nalbandian L, Steele A and Stobbe P (2006), Solar hydrogen production by a two-step cycle based on mixed iron oxides, *J. Solar Energy Engineering*, 128, 125-133.
- Roy Sand Basu S (2002), Improved zinc oxide film for gas sensor applications, *Bull. Mater. Sci.*, 25, 513-515.

- Rusu D I, Rusu G.G. and Luca D (2011), Structural Characteristics and Optical Properties of Thermally Oxidized Zinc Films, *Acta Physica Polonica A*, 119, 6, 850 -856.
- Sagar P, Kumar M and Mehra R M (2005), Electrical and optical properties of sol-gel derive ZnO: Al thin films , *Materials Science-Poland*, 23, 685-691.
- Salem M A (2003), The Dependence of the High Frequency Refractive Index on the Electronegativities in Compound Semiconductors, *ChineseJ. Physics*, 41,288 295.
- Samarasekara P, Nisantha A G K and Disanayake A S (2002), High-photo voltage zinc oxide deposited by DC sputtering, *Chinese J. Phys.*, 40, 196-199.
- Santato C, Ulmann M and Augustynski J (2001), Photoelectrochemical Properties of Nanostructured Tungsten Trioxide Films, *J. Phys. Chem. B*, 2001 , 105,936-940.
- Schell M, Xu Y and Zdraveski Z (1996), Mechanism for the Electrocatalyzed Oxidation of Glycerol Deduced from an Analysis of Chemical Instabilities, *J. Phys. Chem.*, 100,18962-18969
- Schmidt-Mende L and MacManus-Driscoll J L (2007), ZnO - nanostructures, defects, and devices, *Materials Today*, 10 (5), 40 - 48.
- Schneider L, Zaitsev S V, Jin W, Kompch A, Winterer M, Acet M and Bacher G (2009),Fabrication and analysis of Cr-doped ZnO nanoparticles from the gas phase, *Nanotechnology*, 20, 135604.
- Schroder D K (1990), *Semiconductor Material Device Characterization*, John Wiley & Sons, Inc. Seelig E W, Tang B, Chang R P H, Yamilov A and Cao H (2003), Self-assembled 3D photonic crystals from ZnO colloidal spheres, *Mat. Chem. Phys.*, 80, 257-261.
- Sene J J, Zeltner W A and Anderson M A (2003), Fundamental Photoelectrocatalytic and Electrophoretic Mobility Studies of TiO₂ and V -Doped TiO₂ Thin-Film Electrode Materials, *J. Phys. Chem. B* 2003 , 107, 1597-1603.

- Serrano E, Rus G, Garcel 'a-Marti 'nez J (2009), Nanotechnology for sustainable energy, Renewable and Sustainable Energy Reviews, 13, 2373 - 2384.
- Shaogui Y, Xie Q, Xinyong L, Yazhi L, Shuo C and Guohua C (2004), Preparation, characterization and photoelectrocatalytic properties of nanocrystalline Fe₂O₃/TiO₂, ZnO/TiO₂, and Fe₂O₃/ZnO/TiO₂ composite film electrodes towards pentachlorophenol degradation, Phys. Chem. Chem. Phys., 6, 659-664.
- Sharma and Deshpande N G (2008), Modifications in physical, optical and electrical properties of tin oxide by swift heavy Au⁸⁺ ion bombardment, Current Appl. Phys., 8, 181-185.
- Sharma, A., & Lee, B. K. (2016). Rapid photo-degradation of 2-chlorophenol under visible light irradiation using cobalt oxide-loaded TiO₂/reduced graphene oxide nanocomposite from aqueous media. *Journal of environmental management*, 165, 1-10.
- Sharma, A., Thuan, D. V., Pham, T. D., Tung, M. H. T., Truc, N. T. T., & Vo, D. V. N. (2020). The advanced surface of fibrous activated carbon is immobilized with FeO/TiO₂ for photocatalytic evolution of hydrogen under visible light. *Chemical Engineering & Technology*, 43(4), 752-761.
- Sharma P, Kumar P, Deva D, Shrivastav R, Dass Sand Satsangi V R (2010), Nanostructured Zn-Fe₂O₃ thin film modified by Fe-TiO₂ for photoelectrochemical generation of hydrogen, International Journal of Hydrogen Energy, 35, 10883 - 10889.
- Sharma P, Kumar P, Deva D, Shrivastav R, Dass Sand Satsangi V R (2010), Nanostructured Zn-Fe₂O₃ thin film modified by Fe-TiO₂ for photoelectrochemical generation of hydrogen, International Journal of Hydrogen Energy, 35, 10883 - 10889.
- Sharma V K, Xalxo R and Varma G D (2007), Structural and magnetic studies of Mn doped ZnO, Cryst. Res. Technol., 42(1), 34 - 38.
- Sharma V, Kumar P, Shrivastava J, Solanki A, Satsangi V R, Dass Sand Shrivastav R (2011b), Synthesis and characterization of nanocrystalline

- Zn_{1-x}M_xO (M=Ni, Cr) thin films for efficient photoelectrochemical splitting of water under UV irradiation, *International Journal of Hydrogen Energy*, 36,4280-4290.
- Sharma V, Kumar P, Shrivastava J, Solanki A, Satsangi V R, Dass Sand Shrivastav R(2011b), Synthesis and characterization of nanocrystalline Zn_{1-x}M_xO (M=Ni, Cr) thin films for efficient photoelectrochemical splitting of water under UV irradiation,*International Journal of Hydrogen Energy*, 36, 4280-4290.
 - Sharma V, Kumar P, Shrivastava J, Solanki A, Satsangi V R, Dass Sand Shrivastav R(2011a), Vertically aligned nanocrystalline Cu- ZnO thin films for photoelectrochemical splitting of water, *J Mater Sci*, 46, 3792 - 3801.
 - Sheng, P., Yao, L., Yang, P., Yang, D., Lu, C., Cao, K., & Li, W. (2020). The origin of enhanced photoelectrochemical activity in metal-ion-doped ZnO/CdS quantum dots. *Journal of Alloys and Compounds*, 822, 153700.
 - Shi D, He P, Lian J, Wang Land Ooij W J V (2002), Plasma deposition and characterization of acrylic acid thin film on ZnO nanoparticles, 1. *Mater. Res.*, 17, 2555-2560.
 - Shi J, Starr M B, Xiang H, Hara Y, Anderson M A, Seo J H, Ma Z and Wang X (2011),Interface Engineering by Piezoelectric Potential in ZnO-Based Photoelectrochemical Anode, *Nano Lett.* 2011, 11,5587-5593.
 - Shinde V R, Gujar T P, Lokhande C D, Maneb R S and Han S H (2006), Mn doped and undoped ZnO films: A comparative structural, optical and electrical properties study,*Materials Chemistry and Physics*, 96, 326-330.
 - Shishiyanu S, Chow L, Lupan O and Shishiyanu T (2006), Synthesis and characterization of functional nanostructured zinc oxide thin films, *ECS Transactions*, 3, 65-71.
 - Siavash Moakhar, R., Hosseini-Hosseiniabad, S. M., Masudy-Panah, S., Seza, A., Jalali, M., Fallah-Arani, H., ... & Saliba, M. (2021).

Photoelectrochemical Water-Splitting Using CuO-Based Electrodes for Hydrogen Production: A Review. *Advanced Materials*, 2007285.

- Singh A V, Kumar M, Mehra R M, Wakahara A and Yoshida A (2001), Al-doped zinc oxide (ZnO:Al) thin films by pulsed laser ablation, *J. Indian Inst. Sci.*, 81, 527-533.
- Singh P, Kaushal A and Kaur D (2009), Mn-doped ZnO nanocrystalline thin films prepared by ultrasonic spray pyrolysis, *Journal of Alloys and Compounds*, 471, 11-15.
- Singh S, Kumar E Sand Rao M S R (2008), Microstructural, optical and electrical properties of Cr-doped ZnO, *Scripta Materialia*, 58, 866- 869.
- Singh S, Rama Nand Rao M S R (2006), Influence of d-d transition bands on electrical resistivity in Ni doped polycrystalline ZnO, *Applied Physics Letters*, 88, 222111 .
- Singh S, Thiyagarajan P, Kant K M, Anita D, Thirupathiah S, Rama N, Tiwari B, Kortaisamy M and Rao M S R (2007), Structure, microstructure and physical properties of ZnO based materials in various forms : bulk, thin film and nano, *J. Phys. D: App./Phys.*, 40, 6312-6327.
- Sivagurunathan, A. T., Adhikari, S., & Kim, D. H. (2021). Strategies and implications of atomic layer deposition in photoelectrochemical water splitting: Recent advances and prospects. *Nano Energy*, 105802.
- Skyllas Kazacos M, McCann F F and Haneman D (1981), The effects of temperature on the power outputs of two metal dichalcogenide liquid junction cells, *Solar Energy Mater.*, 4, 215-222.
- Sodergren S, Anders H, Jorgen O and Sten-Eric L (1994), Theoretical models for the action spectrum and the current-voltage characteristics of microporous semiconductor films in photoelectrochemical cells, 1. *Phys. Chem.*, 98, 5552-5556.
- Sodergren S, Anders H, Jorgen O and Sten-Eric L (1994), Theoretical models for the action spectrum and the current-voltage characteristics of microporous semiconductor films in photoelectrochemical cells, 1. *Phys. Chem.*, 98, 5552-5556.

- Solanki A, Shrivastava J, Upadhyay S, Sharma V, Sharma P, Kumar P, Kumar P, Gaskell K, Satsangi V R, Shrivastav Rand Dass S (2011), Irradiation-induced modifications and PEC response - A case study of SrTiO₃ thin films irradiated by 120 MeV Ag⁹⁺ ions, *International Journal a/Hydrogen Energy*, 36,5236-5245.
- Song T K, Kim M H, Kim S S, Kim W J, Park C, Ko R K and Song K J (2005), Hydrogen effects on the electrical conductivity of pulsed laser deposited ZnO thin films, *Integrated Ferroelectrics*, 69, 11 3- 118.
- Sowik, J., Miodyńska, M., Bajorowicz, B., Mikołajczyk, A., Lisowski, W., Klimczuk, T. & Malankowska, A. (2019); Optical and photocatalytic properties of rare earth metal-modified ZnO quantum dots. *Applied Surface Science*; (464), 651-663.
- Spanhel L and Anderson M A (1991), Semiconductor clusters in the sol-gel process: quantized aggregation, gelation and crystal growth in concentrated zinc oxide colloids, *1. Am. Chern. Soc.*, 113,2826 - 2833 .
- Srikant V, Valter S and David R (1995), Epitaxial Aluminum-Doped Zinc Oxide Thin Films on Sapphire: I, Effect of Substrate Orientation, *1. Am. Ceram. Soc.*, 78, 1931 -1934.
- Srinivasan G and Kumar J (2006), Optical and structural characterisation of zinc oxide thin films prepared by sol-gel process, *Cryst. Res. Technol.* , 41 ,893 - 896.
- Srinivasan G, Gopalakrishnan N, Yu Y S, Kesavamoorthy Rand Kumara J (2008b), Influence of post-deposition annealing on the structural and optical properties of ZnO thin films prepared by sol-gel and spin-coating method, *Superlattices and Microstructures*, 43 , 112- 119.
- Srinivasana G and Kumar J (2008a), Effect of Mn doping on the microstructures and optical properties of sol-gel derived ZnO thin films, *Journal of Crystal Growth*, 310,1841-1846.
- Steinfeld A (2005), Solar thermochemical production of hydrogen- a review, *Solar energy*, 78, 603-15.
- Steinfeld A (2005), Solar thermochemical production of hydrogen- a reView, *Solar energy*, 78, 603-15.

- Steinfeld A, Brack M, Meier A, Weidenkaff A and Wuillemin D (1998), A solar chemical reactor for co-production of zinc and synthesis gas, *Energy*, 23, 803-814.
- Su X, Si P, Hou Q, Kong X and Cheng W (2009), First-principles study on the bandgap modulation of Be and Mg co-doped ZnO systems, *Physico B.*, 404, 1794-1798.
- Sun B, Hao Y, Guo F, Cao Y, Zhang Y, Li Y and Xu D (2012), Fabrication of Poly(3-hexylthiophene)/CdS/ZnO Core Shell Nanotube Array for Semiconductor-Sensitized Solar Cell, 1. *Phys. Chem. C*, 116, 1395-1400.
- Sun Y, Yan K, Wang G, Guo Wand Ma T (2011), Effect of Annealing Temperature on the Hydrogen Production of TiO₂ Nanotube Arrays in a Two-Compartment Photoelectrochemical Cell, 1. *Phys. Chem. C*, 115, 12844 - 12849.
- Swathi, S., Yuvakkumar, R., Ravi, G., Babu, E. S., Velauthapillai, D., & Alharbi, S. A. (2021). Morphological exploration of chemical vapor-deposited P-doped ZnO nanorods for efficient photoelectrochemical water splitting. *Ceramics International*, 47(5), 6521-6527.
- Szklarski Z and Zakrzewska K (1989), Thin oxide films as gas sensors, *Thin Solid Films*, 174,269 – 275.
- Tan S T, Chen B J, Sun X W, Fan W J, Kwok H S, Zhang X H and Chua S J (2005), Blueshift of optical band gap in ZnO thin films grown by metal-organic Chemical-vapor deposition, 1. *Appl. Phys.*, 98, 013505-1-013505-5.
- Tang X, Clauzonier A, Campbell H I, Prior K A and Cavenett B C (2004), Electrical characterisation of zinc oxide thin films by electrochemical capacitance-voltage profiling, *Appl. Phys. Lett*, 84, 3043-3045.
- Thakur A K, Wantz G, Garcia-Belmonte G, Bisquert J and Hirsch L (2011), Temperature dependence of open-circuit voltage and recombination processes in polymer-fullerene based solar cells, *Solar Energy Materials and Solar Cells*, 95 (8), 2131-2135.

- Tien, H. T., & Chen, J. W. (1992). Photoelectrolysis of water in semiconductor septum electrochemical photovoltaic cells. *Solar energy*, 48(3), 199-204.
- Tiwari A, Snure M, Kumar D and Abiade J T (2008), Ferromagnetism in Cu-doped ZnO films : Role of charge carriers, *Applied Physics Letters*, 92, 062509.
- Tsai C L, Lin Y J, Chin Y M, Liu W R., Hsieh W F, Hsu CH and Chu J A (2009), Lowresistance nonalloyed ohmic contacts on undoped ZnO films grown by pulsed-laser deposition, 1. *Phys. D: Appl. Phys.*, 42, 095108.
- U.Jabeen , Tham A., Dinesh P., Syed Mujtaba S., and Jean-Michel N(2018). ; Structural, optical and photovoltaic properties of P3HT and Mn-doped CdS quantum dots based bulk hetrojunction hybrid layers; *Optical Materials*;(78), 132-141.
- U.Jabeen , Tham A., Dinesh P., Syed Mujtaba S., and Jean-Michel N. ; Structural, optical and photovoltaic properties of P3HT and Mn-doped CdS quantum dots based bulk hetrojunction hybrid layers; *Optical Materials* ,2018,(78), 132-141.
- Upadhyay S, Shrivastava J, Solanki A, Choudhary S, Sharma V, Kumar P, Singh N, Satsangi V R, Shrivastav R, Waghmare U V and Dass S (2011), Enhanced Photoelectrochemical Response of BaTiO₃ with Fe-Doping: Experiments and FirstPrinciples Analysis, *Journal of Physical Chemistry C*, 115,24373-24380.
- Valentin C D (2010), Electronic structure of (Ga_{1-x}Zn_x)N_{1-x}O_x photocatalyst for water splitting by hybrid hartree-fock density functional theory methods, 1. *Phys. Chem. C*, 114 (15), 7054- 7062.
- Vayssieres L (2009), *On Solar Hydrogen & Nanotechnology*, John Wiley & Sons. Vercelli B, Zotti G, Berlin A, Pasini M and Botta C, Gerbasi R, Nelson T Land McCullough R D (2012), Oligo(poly)thiophene sensitization of CdSe nanocrystal and TiO₂ polycrystalline electrodes: A photoelectrochemical investigation, 1. *Phys. Chem. C*, 116,2033- 2039.

- Veziroglu T Nand Sahin S (2008), 21st Century's energy: Hydrogen energy system, *Energy Conversion and Management*, 49, 1820-1831.
- Veziroglu T Nand Sahin S (2008), 21st Century's energy: Hydrogen energy system, *Energy Conversion and Management*, 49, 1820-1831.
- Viswanatha R, Sapra S, Gupta S S, Satpati B, Sat yam P V, Dev B N and Sarma D D (2004), Synthesis and characterization of Mn-doped ZnO nanocrystals, *J.Phys. Chern. B*, 108,6303-6310.
- Walter M G, Warren E L, McKone J R, Boettcher S W, Mi Q, Santori E A and Lewis N S (2010), Solar Water Splitting Cells, *Chern. Rev.*, 110, 6446-6473.
- Wang C, Chen Z, He Y, Li L and Zhang D (2009), Structure, morphology and properties of Fe-doped ZnO films prepared by facing-target magnetron sputtering system, *Appl. Surf. Sci.*, 255, 6881-6887.
- Wang F, Liu Y, Dong W, Shen M and Kang Z (2011), Tuning TiO₂ Photoelectrochemical Properties by Nanoring/Nanotube Combined Structure, *J. Phys. Chern. C*, 115, 14635 -14640.
- Wang G H, Ling Y, Tang Y, Yang X, Fitzmorris R C, Wang C, Zhang J Z, and Li Y (2011), Hydrogen-Treated TiO₂ Nanowire Arrays for Photoelectrochemical Water Splitting, *Nano Lett.*, 11,3026- 3033.
- Wang G, Yang X, Qian F, Zhang J Z and Li Y (2010), Double-Sided CdS and CdSe Quantum Dot Co-Sensitized ZnO Nanowire Arrays for Photoelectrochemical Hydrogen Generation, *Nano Lett.* 2010, 10, 1088-1092
- Wang J, Sallet V, Jomard F, Rego AM, Elamurugu E, Martins R and Fortunato E (2007), Influence of substrate temperature on nitrogen doped ZnO films deposited by RF magnetron sputtering, *Thin Solid Films*, 515, 8785-8788.
- Wang, J., van Ree, T., Wu, Y., Zhang, P., & Gao, L. (2018). Metal oxide semiconductors for solar water splitting. In *Metal Oxides in Energy Technologies*; 205-249.
- Wang M, Wang J, Chen W, Cui Y and Wang L (2006), Effect of preheating and annealing temperatures on quality characteristics of ZnO

- thin film prepared by sol-gel method, *Materials Chemistry and Physics*, 97,219-225.
- Wang Q J, Pflugl C, Andress W F, Ham D, Capasso F and Yamanishi M (2008), Gigahertz surface acoustic wave generation on ZnO thin films deposited by radio frequency magnetron sputtering on III-V semiconductor substrates, *J Vac. Sci. Technol./B.*, 26,1848-1851.
 - Wang, Y. F., Li, K. P., Xu, X. M., & Zhang, Y. R. (2014). Transport energy consumption and saving in China. *Renewable and Sustainable Energy Reviews*; (29), 641-655.
 - Wang Y, Zhang Y, Chang W J, Lu G L, Jiang J Z, Li Y C, Liu J and Hu T D (2005), Mn effect on wurtzite-to-cubic phase transformation in ZnO, *Journal of Physics and Chemistry of Solids*, 66,1775- 1778.
 - Wang, Y., Zhang, F., Yang, M., Wang, Z., Ren, Y., Cui, J., ... & Kang, D. J. (2019). Synthesis of porous MoS₂/CdSe/TiO₂ photoanodes for photoelectrochemical water splitting. *Microporous and Mesoporous Materials*, 284, 403-409.
 - Wang Z L (2004), Zinc oxide nanostructures: Growth, Properties and Application, *J Phys.: Condens. Matter*, 16. R829- R858.
 - Wang, Z., Li, X., Tan, C. K., Qian, C., Grimsdale, A. C., & Tok, A. I. Y. (2019). Highly porous SnO₂ nanosheet arrays sandwiched within TiO₂ and CdS quantum dots for efficient photoelectrochemical water splitting. *Applied Surface Science*, 470, 800-806.
 - Weichsel C, Pagni O and Leitch A W R (2005), Electrical and hydrogen sensing characteristics of Pd/ZnO Schottky diodes grown on GaAs, *Semicond. Sci. Technol.*, 20,840-843.
 - Wellings J S, Chaure N B, Heavens S Nand Dharmadasa I M (2008), Growth and characterisation of electrode posited ZnO thin films, *Thin Solid Films*, 516, 3893- 3898.
 - Wen W, Carim A I, Collins S M, Price M J, Peczonczyk S L, and Maldonado S (2011), Structural and Photoelectrochemical Properties of GaP Nanowires Annealed in NH₃, *J Phys. Chem. C*, 115,22652-22661.

- Wenham S R, Green M A and Watt M E (1994), *Applied photovoltaics*, Centre for Photovoltaic Devices and Systems, Sydney, 239-246.
- Wong K K, Ng A, Chen X Y, Hang Ng Y, Leung Y H, Ho K H, Djurisić A B, Ching Ng A M, Chan W K, Yu L and Phillips D L (2012), Effect of ZnO Nanoparticle Properties on Dye-Sensitized Solar Cell Performance, *ACS Appl. Mater. Interfaces* (in press).
- Wu D, Yanga M, Huang Z, Yin G, Liao X, Kang Y, Chen X and Wang H (2009), Preparation and properties of Ni-doped ZnO rod arrays from aqueous solution, *Journal of Colloid and Interface Science*, 330, 380-385.
- Wu N L and Lee M S (2004), Enhanced TiO₂ photocatalysis by Cu III hydrogen production from aqueous methanol solution, 29 (15), 1601 - 1605.
- Wunderlich W, Oekermann T, Miao L, Hue N T, Tanemura Sand Tanemura M (2004), Electronic properties of Nano-porous TiO₂ and ZnO-Thin Films-comparison of simulations and experiments, *J Ceramic Processing Res.*, 5, 343-354.
- www.h2carco.com
- www.minihydrogen.com
- Xiong, C., Li, B., Lin, X., Liu, H., Xu, Y., Mao, J., & Ni, Y.; The recent progress on three-dimensional porous graphene-based hybrid structure for supercapacitor; *Composites Part B: Engineering*, 2018.
- Xu C, Paul S, Cao L and Gao D (2010), Preferential growth of long ZnO nanowire array and its application in dye-sensitized solar cells, *J Phys. Chem. C*, 114, 125-129.
- Xu H Y (2006), Structural, optical, and magnetic properties of Mn-doped ZnO thin film, *The Journal of Chemical Physics*, 124, 074707.
- Xu L L, Wu X L, Xiong X, Zhu J, Chen H T, Huang G Sand Chu P K (2008), Synthesis and field-emission properties of rose like ZnO nanostructures, *Appl. Phys. A*, 91, 247-250.

- Xu Land Li X (2010), Influence of Fe-doping on the structural and optical properties of ZnO thin films prepared by sol-gel method, *Journal of Crystal Growth*, 312, 851-855.
- Yamabi Sand Imai H (2002), Crystal phase control for titanium dioxide films by direct deposition in aqueous solutions, *J Mater. Chern.*, 12,3773-3778.
- Yan F, Huang L, Zheng J, Huang J, Lin Z, Huang F and Wei M (2010), Effect of surface etching on the efficiency of ZnO-based dye-sensitized solar cells, *Langmuir*, 26, 7153-7156.
- Yan L, Ong C K and Rao X S (2004), Magnetic order in Co-doped and (Mn, Co) codoped ZnO thin films by pulsed laser deposition, *J. Appl. Phys.*, 96, 508-511.
- Yang, X., Zhou, L., Cao, G., Song, Z., & Zhao, M. (2020). Fabrication of reduced graphene oxide wrapped TiO₂/SnO₂ photoanode and its anti-corrosion property. *Optik*, 202, 163573.
- Yilanci A, Dincer I and Qzturk H K (2008), A review on solar - hydrogen/fuel cell hybrid energy systems for stationary applications, *Progress in Energy and Combustion Science*, 35,231-244.
- Yilanci A, Dincer I and Qzturk H K (2008), A review on solar - hydrogen/fuel cell hybrid energy systems for stationary applications, *Progress in Energy and Combustion Science*,35, 231-244.
- Yoshida T, Tochimoto M, Terada K, Schlettwein D, Oekermann T, Wohrle D, Sugiura T and Minoura H (1999), Self-assembly of zinc oxide thin films modified with tetrasulfonated metallophthalocyanines by one-step electrodeposition, internet article.
- Yu Q, Fu W, Yu C, Yang H, Wei R, Sui Y, Liu S, Liu Z, Li M, Wang G, Shao C, Liu Y and Zou G (2007), Fabrication and optical properties of large-scale ZnO nanotube bundles via a simple solution route, *J. Phys. D: Appl. Phys.*, 40,5592-5597.
- Yu, Z., Liu, H., Zhu, M., Li, Y., & Li, W. (2021). Interfacial charge transport in 1D TiO₂ based photoelectrodes for photoelectrochemical water splitting. *Small*, 17(9), 1903378.

- Zaidi T, Fenwick W E, Melton A, Li N, Gupta S, Yu H, Ougazzaden A and Ferguson I(2008), Effects of N doping on ZnO thin films grown by MOVPE, *J. Cryst. Growth*, 310, 5011- 5015.
- Zhang F, Luo Y, Song J, Guo X, Liu W, Ma C, Huang Y, Ge M, Bo Z and Meng Q B (2009), Triphenylamine-based dyes for dye-sensitized solar cells, *Dyes and Pigments*, 81, 224- 230.
- Zhang J, Skomski R and SeUmyer D J (2005), Sample preparation and annealing effects on the ferromagnetism in Mn-doped ZnO, *Journal of Applied Physics*, 97, 303.
- Zhang Y, Lin B, Fu Z, Liu C and Han W (2006), Strong ultraviolet emission and rectifying behavior of nanocrystalline ZnO films, *Opt. Mater.* 28, 1192 - 1196.
- Zhang Z, Hossain M F and Takahashi T (2010), Photoelectrochemical water splitting on highly smooth and ordered TiO₂ nanotube arrays for hydrogen generation, *Int. J. Hydrogen Energy*, 35, 8528-8535.
- Zhang Z, Md F Hand Takakazu T (2010), Photoelectrochemical water splitting on highly smooth and ordered TiO₂ nanotube arrays for hydrogen generation, *Int. J. Hydrogen Energy*, 35 (16), 8528-8535.
- Zhao G, Kozuka H, Lin Hand Yoko Y (1999), Sol-Gel preparation of Ti_{1-x}YxO₂ solid solution film electrodes with conspicuous photoresponse in the visible region, *Thin Solid Films*, 339, 123-128.
- Zheng Y Z, Xia T, Li-Xin W, Hui X, Qian H, Wei-Lie Z and Jian-Feng C (2010), Novel ZnO-based film with double light-scattering layers as photo electrodes for enhanced efficiency in dye-sensitized solar cells, *Chem. Mater.* , 22, 928-934.
- Zhou Z, Kato K, Komaki T, Yoshino M, Yukawa H, Morinaga M and Morita K (2003), Electrical conductivity of Cu-doped ZnO and its change with hydrogen implantation, *Journal of Electroceramics*, 11, 73 - 79.
- Zhou, N., Yan, R., Wang, X., Fu, J., Zhang, J., Li, Y., & Sun, X. (2021). Tunable thickness of mesoporous ZnO-coated metal nanoparticles for

enhanced visible-light driven photoelectrochemical water splitting. *Chemosphere*, 273, 129679.

- Zhu H, Iqbal J, Xu H, and Yu D (2008), Raman and photoluminescence properties of highly Cu doped ZnO nanowires fabricated by vapor-liquid-solid process, *The Journal of Chemical Physics*, 129, 124713.
- Znaidi L, Illia G J A A S, Benyahia S, Sanchez C and Kanaev A Y (2003), Oriented ZnO thin films synthesis by sol- gel process for laser application, *Thin Solid Films*, 428, 257-262.